

**“Therapeutic value of artesunate in  
neuroendocrine cancer treatment inspired  
by EGFR expression”**

**Dissertation**

**zur Erlangung des Grades**

**“Doktor der Naturwissenschaften”**

**im Promotionsfach Pharmazie**

**am Fachbereich Chemie, Pharmazie und  
Geowissenschaften der Johannes Gutenberg-Universität in  
Mainz**

**vorgelegt von Ge Yan**

**geboren am 16.11.1990 in China**

**Mainz, Juli, 2019**

**Betreuer:**

**Gutachter der Arbeit:**

**Datum der mündlichen Prüfung:**

16.07.2019

**Prüfungskommission:**

*D77 (Dissertation Universität Mainz)*

## Erklärung

Hiermit erkläre ich an Eides statt, dass ich diese Arbeit selbständig verfasst und keine anderen als die angegebenen Quellen und Hilfsmittel verwendet habe.

Mainz, 11.06.2019

Keine Unterschrift zwecks Datenschutz

---

---

Ort, Datum

Ge Yan

## **Acknowledgement**

## Abstract

As the second lethal disease, cancer gives rise to about 1 in 6 deaths globally. Despite the enormous efforts, no global cure for cancer has yet been approvingly demonstrated in light of annual escalation of the incidence. In this study, we investigated the prevalence and prognostic value of epidermal growth factor receptor (EGFR) among various solid neoplasms. In spite of the abundance of EGFR in tumors, the EGFR targeted therapies are not seen as optimal due to their induction of rapid drug resistance. Therefore, we were specifically interested in artesunate (ART), which reveals EGFR inhibitory potential and slow resistance development. Since the common EGFR-expressing tumors have multiple therapeutic options, assessing potential of ART in the rather rare neuroendocrine tumors (NETs), which express EGFR and currently lack well-pleasing treatment, presents an especially appealing objective.

Firstly, we looked into the correlation of mRNA level to pathological parameters by analyzing 30 datasets *in silico* and immunohistochemically stained 502 biopsies covering 27 neoplastic types followed by the statistical analysis of the association between the protein expression, which was further classified as membranous/cytoplasmic (mcEGFR) and nuclear (nEGFR) expression patterns, and clinic outcomes. Our results suggest a superiority of protein expression compared to mRNA transcription level concerning the prognostic value. Distinct expression patterns within divergent neoplastic types were described. Unexpectedly, protein expression intensity in both patterns contradicted tumor size. Moreover, mcEGFR was found to significantly correlate with differentiation in an adverse manner. Altogether, these findings imply that the oncogenic property of EGFR is more relevant to the nascent stage than to the advanced stage during the carcinogenesis. Inspired by the current results, we focused on EGFR expressing in the neuroendocrine tumors (NETs), and investigated the cellular response of three EGFR-expressing NET cell lines (BON-1, QGP-1 and NCI-H727) towards ART treatment. Incidentally, we specified a global cellular response that ART induced endoplasmic reticulum stress by eIF2 $\alpha$  activation and gave rise to autophagy. However, the fate of cells considerably diverged associating with a differential regulation of p21 on the long run. In addition to autophagy and apoptosis, ferroptosis was observed in BON-1 cells.

These results implied that ART can be considered as an alternative treatment option or a part of combination therapy for NET patients.

## Zusammenfassung

Krebs führt als die weltweit zweithäufigste tödliche Krankheit zu einem von sechs Todesfällen. Trotz der enormen Bemühungen wurde ein Heilmittel gegen Krebs weltweit noch nicht gefunden, wie die jährliche Zunahme der Krebsinzidenz zeigt. In dieser Studie haben wir die Prävalenz und den prognostischen Wert des epidermalen Wachstumsfaktor-Rezeptors (EGFR) bei verschiedenen Neoplasien untersucht. Trotz der Häufigkeit von EGFR bei Tumoren werden gegen EGFR gerichtete Therapien wegen schneller Resistenzentwicklung als nicht optimal angesehen. Deshalb interessierten wir uns speziell für Artesunat (ART), das ein inhibitorisches Potenzial für EGFR und eine geringe Resistenzentwicklung aufweist. Da die häufig vorkommenden EGFR-exprimierenden Tumoren über eine Vielzahl von therapeutischen Möglichkeiten verfügen, ist die Bewertung des ART-Potenzials bei den weniger häufigen neuroendokrinen Tumoren (NETs), die EGFR exprimieren und derzeit nicht gut behandelt werden, ein besonders attraktives Ziel.

Zunächst haben wir die mRNA Expression mit pathologischen Parametern korreliert unter Verwendung von 30 *in silico* Datensätzen und 502 immunhistochemisch gefärbten Biopsien von 27 verschiedenen neoplastischen Typen. Mittels statistischer Analyse wurde weiterhin der Zusammenhang zwischen der Proteinexpression, die als Expressionsmuster aus membranständig / cytosolisch (mcEGFR) und nukleär (nEGFR) klassifiziert wurde, und dem klinischen Befund hergestellt. Unsere Ergebnisse deuten auf eine Überlegenheit der Proteinexpression im Vergleich zur mRNA-Transkription in Bezug auf den prognostischen Wert hin. Es wurden ausgeprägte Expressionsmuster innerhalb verschiedener neoplastischer Typen beschrieben. Unerwarteterweise widerspricht die Proteinexpression in beiden Mustern der Tumorgröße. Darüber hinaus zeigte sich, dass mcEGFR signifikant negativ mit der Differenzierung korrelierte. Diese Befunde deuten darauf hin, dass die onkogene Eigenschaft von EGFR für frühe Stadien der Karzinogenese relevanter ist als fortgeschrittenen Tumorstadien. Inspiriert durch die aktuellen Ergebnisse fokussierten wir auf EGFR-exprimierende neuroendokrine Tumoren (NETs) und untersuchten die zelluläre Antwort von drei EGFR-exprimierenden NET-Zelllinien (BON-1, QGP-1 und NCI-H727) auf die Behandlung mit ART. ART induzierte Stress im endoplasmatischen Retikulum durch Aktivierung von eIF2 $\alpha$ , was zur Autophagie führte. Das Schicksal der Zellen divergierte jedoch erheblich, was langfristig mit einer differenziellen Regulation von p21 zusammenhing. Neben Autophagie und Apoptose wurde in BON-1-Zellen Ferroptose beobachtet.

Die Ergebnisse deuten darauf hin, dass ART als alternative Behandlungsoption oder als Teil von Kombinationstherapien für NET-Patienten erwogen werden kann.

**Table of contents**

<b>Acknowledgement .....</b>	<b>I</b>
<b>Abstract .....</b>	<b>II</b>
<b>Zusammenfassung .....</b>	<b>III</b>
<b>Table of contents.....</b>	<b>IV</b>
<b>1 Introduction.....</b>	<b>1</b>
<b>1.1 Cancer.....</b>	<b>2</b>
1.1.1 Nature of cancer .....	2
1.1.2 Prevention and management .....	3
<b>1.2 Neuroendocrine neoplasms.....</b>	<b>4</b>
1.2.1 Characteristics of neuroendocrine neoplasms .....	4
1.2.2 Current diagnosis and treatment.....	5
<b>1.3 Epidermal growth factor receptor .....</b>	<b>7</b>
1.3.1 Structure and physiological function.....	8
1.3.2 Signaling pathways and role in cancer .....	11
1.3.3 EGFR and neuroendocrine neoplasms .....	14
<b>1.4 Artesunate .....</b>	<b>15</b>
1.4.1 Structure and utility.....	15
1.4.2 Molecular mechanisms.....	18
<b>2 Aim .....</b>	<b>21</b>
<b>3 Results .....</b>	<b>22</b>
<b>3.1 EGFR and cancer .....</b>	<b>22</b>
3.1.1 Correlation of EGFR mRNA expression and clinic outcomes .....	22
3.1.2 Prevalence of EGFR protein expression in diverse cancer types .....	25
3.1.3 Correlation of EGFR protein expression and clinic outcomes .....	27
3.1.4 Brief summary.....	28

---

<b>3.2</b>	<b>Artesunate against neuroendocrine tumors</b> .....	<b>29</b>
3.2.1	Cytotoxicity of artesunate .....	29
3.2.2	Transcriptomic profiling .....	30
3.2.3	Detection of reactive oxygen species .....	32
3.2.4	Detection of cell cycle arrest .....	34
3.2.5	Detection of ferroptosis .....	36
3.2.6	Detection of autophagy .....	37
3.2.7	Detection of apoptosis by flow cytometer .....	38
3.2.8	Detection of apoptosis in situ .....	39
3.2.9	Western blotting .....	40
3.2.10	Detection of Mitochondrial Membrane Potential .....	43
3.2.11	Brief summary .....	44
<b>4</b>	<b>Discussion</b> .....	<b>46</b>
4.1	EGFR and its role in multiple cancer types .....	46
4.2	Artesunate and its effects on NETs .....	47
<b>5</b>	<b>Material and Methods</b> .....	<b>49</b>
5.1	Tumor cases .....	49
5.2	Statistical evaluation of the GEO and Oncomine databases .....	49
5.3	Search strategy .....	50
5.4	Immunohistochemistry and statistical application.....	50
5.5	Cell lines .....	51
5.6	Cytotoxicity determination .....	51
5.7	Microarray hybridization .....	51
5.8	Quantitative real-time RT-PCR.....	52
5.9	Reactive oxygen species (ROS) generation.....	52

---

<b>5.10</b>	<b>Detection of cell cycle arrest by flow cytometer.....</b>	<b>53</b>
<b>5.11</b>	<b>Ferroptosis inhibition.....</b>	<b>53</b>
<b>5.12</b>	<b>Autophagy inhibition .....</b>	<b>53</b>
<b>5.13</b>	<b>Apoptosis detection with flow cytometer.....</b>	<b>54</b>
<b>5.14</b>	<b>In situ apoptosis detection.....</b>	<b>54</b>
<b>5.15</b>	<b>Western blotting .....</b>	<b>54</b>
<b>5.16</b>	<b>Mitochondrial membrane potential detection .....</b>	<b>55</b>
<b>6</b>	<b>Summary and conclusion .....</b>	<b>56</b>
<b>7</b>	<b>Future perspective .....</b>	<b>58</b>
<b>8</b>	<b>References .....</b>	<b>59</b>
<b>9</b>	<b>Supplementary materials .....</b>	<b>80</b>
<b>10</b>	<b>Appendix .....</b>	<b>85</b>
<b>10.1</b>	<b>Publications List .....</b>	<b>85</b>
<b>10.2</b>	<b>Curriculum Vitae .....</b>	<b>86</b>

## 1 Introduction

Cancer has been a global health issue and perplexed the public for decades. Intensive studies have focused on predominant types of cancer, *e.g.* lung, prostate and breast. By contrast, rare neoplastic types gained sparse attention and scant endeavor.

The project is designed to understand the role of the well-known cancer biomarker epidermal growth factor receptor (EGFR) in multiple neoplastic prognosis to expand the EGFR-targeting strategy in cancer treatment. Instead of the common EGFR-expressing tumors (*e.g.* lung, glioblastoma and colon), which have multiple therapeutical options, we explored the potential of EGFR as a therapeutic target in a rare neoplasm type, namely neuroendocrine tumors (NETs), which lacks effective available treatment.

It has been reported that EGFR is frequently expressed and hyper-activated in NETs [1–3]. Besides, three NET models (BON-1, QGP-1 and NCI-H727) have been proved to express EGFR and the latter two models exhibit *EGFR* aneusomy and elevated *EGFR* gene copy number [4–6]. Thereby, EGFR emerges as a novel biomarker and therapeutic target in NETs. Actually, some clinic trials targeting EGFR in NETs have been undergoing [6–9].

However, the drug resistance towards the standard EGFR-targeted therapies, *e.g.* tyrosine kinase inhibitors (TKIs) and immune-reactive monoclonal antibodies (mAbs), raised our concern in their clinic efficacy. In fact, the resistance to EGFR targeted TKIs due to lack of activating mutations [10,11] and phenotypic neuroendocrine transformation [12] has been shown in several NET cases. In comparison, there is no clear evidence regarding the effect of EGFR directed mAb on NETs. However, the EGFR targeting mAb cetuximab has developed resistance due to increased VEGF and VEGFR production, elevated heterodimerization with HER2/3, EGFR nuclear translocation, mesenchymal-like transformation and constitutive downstream activation [13]. In this case, instead of well-known EGFR-targeted drugs, we are more interested in investigating the utility of other possible candidates in NETs treatment. Artesunate (ART) presents the most potent candidate for the following reason: 1. ART has exhibited inhibitory potential against EGFR [14]. On the other hand, EGFR signaling significantly contributes to the activity of ART in cancer treatment [15–18]. In addition to direct inhibition of EGFR, ART may also exert its effect by impeding HER2, which activates EGFR by forming heterodimerization [19]. This property may allow ART to surpass certuximab. Moreover, the combination of ART and TKIs like gefitinib and OSI-774 has shown the synergistic inhibition against EGFR [20,21]. 2. ART presents patient-friendly safety profile

even with high doses intravenous administration [22]. 3. ART is characterized by comparative reluctance in resistance development. The first resistance case was reported [23] two decades later than the discovery of artemisinin-based therapy in mid-twentieth century [24,25]. This reluctance may be attributed to its multi-target property. 4. ART remains one of the most economic drug in clinic [26]. Based on the mentioned benefits of ART, we investigated the effect of ART in NETs treatment by utilizing the three mature NET models (BON-1, QGP-1 and NCI-H727).

## **1.1 Cancer**

Cancer, alternatively as malignant neoplasms or tumors, is a generic term describing a large group of diseases characterized by the uncontrolled growth of cells invading adjacent tissues due to the accumulation of abnormal molecular alterations. The occurrence of cancer can be traced back to ancient times [27–29]. Despite the long history of cognition regarding cancer, no approvingly radical treatment has yet been demonstrated. Until 2018, cancer remained the second lethal disease and resulted in approximately 9.6 million death according to World Health Organization [30].

### **1.1.1 Nature of cancer**

Briefly, cancer is a consequence of genetic and epigenetic alterations, which eventually break the balance between cell growth-promoting and growth-restraining effects. Generally speaking, cancer is a genetic disease by nature considering the fact that risks of cancer can be inherited and the neoplastic cells present the genetic characteristics of their origins [31]. In order to specify the core traits of cancer, the hallmarks beyond its complexity were announced [32–34], which comprise superior proliferative capacity, resistance to apoptosis and growth suppressors, angiogenesis capability, invasion and metastasis activation, immune modulation, abetting metabolic system and microenvironment.

Aberrantly, the balance between growth-promoting and growth-restraining signals undergoes intimate control under physiological conditions. The qualitative mutations of genes during somatic evolution or quantitative alterations in gene copy number, especially proto-oncogenes and the tumor suppressor genes, allow cells to elude division control and subsequently to form a genetically homogeneous clone. Occurrence of additional mutations in later development gives rise to the sub-clones within the neoplasms and causes heterogeneity. Once the abnormal cells gain metastatic property, cancer rises.

Oncogenes are literally derived from proto-oncogenes, which promote cell growth under physiological conditions. However, once proto-oncogenes become hyper-activated due to mutations or increased gene copy number, they turn into oncogenes. Similarly, tumor suppressor genes exist to slow down the cell division. However, the inactivation of these suppressor genes leads to the unlimited cell proliferation. Cancer hence can rise from activation of oncogenes and inactivation of tumor suppressor genes through direct mutations and alterations of gene copy number. Indirectly, epigenetic modulators [35] in post-translation modification can also tune the oncogenesis. Taken all together, gain or loss of the entire chromosomes, accumulative mutations directly affecting the gene-coding protein function or indirectly affecting the microRNA that controls the expression of numerous genes eventually alter cells behavior and enable cells to display the hallmarks of cancer. A number of oncogenes and tumor suppressor genes have been identified during the last decades. Many types of cancer are specifically associated with the defined genetic alteration events [36]. In our study, we investigated a specific oncogene encoding protein, EGFR.

### **1.1.2 Prevention and management**

Reducing the likelihood of cancer significantly relies on the avoidance of specific factors, which are able to cause carcinogenic gene alterations. The environmental factors (*e.g.* special chemical substances and radiation) and biological factors (*e.g.* certain types of pathogens or life habits) have been intensively investigated in epidemiology studies [37–41]. Nevertheless, there are also age- and family history-related factors, which cannot be intentionally avoided.

Concrete management of cancer differs from one cancer type to another. In general, the management of cancer involves diagnosis, treatment and follow-up care.

Classical diagnosis methods include physical test, fluid test, image and biopsy [42–44]. The advanced diagnosis methods incorporate tests on the cell-free DNA and non-coding long RNA in circulating fluids [45–48]. Further classification regarding the stage and grade of cancer is concluded according to the histologic characterizations, which are pivotal for the treatment recommendations [49]. TNM stage system developed by American Joint Committee on Cancer and Union for International Cancer Control is considered to be a globally accepted standard for cancer progressive classification [50]. The system shows its strength in tackling the heterogeneity of innumerable variables (*e.g.* patient age, gender, family history, primary neoplasm location, and so forth) by focalizing on tumor size and invasion capability. On the

other hand, the classification system fails to provide reliable and accurate prognostic information [51] due to the neglect of some crucial variables.

Despite the diversity of cancer, a combination of available treatments involving physical treatment, *e.g.* surgery, transplant, and radiation therapy, chemical treatment, *e.g.* chemotherapy, biochemical treatment, *e.g.* targeted therapy, immunotherapy and hormone therapy are commonly given to patients [52–55]. Additional supportive treatments are also incorporated to relieve some unspecific symptoms or unpleasant side effects, *e.g.* pain, anemia and diarrhea. Lastly, follow-up visit is essential to record and supervise the conditions of currently cured patients.

## 1.2 Neuroendocrine neoplasms

Present research work prevalingly concentrates on the most frequent cancer types. Neuroendocrine tumors (NETs) obtain very limited attention worldwide and is considered as an orphan disease [56]. By contrast, a retrospective study showed that the incidence of NETs steadily rose by 6.4-fold from 1973 (1.09 per 100 000) to 2012 (6.98 per 100 000) [57].

### 1.2.1 Characteristics of neuroendocrine neoplasms

NETs arise from the cells of the endocrine and nervous system. In addition to the paucity and steadily increased incidence, NETs are characterized by the extraordinary heterogeneity, which can be attributed to multiple origins, diverse histopathological and clinical features, hormone secretion capacity as well as various cellular and genetic features [58] (**Figure 1**).

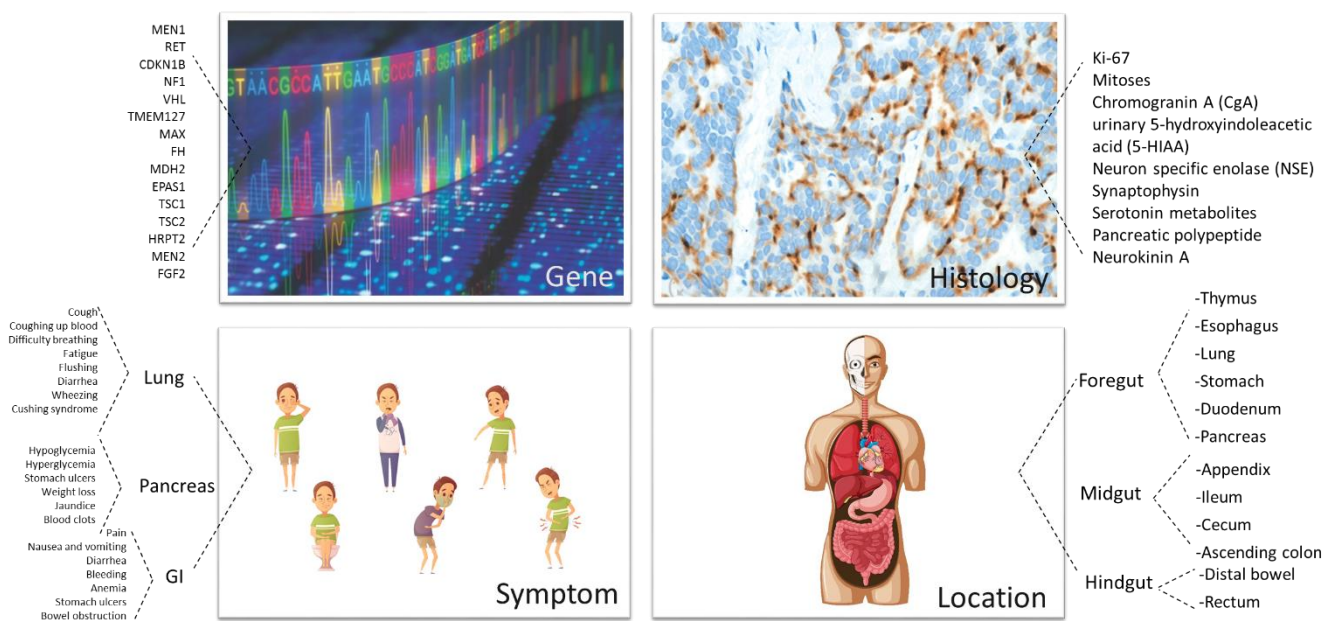


**Figure 1. Heterogeneity of neuroendocrine tumors**

Heterogeneity of neuroendocrine tumors. The heterogeneity is presented on gene level, protein level, tissue level and consequent symptoms. The whole figure was constructed by the thesis author. The upper two figures were cited from website (<http://www.clpmag.com/2018/03/delivering-promise-ngs-clinical-diagnostics/> and <https://biocare.net/product/chromogranin-a-antibody/>) and the below two figures were obtained from freepik online resources.

NETs can generate from tissues in the entire body. According to the Surveillance Epidemiology and Ends Results database, the lung was the most common site of NETs (30.6%), followed by the small intestine (22.2%), rectum (16.2%), colon (13.4%), pancreas (10.8%), and stomach (6.8%), respectively [59].

The clinical features of neuroendocrine tumors in lung involve non-specific respiratory symptoms (*e.g.* cough, dyspnea, hemoptysis or wheezing), hormonal symptoms (*e.g.* hyperhidrosis, flushing or diarrhea) or no symptoms [60,61]. For the patients diagnosed with gastroenteropancreatic neuroendocrine tumors (GEP-NET), they present hypoglycemia, peptic ulcer, hypokalemia or no symptoms [62]. Noticeably, a majority of patients show no symptoms at the early stage, which lead to a delayed diagnosis [63,64]. Besides, the terminology and criteria regarding NETs in histopathological aspect remains controversial.

From the cellular point of view, neuroendocrine cells comprise a group of cells, *e.g.* enterochromaffin-like (ECL) cells and pancreatic polypeptide (PP) cells [58]. They receive neuronal input and, as a consequence, release message molecules into the blood, by which the neuroendocrine integration is formed. From the genomic point of view, NETs with different anatomical location usually harbor different gene mutation features [65,66].

Collectively, neuroendocrine tumors are characterized by paucity, rising incidence, heterogeneity and late diagnosis.

### 1.2.2 Current diagnosis and treatment

The diagnosis of NETs is conducted by a combination of means involving general tests, (*e.g.* medical history survey, physical exam and blood/urine tests), defined tests (*e.g.* biopsy and biochemical markers test) and image tests (endoscopy, ultrasound scan, X-ray scan, computed tomography (CT) scan, magnetic resonance imaging (MRI), octreotide scan, metaiodobenzylguanidine (MIBG) scan and positron emission tomography (PET) scan) (**Figure 2**).

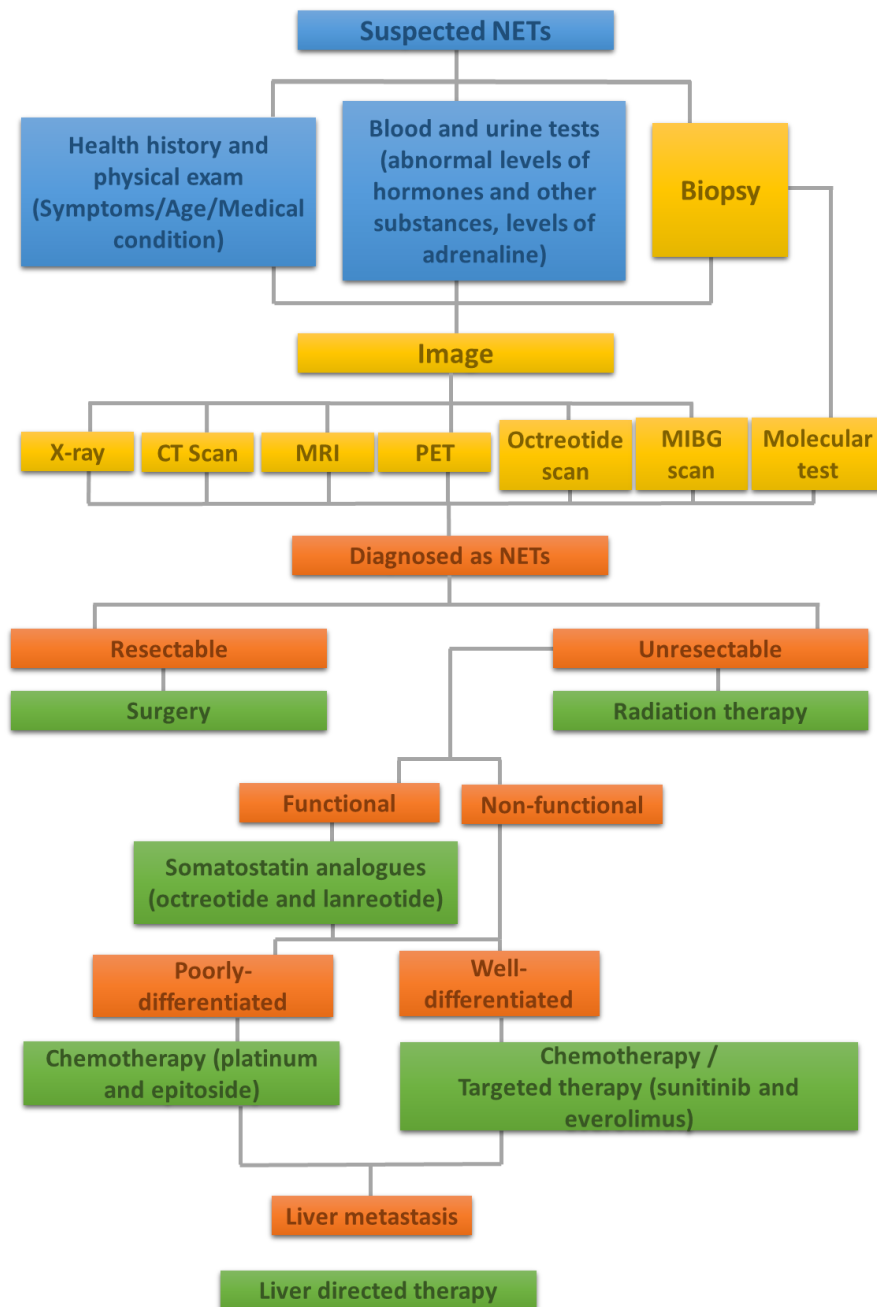


**Figure 2. Treatment algorithms**

Treatment algorithms for neuroendocrine tumors. Blue background indicates general tests. Yellow background indicates defined tests. Orange background indicates the condition of patients. Green background indicates the corresponding treatment options under each condition. The diagram was constructed by the thesis author through office PowerPoint.

Among these diagnostic methods, the general physical exam and fluidic tests merely provide suggestions for the existence of NETs. Conclusions are normally drawn from biopsy and image results, which further provide information on the malignancy property. In addition, circulating biomarkers, *e.g.* chromogranin A (CgA) and serotonin metabolites, which originally are neuroendocrine secretory proteins, are included alone or in concert to monitor neoplasm progress and therapy efficacy [67]. Some other tumor-based biomarkers (Ki-67 and mitotic

count) help to determine the grade of NETs [68–70] (**Table 1**). However, the current grading system, which distributes NETs according to the anatomical locations, causes considerable confusion and controversy. Recently, a grading framework for NETs has been discussed by the International Agency for Research on Cancer (IARC), which allows unification despite the diverse locations, neoplasm biology and prognostic factors [70]. Moreover, the currently applied biomarkers fail diagnostic capacity in sensitivity and specificity. Some novel determinants (*e.g.* gene transcripts and microRNA) represent emerging alternative biomarkers [65,71,72].

**Table 1. Grading system for pancreatic NETs**

WHO Grading System for Pancreatic NETs		
<b>Well differentiated NENs</b>	<b>Ki-67 Index</b>	<b>Mitotic Index</b>
Grade 1	< 3 %	< 2 mit/10 HPF
Grade 2	3-20 %	2-20 mit/10 HPF
Grade 3	>20 %	> 20 mit/10 HPF
<b>Poorly differentiated NENs</b>		
Grade 3	>20 %	> 20 mit/10 HPF
Small cell type		
Large cell type		
<b>Mixed neuroendocrine-non neuroendocrine neoplasm(MiNEN)</b>		
Mit, mitoses; HPF, high power field		

Irrespective of the advancement in diagnosis, the management of NETs remains challenging and the benefits from current treatment are dissatisfactory. Present therapeutic guidelines are confined to surgical and systemic treatment committed to relieve hormone excess (*e.g.* somatostatin analogs (SSAs)) and restrain neoplasm growth (standard chemotherapy, *e.g.* etoposide) [73–76].

### 1.3 Epidermal growth factor receptor

Cumulative cognition regarding the nature of cancer and inclusive identification of networks behind oncogenesis grant the possibility of improving treatment. The epidermal growth factor receptor (EGFR) is one typical representative. Following the discovery of epidermal growth factor (EGF) by Dr. Stanley Cohen [77], EGFR and its role as a tyrosine kinase was firstly described [78–80]. Elegant studies have established that the EGFR, also known as ErbB1 or HER1, together with other three homologues (HER2, HER3 and HER4) composing ErbB family of tyrosine kinase receptors (TRKs), promotes multiple pro-oncogenic biological processes, including cell proliferation, angiogenesis, differentiation and migration [81].

### 1.3.1 Structure and physiological function

EGFR represents a transmembrane glycoprotein comprising one extracellular domain, a short hydrophobic transmembrane domain (TM), a flexible juxtamembrane segment (JM), a tyrosine kinase domain and a C-terminal tail [82,83].

EGFR is synthesized by a gene locating at short arm of chromosome 7. The whole gene covers a span of nearly 200 kb and contains 28 exons [84] (**Figure 3**). There are 4 isoforms of EGFR, namely, isoform 1 (175 kDa), 2 (60 kDa), 3 (80 kDa) and 4 (110 kDa [85], produced by alternative mRNA splicing. Taking the canonic isoform 1 (UniProtKB - P00533-1) as an example, the coding sequence incorporates 3633 nucleotides (nt) including a stop codon “TGA” at the end. Thereby, EGFR precursor harbors 1210 amino acids (aa), which later experiences a cleavage of 24-residue signal peptide to form the mature protein [86]. There are two number system describing EGFR sequence [87]. The system applied in this chapter is according to the nascent protein including 24 amino acids signal peptide.

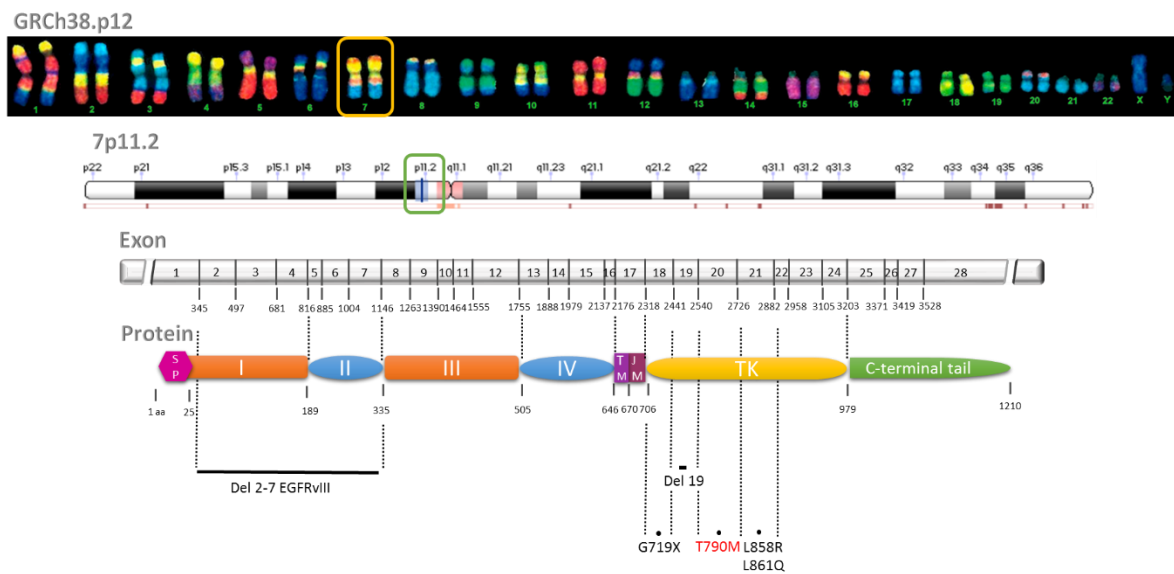


**Figure 3. Sequence and structural model of EGFR**

Sequence and structural model of EGFR. The top figure represents the whole set of human genome and the yellow rounded rectangle emphasizes the chromosome 7. The second top figure indicates the chromosome 7 and the location of *EGFR* gene is shown in green rounded rectangle. The 28 exons of *EGFR* gene are shown in the third figure and the corresponding structural model of EGFR (labelled with amino acid number and common mutations. The black indicates activating mutations while the red indicates resistance mutation) is shown in the bottom figure. The whole diagram was constructed by the thesis author. The set of chromosomes on top was cited from <http://pulpbits.net/5-human-chromosome-structure/human-chromosome-pictures/>. The chromosome 7 was cited from NCBI genome (<https://www.ncbi.nlm.nih.gov/genome>). The rest was constructed by the thesis author through office PowerPoint.

The extracellular domain of the EGFR is composed of 621 aa and contains four subdomains I–IV. Domain I (also known as L1, amino acids 25–189, exons 1–4) and III (also known as L2, amino acids 335–504, exons 8–12) harbor  $\beta$ -helix structures and share 37% protein sequence identity [88]. Leucine-rich domain I and III exclusively participate in ligand binding through simultaneous attachment to the ligand [83,87,89,90]. Although domain II (also known as CR1, amino acids 190–334, exons 5–7) and IV (also known as CR2, amino acids 505–645, exons 13–16) do not directly interact with the ligand, they putatively participate in the formation of an autoinhibitory configuration of the receptor. Domain II has a 20 aa long  $\beta$ -hairpin structure called the dimerization arm that extends out of the center of the domain and connects the analogous domain of the family members. In unbound EGFR, the domain II dimerization arm is completely occluded with domain IV through the intramolecular interaction between a tyrosine residue in domain II and an aspartic acid residue and a lysine residue in domain IV, in addition to which, extensive hydrogen bonds and van der Waals interactions assist to maintain the connections between the two domains. These interactions subsequently pull domains I and III away from each other [91–93] (**Figure 4**). Upon the binding of the ligand to domain I, domain III establishes a tendency to bind to the same ligand. In order to stabilize the arrangement, a conformational alteration occurs that the connection between domains II/IV breaks and rigid body of domain I/II anticlockwise rotates by  $130^\circ$  [91] (**Figure 4**).

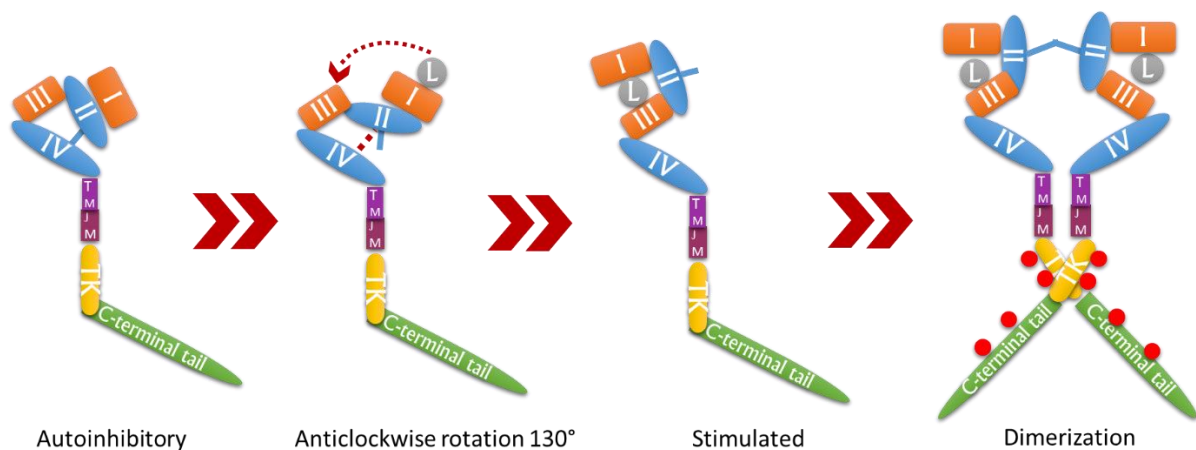


**Figure 4. EGFR extracellular domain transformation**

EGFR extracellular domain transformation. The diagram describes the proposed process of EGFR configuration changing from autoinhibitory status to activated dimerization upon ligand binding. The figure was constructed by the thesis author through office PowerPoint.

The TM domain, as a 23 aa long hydrophobic single pass membrane structure connecting directly to extracellular domain IV and the intracellular flexible juxtamembrane segment (JM), anchors the receptor to the membrane [94].

The intracellular domain is composed of 542 aa comprising JM segment (~40 aa), the tyrosine kinase domain (amino acids 706–978, exons 18–24) and the C-terminal tail (amino acids 979–1210, exons 25–28) [87,90,95]. There are 20 tyrosine residues in the intracellular domain, of which 12 tyrosine residues can be phosphorylated [90]. The tyrosine kinase domain contains an NH<sub>2</sub>-terminal lobe (N-lobe) and a COOH-terminal lobe (C-lobe). The N-lobe is predominantly formed of  $\beta$ -sheets and one  $\alpha$ -helix ( $\alpha$ C), whereas the larger C-lobe is mostly  $\alpha$ -helical. Upon binding to ligands, the homo- or hetero-dimerization of EGFR subsequently lead to the trans-autophosphorylation, which depends on the interaction of the N-lobe of one receptor to the C-lobe of the other [96,97]. The cleft between these two lobes is the ATP-binding site [98], where a large flexible loop lies and is referred to as the activation loop (A-loop). Both  $\alpha$ C helix in N-lobe and A-loop are frequently reoriented during the transition between the active and inactive states. In the active kinase state, the  $\alpha$ C helix rotates inward against the N-lobe and towards the active site. This distortion allows a glutamate residue in  $\alpha$ C helix to get closer to a lysine residue in the  $\beta$ 3-strand (in N-lobe) and build a stable ionic interaction that coordinates the  $\alpha$ - and  $\beta$ -phosphates of ATP. Meanwhile, A-loop reorients away from the cleft to allow peptide substrate binding. The Asp-Phe-Gly (DFG) motif at the beginning of A-loop pointed into ATP-binding site and coordinate the Mg<sup>+2</sup> ion [98–100]. However, phosphorylation of A-loop itself is not necessary for kinase activity [101] of EGFR. Furthermore, the C-terminal tail of EGFR contains 9 tyrosine residues [102,103]. Upon stimulation, the C-terminal tail becomes tyrosine-phosphorylated and recruits a variety of intracellular Src homology-2 (SH2) domain containing effectors [83].

Currently, there are two models describing the mechanism of EGFR. One is ligand-induced dimerization model, which assumes EGFR pre-exists as monomers. The ligand binding drives the dimerization and induces subsequent activation. The other emerging model is the rotation model, which claims the dimerization is pre-formed by the extracellular domain II. The ligand binding promotes its transmembrane domains rotate or twist parallel to the plane of the cell membrane, resulting in the reorientation of the intracellular kinase domain dimer from a symmetric inactive configuration to an asymmetric active form, which subsequently lead to phosphorylation and activation [90].

The EGFR is universally expressed in multiple organs and its activation is essential for development of mammals. The EGFR can be activated by several growth factors including epidermal growth factor (EGF), transforming growth factor- $\alpha$  (TGF- $\alpha$ ), heparin-binding EGF-like growth factor (HBEGF),  $\beta$ -cellulin (BTC), amphiregulin (AREG), epiregulin (EREG), and

epigen (EPGN) [104]. All of these ligands can exist in soluble form. Nevertheless, TGFA, HBEGF, BTC and AREG, are also present as biologically active precursors anchored to the plasma membrane [105]. The physiological function of the EGFR is to regulate epithelial tissue development and modulate proliferation, survival, and differentiation [106].

### 1.3.2 Signaling pathways and role in cancer

The EGFR downstream signaling axis can be further divided into cytoplasmic signaling and nuclear signaling (**Figure 5**).

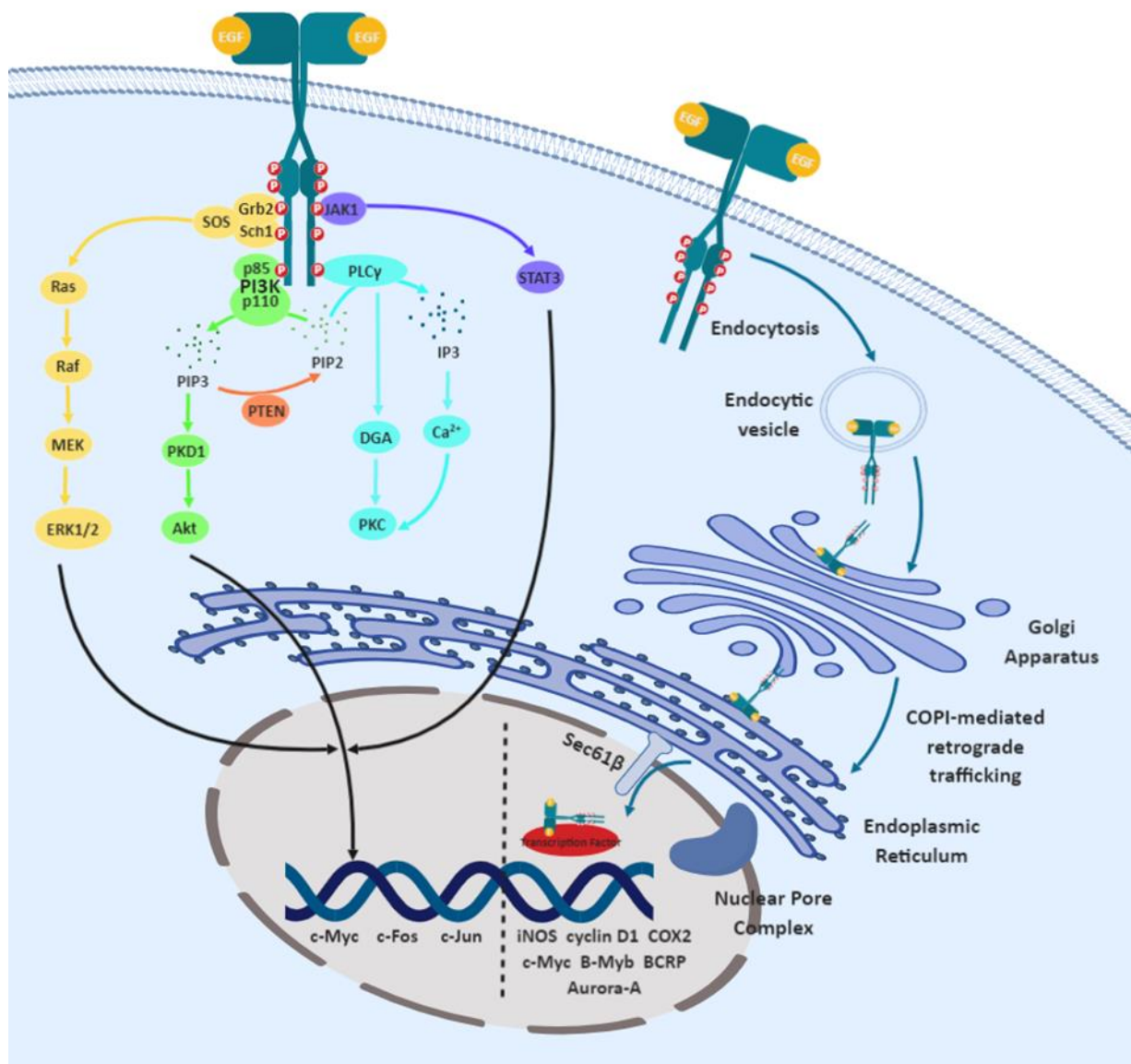


**Figure 5. EGFR downstream signaling**

EGFR downstream signaling. Both cytoplasmic and nuclear signaling pathways are presented. The figure was constructed by the thesis author through the online tool BioRender (<https://biorender.com/>).

The cytoplasmic signaling pathways involve phospholipase- $C\gamma$ / protein kinase C (PLC $\gamma$ /PKC) pathway, mitogen-activated protein kinase (Ras/Raf/MEK/ERK) pathway, phosphatidylinositol 3-kinase/protein kinase B/mammalian target of rapamycin (PI3K/Akt/mTOR) pathway, and Janus kinase/signal transducers and activators of transcription (JAK/STAT) pathway [107,108].

PLC $\gamma$  contains two SH2 motifs and one SH3 motif. The PLC $\gamma$  can be directly phosphorylated by the activated EGFR at the tyrosine residue via interaction between its SH2 domain and the cytoplasmic part of the receptor [109]. Activation of the PLC $\gamma$  leads to the hydrolysis of phosphatidylinositol-4,5-bisphosphate (PIP<sub>2</sub>) to the second messenger inositol 1,4,5-trisphosphate (IP<sub>3</sub>) [110], which thereafter mediates intracellular release of Ca<sup>2+</sup>, and diacylglycerol (DAG). The latter functions as the ligand of protein kinase C (PKC) [111]. The signal transduction cascades modulate cytoskeletal dynamics and immediate post receptor mitogenic pathway and other cellular functions including differentiation and growth [112].

Growth factor receptor-bound protein 2 (Grb2) contains one SH2 motif and two SH3 motifs. Similar to PLC $\gamma$ , Grb2 binds to phosphorylated tyrosine in the activated EGFR via SH2 motif. The N-terminal SH3 motif recruits the son of sevenless (SOS), a guanine nucleotide exchange factor (GEF) for Ras. Ras activation is mediated by the Grb2/SOS complex or Grb2/SOS/Shc triplex in a ligand-dependent manner [113–115], which consequently activates Raf/mitogen-activated protein kinase (MEK)/extracellular-signal-regulated kinase (ERK) (also known as MAP3K/MAP2K/MAPK) signaling cascade. Finally, the ERK translocates to the nucleus and promotes the expression of several transcriptional factors such as c-Myc [116], c-Fos [117] and c-Jun [118], which are implicated in driving DNA synthesis, cell proliferation and other processes [119].

PI3K plays a pivotal role in the regulation of many cellular processes, including cell growth, motility, proliferation, and survival. The EGFR activates class I PI3K by interacting with its p85 subunit which contains SH2 motifs. The activated PI3K catalyzes the phosphorylation of PIP<sub>2</sub> to produce the second messenger PIP<sub>3</sub> [120], which further specifically recruits PH domain containing protein PI3K-dependent serine/threonine kinases (PDK1) and Akt (also known as protein kinase B, PKB) and allows PDK1 to access and partially phosphorylates the Akt at T308 [121]. Partial phosphorylation of Akt is sufficient to activate mTORC1 [122]. The full enzymatic activity of Akt attributes to the additional phosphorylation at S473 by mTORC2 [123] or DNA dependent protein kinase (DNA-PK) [124]. Akt is the major element of the anti-apoptotic effects of the PI3K pathway and can be dephosphorylated by the protein phosphatase

2A (PP2A) [125] and the PH-domain leucine-rich-repeat-containing protein phosphatases (PHLPP1/2) [126]. In addition, the tumor suppressor phosphatase and tensin homolog (PTEN) adversely regulates Akt activity by dephosphorylating PIP3 [127].

Activation of EGFR also phosphorylates signal transducers and activators of transcription (STAT) in a Janus kinase (JAK) dependent [128] or independent way [129] (both proteins contain SH2 domains) and activation of STAT3 gives rise to cell proliferation *in vitro* and tumor growth *in vivo* [130].

These cascades interlink with each other and form a complex network. Both PLC $\gamma$ /PKC and PI3K/Akt pathways are implicated in phospholipid metabolism and consume PIP2 as the substrate [131]. Instead of activating Akt, the PDK1 can phosphorylate PKC in a direct manner [132]. Activation of PKC through PLC $\gamma$  leads to PKC-dependent induction of MAPK [133]. In addition to mediate MAPK signaling, Ras can regulate PI3K [134]. Besides that, inhibition of one pathway can trigger the activation of one another as a compensatory pathway [135].

In addition to the cytoplasmic signaling, EGFR can also internalize and translocate to the nucleus upon stimulation and act as a transcriptional co-activator for seven identified genes: cyclin D1, inducible nitric oxide synthase (iNOS), B-Myb, aurora kinase A (Aurora-A), cyclooxygenase-2 (COX2), c-Myc, and breast cancer resistant protein (BCRP) [136]. Moreover, nuclear EGFR (nEGFR) promotes DNA replication and repair through associating with proliferating cell nuclear antigen (PCNA) [137] and DNA dependent protein kinase (DNA-PK) [138]. Emerging evidences demonstrate that nEGFR mediates resistance to cetuximab [139], gefitinib [140] and radiation therapy [141].

The link between EGFR and cancer was firstly recognized when the transforming v-ErbB oncogene of the avian erythroblastosis virus (AEV) was found to be a mutant homolog of human EGFR. EGFR hyper-activation due to the ligands overload, overexpression or mutations was soon found in most solid neoplasms and considered as a target for cancer therapy since early 90s [142]. The EGFR driven therapeutic strategies, *e.g.* neutralizing monoclonal antibodies (mAbs) and small molecule tyrosine kinase inhibitors (TKIs), have gained enormous success in clinic implication in the past years. EGFR-targeting antibodies can induce antibody-dependent cellular cytotoxicity (ADCC) and complement-mediated cytotoxicity which contributes to their efficacy additionally [143–145]. There are also studies demonstrating these antibodies trigger internalization and thereafter degradation of EGFR, which further downregulate total EGFR level [146]. Alternatively, three generations of tyrosine kinase

inhibitors (TKIs) were brought into market to improve clinic efficacy and overcome *de novo* or secondary resistance due to mutations.

Mutations of EGFR have been intensively studied (**Figure 3**). The most common deletion mutations are EGFRvIII (exon 2-7 deletion) found in glioblastoma and Del 19 (6 amino acids deletion in exon 19) found in pulmonary cancer. EGFRvIII lacks extracellular ligand-binding domain and shows constitutive activation. Point mutations are more frequently found in tyrosine kinase domain (exon 18-21) of pulmonary cancer patients, *e.g.* G719C/S/A (exon 18), T790M (exon 20), L858R (exon 21) and L861Q (exon 21). These mutations can be further divided into activating mutations and resistance mutations according to the drug response. Activating mutations are associated with higher than wild type sensitivity to TKIs, *e.g.* Del 19, G719C/S/A (exon 18), L858R (exon 21) and L861Q (exon 21). Resistance mutations are associated with resistance to TKIs, *e.g.* exon 20 insertion and T790M. There are also some other comparatively sparse mutations found in patients. These mutations alone or in concert lead to different drug responses in clinic [147–149].

In addition to the role as a prominent anti-cancer target, EGFR and its downstream signaling are well considered as an emerging determinant for drug resistance towards several first line chemotherapies and ironizing radiation treatment [139,150,151].

Despite its unambiguous role as an oncogene, the documentation of its clinical relevance is surprisingly heterogeneous [152]. In this case, we were interested to estimate the prevalence of EGFR in diverse cancer types at both mRNA and protein levels and their clinic relevance. The protein expression was subdivided into membranous/cytoplasmic (mcEGFR) and nuclear (nEGFR) expression patterns due to the distinct cellular functions of mcEGFR and nEGFR.

### 1.3.3 EGFR and neuroendocrine neoplasms

The correlation between EGFR and neuroendocrine tumors (NETs) has been investigated by several studies based on gene copy numbers, transcription level, protein expression and activation level. Papouchado *et al.* showed EGFR was highly expressed and activated in gastrointestinal neuroendocrine tumors (GI-NETs) and pancreatic neuroendocrine tumors (PNETs) by immunohistochemistry, Western blotting and RT-PCR [153]. Later on, Shah *et al.* [3] immunohistochemically evaluated EGFR expression and activation on a larger scale in patients diagnosed with NETs originating from foregut, midgut, hindgut, paragangliomas and unknown origins. Besides, the downstream signaling molecules were also investigated in this study. The results were consistent with previous findings and further proved the activation of

Atk and ERK [3]. Moreover, high EGFR aneusomy and elevated *EGFR* gene copy number were found in NETs [1].

Interestingly, the presence of neuroendocrine cells in gastric adenocarcinomas showed significant correlation to EGFR expression [154]. Similarly, pulmonary neuroendocrine cell hyperplasia exhibited a maximum EGFR expression [155].

In a practical sense, some TKIs targeting at EGFR have been implicated in clinical trials to treat patients harboring NETs [156]. Among these TKIs, a multi-target receptor tyrosine kinases (RTKs) inhibitor, sunitinib malate, has been approved by the regulatory agencies (European Medicine Agency, EMA and United States Food and Drug Administration, FDA) in unresectable and progressing differentiated (grade 1 or grade 2) PNETs [157].

These findings indicate the rationale for considering EGFR inhibitors as a potential therapeutic approach in the NETs treatment. However, cumulative research results raise the concern on efficacy of these TKIs. Development of phenotypic neuroendocrine transformation from adenocarcinoma to large cell neuroendocrine cancer (LCNEC) and occurrence of resistance mutations impede the patients response to the EGFR-TKIs [12,12,158]. Besides, EGFR activating mutations were less frequently found in GEP-NET and LCNEC patients [10,11].

Briefly, EGFR inhibition provides new possibility in NETs treatment. However, novel mechanisms rather than interfering with EGFR tyrosine kinase domain should be investigated.

## **1.4 Artesunate**

Artesunate (ART), an artemisinin-like compound, was initially designed to treat severe malaria [159,160]. This was a breakthrough in malaria research, since it was able to combat otherwise drug-resistant plasmodium. Due to its potent effect, it has been listed on the World Health Organization's List of Essential Medicines and made available in the US under the investigational new drug protocol [161,162]. It turned out that artemisinin-type drugs including artesunate are not only active against malaria, but also against other infectious diseases (*e.g.* viruses, schistosomiasis and trypanosomiasis) and cancer [163–165].

### **1.4.1 Structure and utility**

Artesunate represents a water-soluble, semi-synthetic derivative of the sesquiterpene lactone artemisinin, which is isolated from the plant *Artemisia annua* L. The molecule is characterized

by a fused ring system containing a six-membered ring C which includes an oxygen bridge and a peroxy-bridge [166] (**Figure 6**).

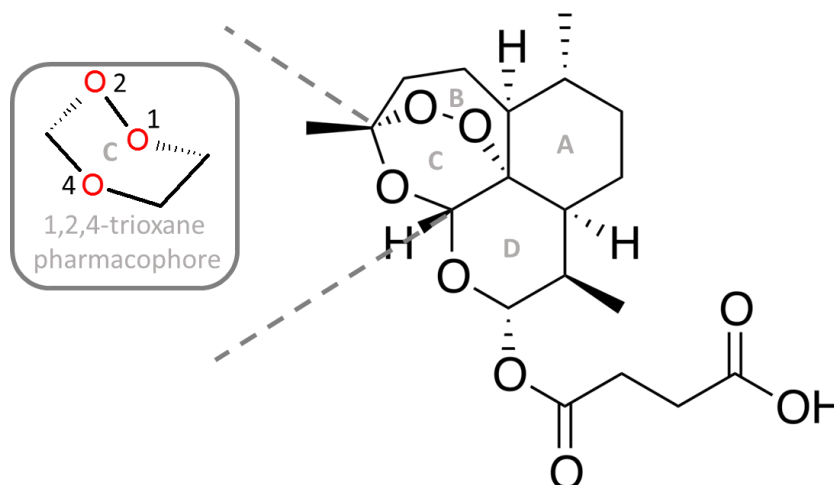


**Figure 6. Structure of Artesunate**

Structure of artesunate. Artesunate contains the pharmacophore trioxolane structure (a ring containing three oxygen atoms). The pharmacophore was constructed by the thesis author through ChemSketch. The structure was cited from Wikipedia (<https://en.wikipedia.org/wiki/Artesunate>).

From a pharmacological point of view, ART is specifically applied for the treatment of severe malaria caused by *plasmodium falciparum* in adults and children, which shows resistance to quinidine treatment [167]. ART inhibits the asexual erythrocytic stage of the malaria parasites [168], blocks transmission of gametocytes [169] and increases the splenic clearance of infected erythrocytes by reducing cytoadherence [170] (**Figure 7**). In clinic, ART is often administered by an intravenously (IV) or intramuscularly (IM) at a dose of 2.4 mg/kg body weight (bw), then is injected twice in 12h and 24h followed by once per day injection until the patient is able to take oral medication [171]. According to the pharmacokinetic studies, the parent drug artesunate is rapidly converted to dihydroartemisinin (DHA) by plasma esterases *in vivo* after either oral or IV administration. The IV administration surpasses oral therapy in bioavailability if comparing their intravenous concentration peaks. Expectedly, the half-life of the active metabolite DHA is much longer than the parent drug ART [172]. DHA is afterwards glucuronidated to the  $\alpha$ -dihydroartemisinin- $\beta$ -glucuronide ( $\alpha$ -DHA-G) through two UDP-glucuronosyltransferases UGT1A9 and UGT2B7 in the liver and excreted through urine. Partial  $\alpha$ -DHA-G can be non-enzymically isomerized in the presence of iron in urine [173].

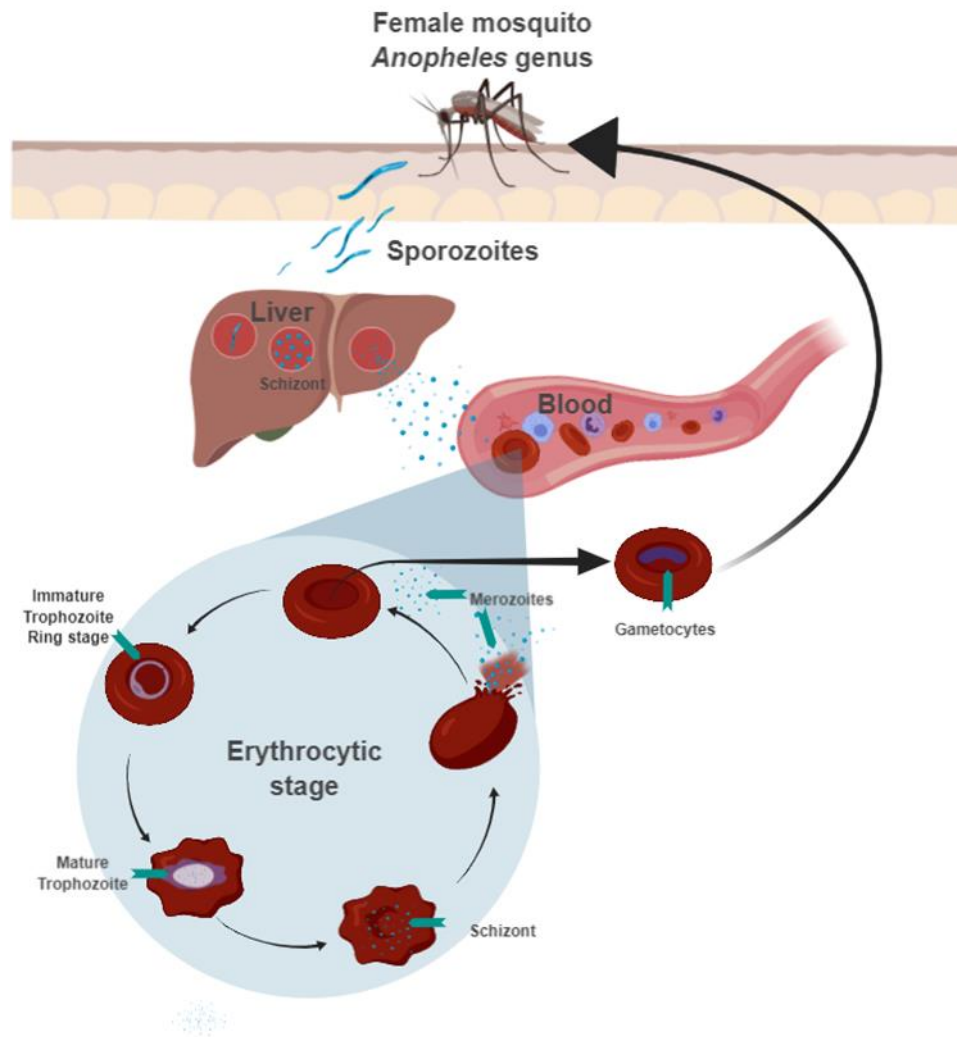


**Figure 7. Plasmodium life cycle**

Plasmodium life cycle. The infected female mosquitoes transmit Plasmodium as sporozoites to human. The sporozoites invade liver tissue dividing into merozoites, which can be released into blood vessels. Infection of erythrocytic cells initiates the disease specific symptoms. The merozoites are able to develop into gametocytes and taken up by non-infected mosquitoes to rapidly spread the infection span. The whole diagram was constructed by the thesis author through the online tool BioRender (<https://biorender.com/>).

The ART has shown robust effects beyond anti-malaria activity. It inhibits a broad range of viruses (*e.g.* cytomegalovirus, CMA; herpes simplex virus type 1, HSV-1; Epstein-Barr virus and hepatitis B virus) [161,163] and parasites other than Plasmodium (*e.g.* Schistosoma, Fasciola hepatica and Trypanosoma) [164,174,175]. ART also shows potent anti-inflammatory, anti-allergic and immune suppressive activity [176]. Moreover, applying alone or in combination with other standard chemotherapies, ART surprisingly suppressed the growth of diverse tumors [20,24,177].

In fact, there have been 214 clinical trials regarding ART (24 phase I studies, 3 phase I/II studies, 26 phase II studies, 9 phase II/III studies, 50 phase III studies, 53 phase IV studies and 49

unclear studies) recorded in the U.S. National Library of Medicine database (<https://clinicaltrials.gov/ct2/home>) purposing the treatments for malaria, schistosoma, CMA, lupus nephritis and multiple cancers.

#### 1.4.2 Molecular mechanisms

In the asexual erythrocytic stage of plasmodium life cycle (**Figure 7**), parasites invade the erythrocytes and thereafter develop into ring forms, mature trophozoites, and multinucleated schizonts, respectively, which finally rupture the erythrocytes and release more merozoites. This repeated cycle physically caused chill, fever, headache, fatigue and other nonspecific symptoms. Hemoglobin (Hb) is one iron-containing oxygen-transport metalloprotein in the erythrocytes, which carries oxygen from the lung to other body tissues. The host Hb is enzymatically processed in the food vacuole of the parasites to form heme and peptides required for its own development. The metabolism of heme is utilized by many therapeutic approaches. Heme is transiently converted in parasites into hematin, which is toxic, and eventually become the non-toxic hemozoin through biomineralization. The predominantly acknowledged action of artemisinin-based drugs including ART is heme-mediated alkylation activity (also known as heme activation theory), which involves the formation of free radicals via the cleavage of the endoperoxide bond present in its structure through the reaction with heme and the consequently generated free radicals alkylate parasitic proteins. In this scenario, the selectivity and activity of artemisinin-based drugs can be rationalised by the iron mediated cleavage of the endoperoxide bridge [178,179]. Interestingly, among all the iron-containing proteins, heme is considered as the preferable activator [180]. The generated free radicals following cleavage of endoperoxide bridge damage the lipid membranes of parasites, alkylate and inactivate plasmodium proteins [181] and interfere with detoxification of hematin via inhibition of a glutathione S-transferase found on the membrane of plasmodium, namely EXP1 [182] and finally lead to parasites death. However, the fact that artemisinin localizes to the parasite membrane but not food vacuole membrane [183] and eliminates tiny rings lacking haemozoin at the early ring stage [184] argue against the heme activation theory. Alternatively, interference with the sarco/endoplasmic calcium ATPase (SERCA) and depolarize mitochondrial membranes are believed to be implicated in the actions of artemisinin-based drugs [185].

Like all medications, ART can non-specifically bind to plasma proteins *e.g.* human serum albumin, lipoprotein, glycoprotein and globulins. Based on the structural similarity of ART and thapsigargin, which is a known selective SERCA inhibitor, PfATP6 (also known as plasmodium SERCA) is assumed to be a potential binding target for ART and other

artemisinins. It is hypothesized that structurally similar compounds may act in a similar way. PfATP6 is the only SERCA-type enzyme present in the malarial parasite and it is considered to be the suitable molecular target for artemisinins. An *in vitro* study suggested that artemisinins inhibit the PfATP6 activity of *P. falciparum* in *Xenopus* oocytes [186]. By contrast, Arnou and Cardi *et al* [187,188] demonstrated there was no inhibition of artemisinins against PfATP6. Lisewski *et al.* [182] has suggested another target EXP1 in the parasite *P. falciparum* based on the supergenomic network compression prediction. The study revealed EXP1 is able to catalyze the conjugation of reduced glutathione (GSH) and heme/hemetin and subsequently degrade hemetin. This process is dramatically blocked in the presence of ART. However, in the same study, it demonstrated that the inhibition against the capacity of EXP1 conjugating GSH and 1-chloro-2, 4-dinitrobenzene (CDNB, a common substrate for GSTs) was 100-fold less potent than the inhibition against the capacity of EXP1 conjugating GSH and hematin, which indicated ART inhibited EXP1 by affecting its substrate hematin instead of inhibiting EXP1 itself. Wang *et al.* [189] identified 124 covalent protein targets of artesiminin by including alkyne-tagged artemisinin analogue (AP1). However, the covalent bond was only observed at the presence of hemin detected by *in vitro* binding assay, which further indicated ART itself was not able to bind to these proteins. No convinced specific biological target of ART has yet been identified. However, Kasaragod *et al.* recently revealed the first binding crystal structure of artesunate and gephyrin, which is implicated in neurotransmission regulation [190] and was previously reported to play a role in rapamycin-sensitive signaling [191].

The anti-inflammatory, anti-allergic, immune suppressive and anti-tumor activity of ART can be attributed to its effect on a complex of signaling pathways and the regulation of a considerable number of relevant molecules, which involves the negative regulation of specificity protein 1 (Sp1), nuclear factor kappa B (NF- $\kappa$ B), toll-like receptors (TLRs), spleen tyrosine kinase (Syk), PLC $\gamma$ , PI3K/Akt, MAPK and STAT-1/3/5 [192] and the activation of nuclear factor (erythroid-derived 2)-like/ antioxidant response element 2 (Nrf2/ARE2). These regulations subsequently suppress numerous cytokines like tumor necrosis factor  $\alpha$  (TNF- $\alpha$ ), interferon gamma (IFN- $\gamma$ ) and interleukins (IL-1 $\beta$ , IL-2, IL-6, IL-8, IL-17 $\alpha$  and IL-33) and downregulate pro-oxidants via inhibition of NADPH oxidases (NOXs) and inducible nitric oxide synthase (iNOS)[193–196].

Multiple mechanisms of ART incorporating induction of oxidative stress, anti-angiogenesis, oxidative DNA damage, cell cycle arrest, immunomodulatory impact and neoplasm-related signal transduction inhibition, finally converge on neoplastic cell death [24].

---

Obviously, ART affects cascades which are commonly stimulated by EGFR activation. In fact, several studies have shown the inhibitory potential of ART on EGFR [14,197] and its interference with its downstream signaling [198]. In addition, the combination of ART with EGFR selective TKI erlotinib demonstrated a synergetic inhibition of cell growth [20]. Some *in silico* studies also proved the possibility of ART co-localization with EGFR [199]. All the cumulative evidences encouraged us to investigate the effect of ART on EGFR signaling.

## 2 Aim

The aim of the study was exploring alternative treatments for a rare cancer types such as neuroendocrine tumors (NETs). The abundant expression of epidermal growth factor receptor (EGFR) in NETs has been previously demonstrated. Therefore, the well-known oncogene encoding protein EGFR can possibly be a potent therapeutic target for NETs. However, the emerging drug resistance of EGFR-targeted therapy weakens our faith in the practical value of anti-EGFR antibodies and specific EGFR tyrosine kinase inhibitors. It has been well-established that artesunate (ART) showed favorable potential in inhibiting EGFR expression and its downstream signal. Moreover, as a potent therapeutic agent to treat severe malaria, ART develops drug resistance in a dramatically slow manner, which may attributed to its multiple-mechanism property. Obviously, ART has exhibited a broad range of bioactivity. In this case, we are specifically interested in investigating the therapeutic value of ART in the treatment of NETs by utilizing three EGFR-expressing NET cell lines (BON-1, QGP-1 and NCI-H727, the latter two cell lines also showed EGFR aneusomy and elevated *EGFR* gene copy number) [4–6].

To address this issue, we focused on two aspects. The first aspect was to survey the extended value of EGFR in solid tumors including but not limited to lung cancer. We evaluated the prognostic value of *EGFR* mRNA level *in silico*, the protein expression pattern and the prognostic capacity of EGFR in 27 cancer types *in house*. The second aspect was to investigate the potential of ART in NETs by using three neuroendocrine tumor cell lines (BON-1, QGP-1 and NCI-H727). The concrete mechanisms were further explored by taking advantage of mature biological methods. Our results supported the possible utilization of ART in NETs treatment.

### 3 Results

#### 3.1 EGFR and cancer

Although a large and growing body of literature has investigated EGFR, its prognostic role in research is surprisingly controversial and confusing [200]. Besides, much of the current literature regarding EGFR particularly focuses on lung cancer despite its vital role in the development of broad neoplasms. Therefore, we were interested to broaden the application span of EGFR and assess its prognostic value in multiple cancer types.

In order to have an overview of EGFR expression in the neoplasms landscape and further study the association between clinic outcomes and its expression patterns, which are categorized into transcription level, membranous/cytoplasmic expression (mcEGFR) and nuclear translocation (nEGFR), we correlated *EGFR* mRNA level to pathological parameters by analyzing 30 datasets *in silico*, immunohistochemically stained 502 biopsies from 27 tumor types and afterwards statistically assessed the data.

##### 3.1.1 Correlation of EGFR mRNA expression and clinic outcomes

Thirty datasets were screened with filters in the Oncomine database. The filter flow is shown in **Figure 8**. Among 30 datasets (**Table 2-4**), 23 datasets (=76.7%) did not show any significant association between *EGFR* mRNA level and clinical outcome or pathological characteristics of patients. Datasets GSE22226 and GSE10846 showed significant associations between high *EGFR* mRNA expression levels and poor overall survival (cutoff mean,  $p=0.03$ ; cutoff mean,  $p=0.03$ ; respectively) (**Table 2**). However, adverse effects were indicated from datasets GSE4412 and GSE15081 with statistical significance (cutoff median = mean,  $p=0.02$ ; cutoff median, probe AGhsB031519,  $p=0.04$ ).

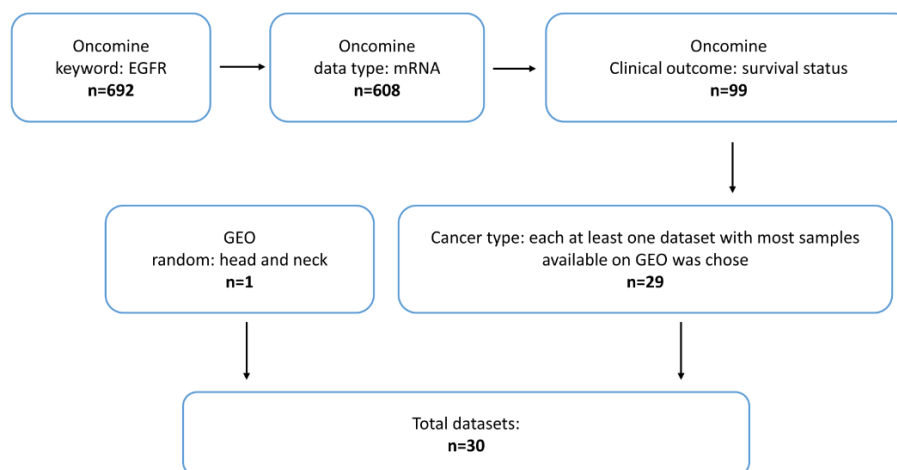


**Figure 8. Filter flow for datasets screen**

Filter flow for datasets screen. In total 30 quantified datasets were collected through stepwise filters (EGFR, mRNA, survival status, sample number). The figure was constructed by the thesis author through office PowerPoint.

Regarding tumor grade, datasets GSE5206 and GSE3538 showed a significant correlation between high *EGFR* mRNA expression and poor differentiation (cutoff median,  $p=0.03$ ; cutoff median = mean,  $p=0.02$ ; respectively) (Table 3). Conversely, dataset GSE4412 indicated a conflicting trend (cutoff median = mean,  $p=0.02$ ). In addition, dataset GSE15081 conveyed a trend for association of *EGFR* mRNA with N stage, GSE9899 with grade (Table 3-4).

**Table 2. Correlation of *EGFR* mRNA expression and overall survival**

Cancer Type	GEO Accession	Jetset Probe	OS (p value)	
			Median	Mean
Bladder	GSE13507	ILMN_1696521	0.47	0.25
Brain	GSE7696	211607_x_at	0.12	0.28
	GSE4271	211607_x_at	0.19	0.19
	GSE4412	211607_x_at	0.02*	0.02*
Breast	GSE22226	A_23_P215790	0.07	0.03*
	GSE20685	211607_x_at	0.72	0.54
Colorectal	GSE17536	211607_x_at	0.01	0.01
Gastric	GSE15081	AGhsA201212	0.52	0.32
		AGhsB031519	0.04*	0.11
Head-Neck	GSE2379	1537_at	0.07	0.27
	GSE65858	ILMN_1696521	0.88	0.28
Leukemia	GSE12417	211607_x_at	0.17	0.14
Liver	GSE10186	DAP2_6059	0.12	0.08
	GSE364	NM_005228	0.33	0.28
Lung	GSE19188	211607_x_at	0.93	0.46
	GSE31210	211607_x_at	0.64	0.96
	GSE5123	X00588	0.50	0.61
Lymphoma	GSE4573	211607_x_at	0.22	0.27
	GSE4475	211607_x_at	0.53	0.76
	GSE10846	211607_x_at	0.08	0.03*
Melanoma	GSE8401	211607_x_at	0.64	0.47
	GSE2658	211607_x_at	0.59	0.52
	GSE19234	211607_x_at	0.97	0.60
Ovarian	GSE26712	211607_x_at	0.65	0.65
	GSE9899	211607_x_at	0.68	0.84
Pancreas	GSE14764	211607_x_at	0.93	0.66
	GSE17891	211607_x_at	0.95	0.89
Prostate	GSE6919	1537_at	0.67	0.67
	GSE10645	GI_29725608-S	0.43	0.51
Renal	GSE3538	AA234715	0.59	0.26

W48712	0.20	0.20
H80438	0.94	0.99

*P* value < 0.05 was labelled with asterisk mark. OS, overall survival. Median, group *EGFR* mRNA expression as “high” and “low” by median. Mean, group *EGFR* mRNA expression as “high” and “low” by mean.

**Table 3. Correlation of *EGFR* mRNA expression and grade**

Cancer Type	GEO Accession	Jetset Probe	Grade ( <i>p</i> value)	
			Median	Mean
Bladder	GSE13507	ILMN_1696521	0.86	0.81
Brain	GSE4271	211607_x_at	0.35	0.35
	GSE4412	211607_x_at	0.02*	0.02*
Breast	GSE22226	A_23_P215790	0.06	0.05
Colorectal	GSE17536	211607_x_at	0.06	0.10
	GSE5206	211607_x_at	0.03*	0.08
Gastric	GSE15081	AGhsA201212	0.08	0.17
		AGhsB031519	0.64	0.23
Head-Neck	GSE2379	1537_at	0.54	0.63
Liver	GSE364	NM_005228	0.19	0.16
Lung	GSE5123	X00588	0.38	0.08
	GSE4573	211607_x_at	0.46	0.42
Ovarian	GSE9899	211607_x_at	0.05	0.02*
	GSE14764	211607_x_at	0.83	0.85
Pancreas	GSE17891	211607_x_at	0.37	0.85
Renal	GSE3538	AA234715	0.36	0.28
		W48712	0.02*	0.02*
		H80438	0.34	0.36

*P* value < 0.05 was labelled with asterisk mark. Median, group *EGFR* mRNA expression as “high” and “low” by median. Mean, group *EGFR* mRNA expression as “high” and “low” by mean.

**Table 4. Correlation of *EGFR* mRNA expression and TNM stage**

Cancer Type	GEO Accession	Jetset Probe	T ( <i>p</i> value)		N ( <i>p</i> value)		M ( <i>p</i> value)	
			Median	Mean	Median	Mean	Median	Mean
Bladder	GSE13507	ILMN_1696521	0.56	0.47	0.08	0.31	0.66	0.53
Breast	GSE22226	A_23_P215790	0.29	0.26				
	GSE20685	211607_x_at	0.92	0.98	0.59	0.60	0.48	0.14
Colorectal	GSE5206	211607_x_at	0.63	0.78	0.68	0.59	0.73	0.62
Gastric	GSE15081	AGhsA201212			0.02*	0.10		
		AGhsB031519			0.35	0.97		
Head-Neck	GSE2379	1537_at	0.25	0.24	0.55	0.48		
	GSE65858	ILMN_1696521	0.26	0.11	0.13	0.09	0.25	0.09
Liver	GSE364	NM_005228					0.46	0.73
Lung	GSE5123	X00588			0.63	0.65	0.23	0.12
	GSE4573	211607_x_at	0.56	0.45	0.60	0.38		
Melanoma	GSE8401	211607_x_at	0.32	0.25	0.38	0.73	0.12	0.08
Pancreas	GSE17891	211607_x_at	0.97	0.46	0.87	0.42		
Prostate	GSE6919	1537_at	0.32	0.32	0.61	0.61		
	GSE10645	GI_29725608-S	0.34	0.28	0.84	0.51		

*P* value < 0.05 was labelled with asterisk mark. T, N and M represented T stage, N stage and M stage, respectively. Median, group *EGFR* mRNA expression as “high” and “low” by median. Mean, group *EGFR* mRNA expression as “high” and “low” by mean.

*EGFR* at the mRNA level failed to correlate with the survival times of patients by Kaplan-Meier curve analysis. In addition, few clinic parameters including TNM stage and grade were correlated with *EGFR* mRNA level. However, the irrelevance between *EGFR* transcription level and clinical outcomes should be interpreted with caution. The mRNA level alone lacks necessary information on the post-translational epigenetic regulation and mutation status, which can dramatically affect the ultimate effect of *EGFR*. Undeniably, *EGFR* gained its reputation regarding therapy development and personalized drug design in clinic practice. The prognostic weakness of *EGFR* mRNA drove us to assess, whether or not *EGFR* protein expression is of

prognostic value. We evaluated 30 studies with certain screen filters described in materials and methods, among which 18 studies revealed the correlation between EGFR protein expression and clinic outcomes or pathological parameters.

### 3.1.2 Prevalence of EGFR protein expression in diverse cancer types

To address this question, we investigated EGFR protein expression by immunochemical staining. Moreover, we looked into the expression patterns as membranous/cytoplasmic expression (mcEGFR) and nuclear translocation (nEGFR) (**Figure 9**).

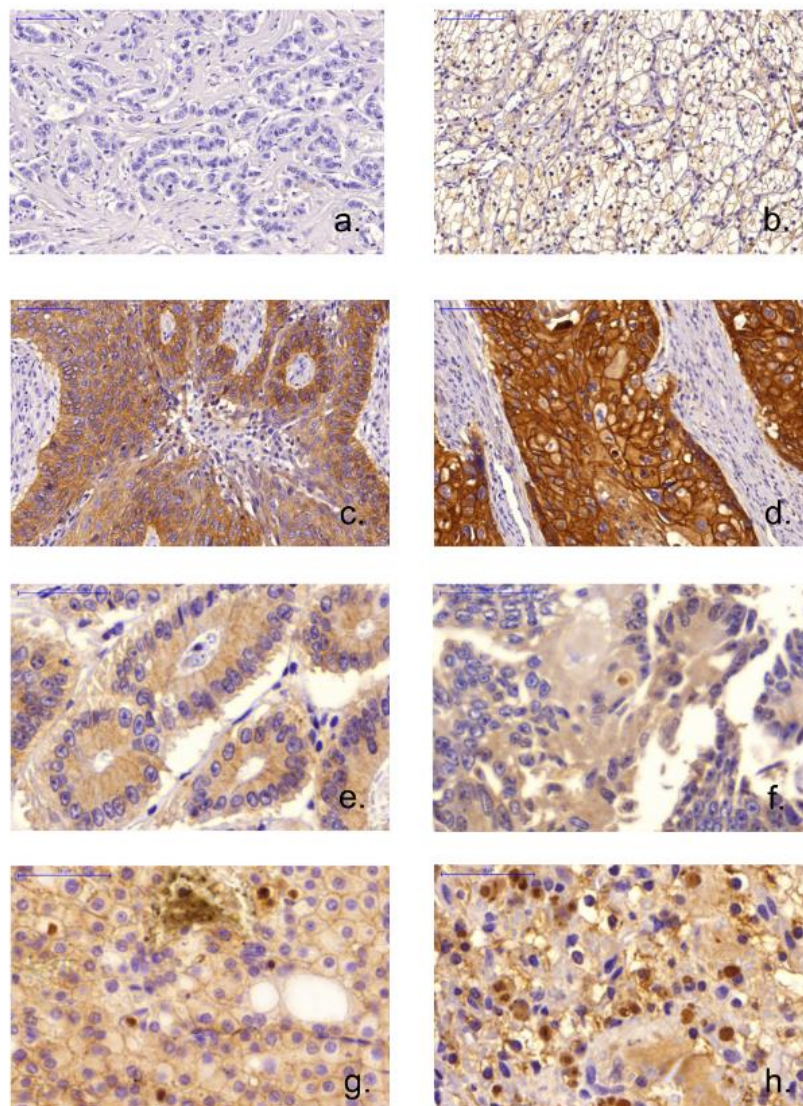


**Figure 9. Immunohistochemical staining of mcEGFR and nEGFR**

(a), Negative mcEGFR, breast tumor, 20×magnification; (b), Weak mcEGFR, kidney tumor, 20×magnification; (c), Moderate mcEGFR, lung tumor, 20×magnification; (d), Strong mcEGFR, esophagus tumor, 20×magnification; (e), Negative nEGFR, colon tumor, 40×magnification; (f), Weak nEGFR, colon tumor, 40×magnification; (g), Moderate nEGFR, kidney tumor, 40×magnification; (h), Strong nEGFR, kidney tumor, 40×magnification (The photos were obtained through Panoramic Desk scanner and arranged by the thesis author through office PowerPoint.)

We identified the distribution of mcEGFR and nEGFR expression in different tumor types (**Figure 10**). As shown in **Figure 10a**, mcEGFR was highly expressed in brain tumors followed by lung tumors. Compared to lung tumors, the expression in brain tumors tend to be more intensive if the whisker range is put into consideration. Uterus, colorectal and kidney tumors expressed mcEGFR in a similar manner. Breast, ovary, pancreas and prostate tumors revealed comparatively low expression levels. Noticeably, there were a few cases of breast tumors with strong mcEGFR expression, which exceeded the whisker range. Tumor types comprising less than 5 cases were classified as “others” (**Figure 10b**), among which fallopian tube tumor ranked top while parotid and testis ranked the lowest. However, the results could not provide accurate information due to the limited available cases. In the case of nEGFR, brain tumors were excluded from analysis due to the difficulty in determining nEGFR in this tumor entity. By contrast, nEGFR was frequently found in lung tumors followed by kidney, colorectum, pancreas, ovary and uterus, respectively (**Figure 10c**). In addition, stomach tumors also expressed high nEGFR (**Figure 10d**). However, nEGFR expression in breast and prostate was comparatively rare.

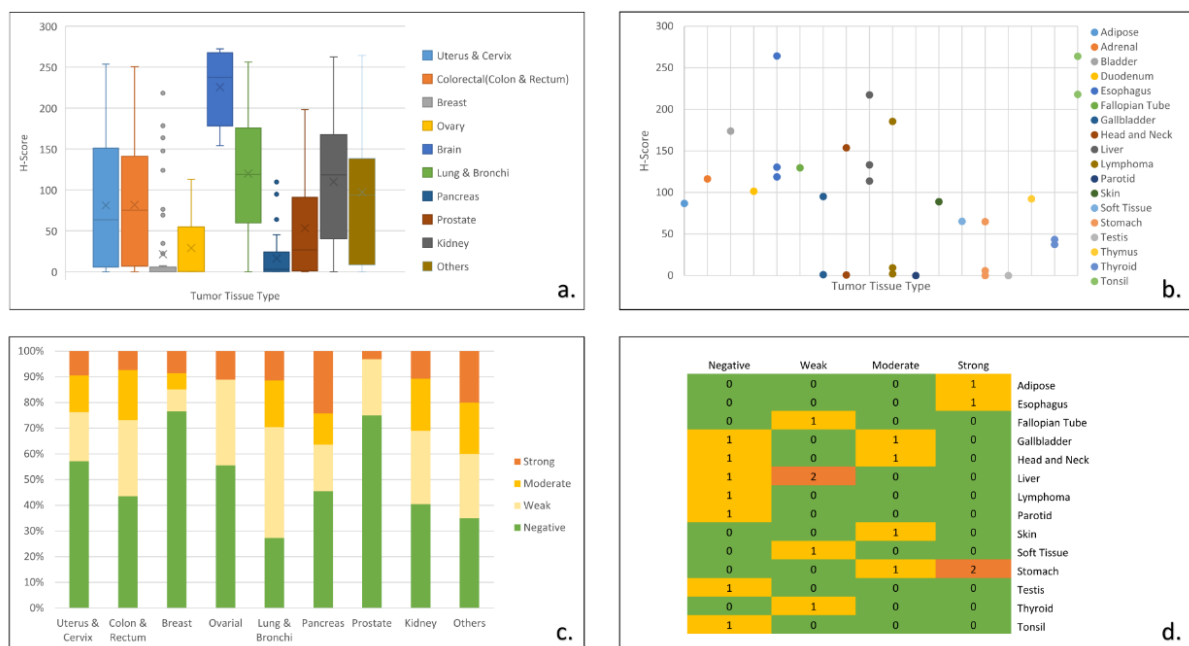


**Figure 10. Distribution of EGFR in different tumor tissue type**

(a), H-score, as indicator of mcEGFR expression, distribution in different tumor types. All the tumor types comprising less than 5 cases were grouped as “others”. Tissue types were color coded as shown in legend.(b), H-score distribution among “others”. In this figure, cases of each tumor type were less than 5. Plot was drawn according to H-score and tumor types. Tissue types were color coded as shown in legend.(c), Distribution of nEGFR among different tumor types. nEGFR levels were classified as “Negative”, “Weak”, “Moderate” and “Strong” and each level was coded with green, light yellow, yellow and orange respectively.(d), nEGFR expression among tumor types with less than 5 cases. Heat map was drawn according to nEGFR level and tissue type. 3-Color scale indicated frequency of nEGFR expression where green showed 0 case, yellow showed 1 case while orange showed 2 cases.Detailed information about “others” refers to **Supplementary Table S2**. The figure was constructed by the thesis author through office Excel.

To explore the relationship between mcEGFR and nEGFR, we performed independent t-tests with negative or positive expression of nEGFR as grouping variable. Furthermore, we categorized the H-score into four levels. H-score values below 20 were grouped as negative; H-scores ranging from 20 to 115 as weakly positive, from 115 to 210 as moderate positive and above 210 as strongly positive. The later three groups were all considered as positive. Pearson's  $\chi^2$ -test was applied to assess the independence between H-score levels and nEGFR levels (**Table 5**). The result provided a compelling argument that mcEGFR and nEGFR are dependent factors ( $p < 0.001$ ). Besides, there was a significant difference of H-score mean value between negative nEGFR and positive nEGFR groups ( $p < 0.001$ ) which indicated cases harboring negative nEGFR also showed lower mcEGFR expression compared to positive nEGFR cases.

**Table 5. Correlation between mcEGFR and nEGFR**

		mcEGFR No. patients (% within H-score)						
		Independent t-test		Pearson's $\chi^2$ -test				
		Mean	P Value	Negative	Weak	Moderate	Strong	P Value
nEGFR	Negative	37.416		Negative 115(70.12)	54(46.55)	21(21.43)	2(10.00)	
	Positive	101.528	8.44E-11*	Weak 23(14.02)	35(30.17)	40(40.82)	6(30.00)	
				Moderate 12(7.32)	18(15.52)	22(22.45)	8(40.00)	
				Strong 14(8.54)	9(7.76)	15(15.31)	4(20.00)	2.85E-13*

*P* value < 0.05 was labelled with asterisk mark.

### 3.1.3 Correlation of EGFR protein expression and clinic outcomes

To further explore the correlation of EGFR protein expression and pathological characteristics, we firstly run ANOVA mean comparison test for mcEGFR H-score within different TNM stages and grades. Then, we used Pearson's  $\chi^2$ -test to determine the independence of H-score as negative and positive groups with TNM stages and grades, respectively.

Unexpectedly, there was an adverse association between mcEGFR and T stage as mean comparison (**Figure 11**,  $p < 0.001$ ). In addition, H-score and T stage were dependent in an adverse manner as well ( $p < 0.001$ ). Moreover, positive mcEGFR was associated with low grade ( $p = 0.027$ ) in Pearson's  $\chi^2$ -test. The same trend was also found in one-way ANOVA mean comparison test but without significance ( $p = 0.233$ ). However, no significant difference was found among any other pathological parameters. Neither were any dependent relationships in between these parameters (**Table 6**). Interestingly, nEGFR revealed consistent results that its expression and T stage was adversely dependent ( $p = 0.004$ ) by Pearson's  $\chi^2$ -test (**Table 6**).

The most striking indication from the results was that EGFR expressed more intensive in the nascent stage than advanced stage during carcinogenesis. Coincidentally, several studies have also found that positive EGFR [201,202] or activation of EGFR [203] was correlated with well differentiation and better clinic outcomes [204]. Our findings may as well partially explain the development of resistance against EGFR-targeted therapy during the treatment in a way that advancement of neoplasm is accompanied with the reduction of EGFR expression.

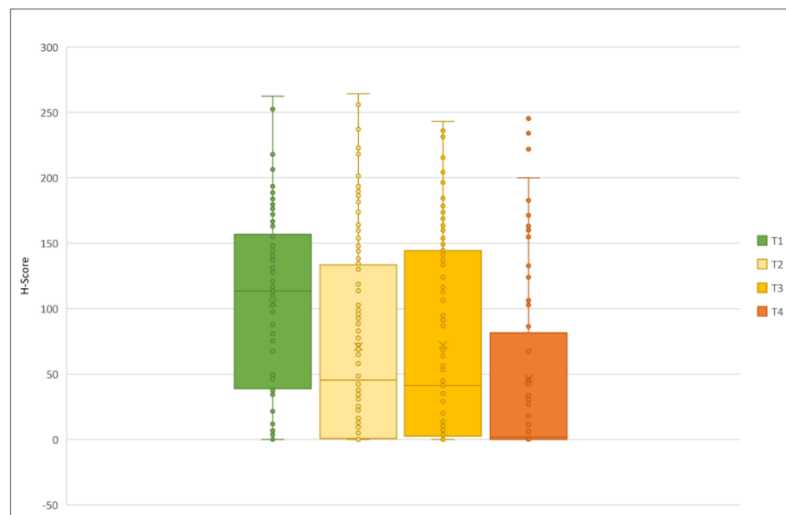


**Figure 11. Correlation between H-score and T stage**

Correlation between H-score and T stage illustrated by box plot. Tissues were classified by T stages (Green, T1 stage; light yellow, T2 stage; yellow, T3 stage; orange, T4 stage). The Y-axis indicates H-scores. The figure was constructed by the thesis author through office Excel.

**Table 6. Correlation of EGFR protein expression and pathological characteristics**

		mcEGFR No. patients (% within pathological parameters)				nEGFR No. patients (% within pathological parameters)			
		One way ANOVA /independent t-test		Pearson's $\chi^2$ -test		Pearson's $\chi^2$ -test			
		Mean	P value	Negative	Positive	P Value	Negative	Positive	P value
T Stage	T1	104.460		14(15.7)	75(84.3)		26(39.4)	40(60.6)	
	T2	70.918		55(41.7)	77(58.3)		58(54.2)	49(45.8)	
	T3	72.144		46(40.0)	69(60.0)		40(40.4)	59(59.6)	
	T4	46.390	3.18E-05*	37(61.7)	23(38.3)	2.19E-07*	32(68.1)	15(31.9)	0.004*
N Stage	N0	63.121		100(47.2)	112(52.8)		93(55.4)	75(44.6)	
	N1	67.407		36(46.8)	41(53.2)		31(44.3)	39(55.7)	
	N2	73.402	0.812	5(29.4)	12(70.6)	0.365	7(63.6)	4(36.4)	0.224
M Stage	M0	72.587		133(39.9)	200(60.1)		134(50.2)	133(49.8)	
	M1	62.534	0.606	11(44.0)	14(56.0)	0.690	10(50.0)	10(50.0)	0.987
Grade	Low	81.664		76(32.3)	159(67.7)		95(50.8)	92(49.2)	
	High	70.133	0.233	64(43.5)	83(56.5)	0.027*	50(42.4)	68(57.6)	0.151

P value < 0.05 was labelled with asterisk mark. G0 and N3 cases were excluded for analysis. Well differentiated to moderate differentiated cases were grouped as low grade while moderate-to-poorly differentiated to poorly differentiated cases were grouped as high grade.

### 3.1.4 Brief summary

The results in this chapter further prove that application of EGFR-targeted therapy should not be confined. Inhibition of EGFR and its downstream signaling strategy may be implicated in the treatment of multiple solid neoplasms. Besides that, we firstly demonstrated that EGFR

therapy should be given to the patients characterized with overexpression or hyper-activation of EGFR as early as possible, if the tumor remains at the nascent stage. Additionally, patients harboring well-differentiated tumors may benefit more from the EGFR therapy. By contrast, the advanced and poor-differentiated tumors may develop drug resistance towards EGFR therapy due to the reduction of EGFR expression.

### 3.2 Artesunate against neuroendocrine tumors

In this study, artesunate was investigated for its inhibitory activity against EGFR. Frequently occurring and well-known EGFR-expressing solid tumors, *e.g.* lung cancer, colon cancer and head and neck cancer, did not present appealing target for us, since there are multiple therapeutic options available for these tumor types. Instead, EGFR-expressing NETs without accessible satisfactory treatment have drawn our attention. The abundance of EGFR in NETs has been well documented [1,3,153]. Concerning the occurrence of TKIs resistance in practice, we attempted to discover the potential of ART in NETs treatment.

#### 3.2.1 Cytotoxicity of artesunate

To assess the activity of ART against NETs, we performed resazurin-reduction assay. As resazurin results demonstrated (**Figure 12**), ART inhibited cell viability of the BON-1 cell line with a  $\log\text{IC}_{50}$  value of  $0.22 \pm 0.09 \mu\text{M}$ , while the  $\log\text{IC}_{50}$  values of the other two cell lines tested were much higher ( $\log\text{IC}_{50}$  of QGP-1:  $1.33 \pm 0.10 \mu\text{M}$  and  $\log\text{IC}_{50}$  of NCI-H727:  $1.34 \pm 0.10 \mu\text{M}$ ). The BON-1 cell line was approximately 13-fold more sensitive than the QGP-1 and NCI-H727 cell lines.

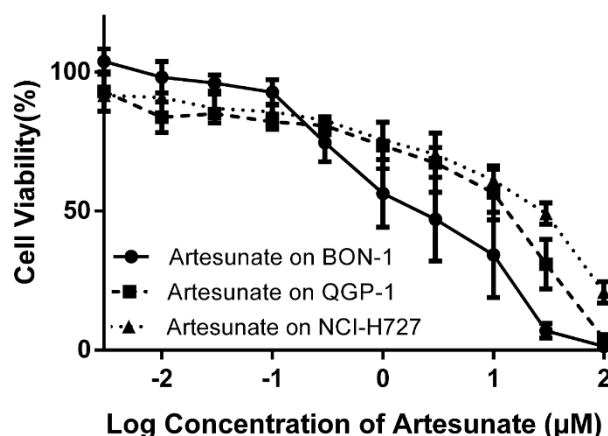


**Figure 12. Cytotoxicity of artesunate towards NET cell lines**

Cytotoxicity of artesunate towards NET cell lines. The cells were treated with ART in a range from  $0.003 \mu\text{M}$  to  $100 \mu\text{M}$ . The X-axis shows  $\log_{10}$  transformed concentrations of ART, while the Y-axis shows cell viability. The cell viability of untreated cells was considered as 100%. The figure was constructed by the thesis author through GraphPad Prism 8.

### 3.2.2 Transcriptomic profiling

To clarify the possible mechanisms by which ART inhibited growth of NET cell lines, total RNA from cells was extracted after  $2 \times IC_{50}$  ART treatment for 24 h. Quantile normalized data from microarray analysis were screened with Chipster software to obtain differentially expressed genes for downstream analysis. In total, 877 genes were filtered for BON-1 cells, 880 genes for QGP-1 cells and 758 genes for NCI-H727 cells. In order to validate the quality of microarray data, we performed quantitative real-time RT-PCR analyses of 6 exemplarily selected genes for each cell line (**Figure 13A**). The primers sequences are available in **Supplementary Table S3**. As shown in **Figure 13B**, there was a reasonable concordance ( $R^2 = 0.8666$ , two outliers were excluded) between microarray data and quantitative real-time RT-PCR data, which proved the reliability of the microarray results.

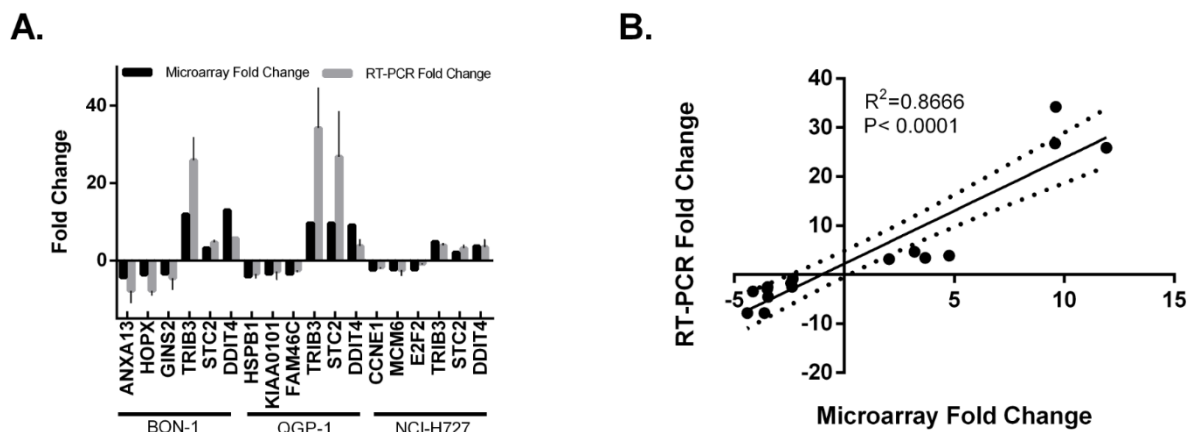


**Figure 13. Correlation between mRNA expression values**

Correlation between mRNA expression values obtained from microarray hybridization and quantitative real-time RT-PCR. (A) Fold changes obtained from 6 exemplarily selected genes for each cell line (BON-1, QGP-1 and NCI-H727). (B) Pearson correlation coefficient linear regression. The figure was constructed by the thesis author through GraphPad Prism 8.

We built a network involving common genes regulated upon ART treatment for all three cell lines by using Ingenuity Pathway Analysis software (**Figure 14**). Top 10 regulated networks (**See supplementary table S4**) from each cell line after ART treatment were chosen and common genes regulated within these networks were selected to build a novel network. We discovered a global cellular response of NET cell lines, which can also possibly be triggered by EGFR inhibition, towards ART [205]. The convergent network extracted from microarray results demonstrated a clear clue for endoplasmic reticulum (ER) stress, which was highly relevant to ROS generation, autophagy and cell cycle arrest. Among all involved genes, activating transcription factor 4 (*ATF4*) played a top hierarchical role which regulates the transcription of a cohort of downstream target genes involved in cell survival, apoptosis, autophagy and senescence. The ultimate outcome following *ATF4* activation is context

dependent. To predict subsequent cellular events after *ATF4* activation, we evaluated robust genes related to cell death by using the transcriptomic data (**Table 7**). Genes implicated in apoptosis, autophagy and ferroptosis were significantly deregulated upon ART treatment, especially in the BON-1 cell line, which may explain its superior sensitivity towards ART compared to the other two cell lines. However, considerable alterations of genes related to necrosis or necroptosis were not observed.

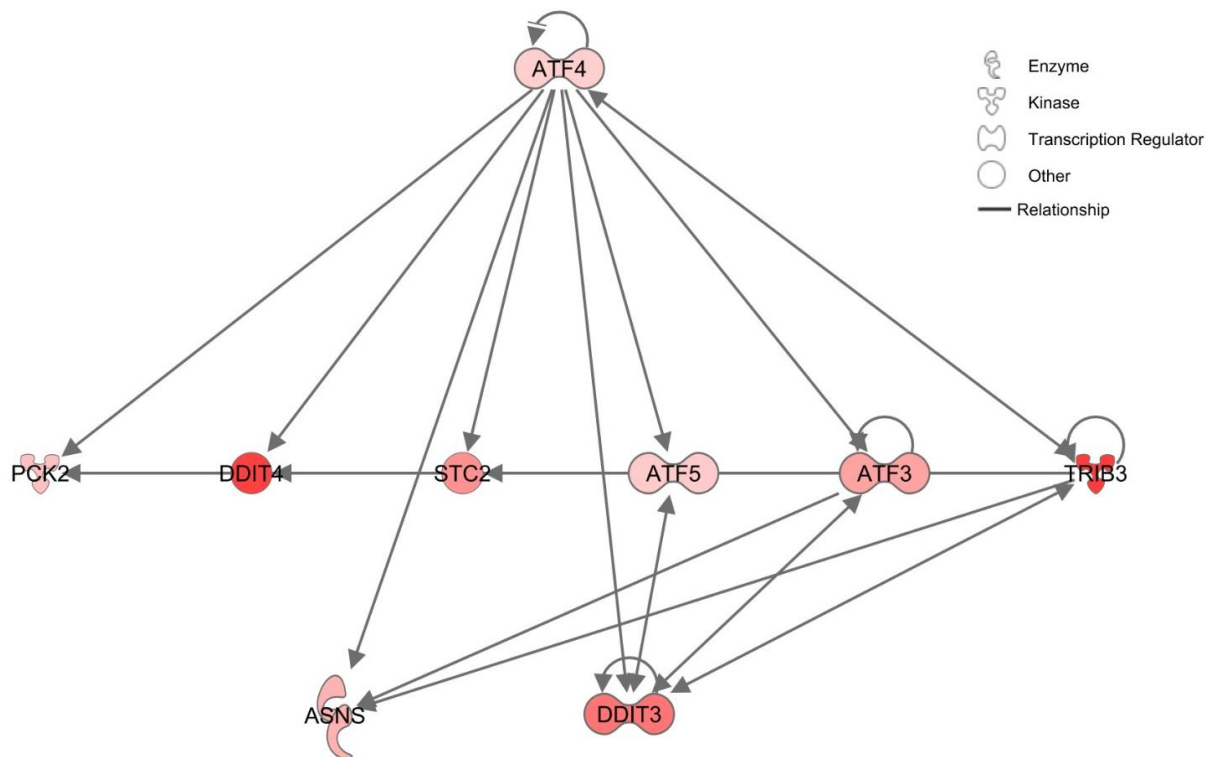


**Figure 14. Convergent network in NET cell lines**

Convergent network in NET cell lines. Color intensity demonstrates the average regulation level among three cell lines. The figure was constructed by the thesis author through Ingenuity Pathway Analysis software.

Table 7. Regulation of cell death determinants.

		Genes	Regulation Fold Change			Reference
			BON-1	QGP-1	NCI-H727	
Apoptosis	Positive regulators	ABL1	1.71			Jean YJ Wang, 2000
		APP	1.63			Han Zhang,2012
		BAX		-1.35		Y Xie,2016
		CASP10		-1.26		UniProtKB - Q92851
		CASP2		-1.25		Droin N,1998
		CASP4	1.61	1.60		Droin N,1998
		DFFB	1.38			Yong Fu,2013
	Negative regulators	GADD45A	1.21	2.09		UniProtKB - P24522
		TNFRSF10A	1.34			Thorburn, A.,2007
		TNFRSF1A	2.38	2.41	1.66	UniProtKB - P19438
		AKT1		-1.48		Luo, Y.,2006
		BCL2			-1.36	Y Xie,2016
		HSPA1B	-1.64	-1.73		Li, C. Y.,2000
		MCL1	1.31	1.24	1.72	Opferman, J. T.,2012
Autophagy	Positive regulators	TNFRSF11B		-1.51		Thorburn, A.,2007
		BIRC5	-1.80	-1.63		UniProtKB - O15392
		ATG16L1	1.31			Mizushima, N.,2007
		ATG7	1.36			Y Xie,2016
	Negative regulators	BECN1	1.20			Y Xie,2016
		SQSTM1	3.06	2.01	1.66	Guan, J. L.,2017
		ULK1	1.73	1.24	1.72	Zhong, Q.,2013
Ferroptosis	Positive regulators	SNCA	-1.52	-1.74		Ashley R. Winslow,2010
		ATF4	2.28	2.73	1.94	Chen, D.,2017
	Negative regulators	CARS	2.69	2.71	2.11	Cao, J. Y.,2016
		NOX		3.32		Y Xie,2016
		SLC38A1	1.96	2.03	1.81	Minghui Gao,2016
		TFR1	1.36	1.92		Y Xie,2016
		SLC7A11	3.64	1.97	1.77	Y Xie,2016
		HSPB1	-2.09	-4.16	-1.39	Y Xie,2016
		NRF2	1.21	1.71	1.38	Y Xie,2016
		SLC3A2	5.31	3.81	2.77	Y Xie,2016

### 3.2.3 Detection of reactive oxygen species

Upon treatment of BON-1 cells with 3, 6 and 9  $\mu\text{M}$  ART and QGP-1 and NCI-H727 cells with 40, 60 and 80  $\mu\text{M}$  ART, ROS were generated in all three cell lines in a dose-dependent manner. TBHP (500  $\mu\text{M}$ ) was applied as positive control, which increased ROS levels  $1.97 \pm 0.29$  ( $p < 0.0001$ ) fold in BON-1 cells,  $2.53 \pm 0.17$  fold ( $p = 0.0009$ ) in QGP-1 cells and  $2.49 \pm 0.11$  fold ( $p < 0.0001$ ) in NCI-H727 cells compared to untreated controls. Although ROS were induced by ART from  $1.29 \pm 0.01$  to  $1.49 \pm 0.05$  ( $p = 0.0067$ ) times more in BON-1 cells compared to untreated samples, the induction effects on QGP-1 and NCI-H727 cells were stronger with  $3.12 \pm 0.63$  ( $p = 0.0002$ ) to  $3.69 \pm 0.36$  ( $p < 0.0001$ ) and  $1.69 \pm 0.09$  ( $p < 0.0001$ ) to  $1.97 \pm 0.11$  ( $p$

< 0.0001) fold change, respectively (**Figure 15**). ROS induction was inhibited by pre-incubation with *N*-acetylcysteine (20 mM) (data not shown).

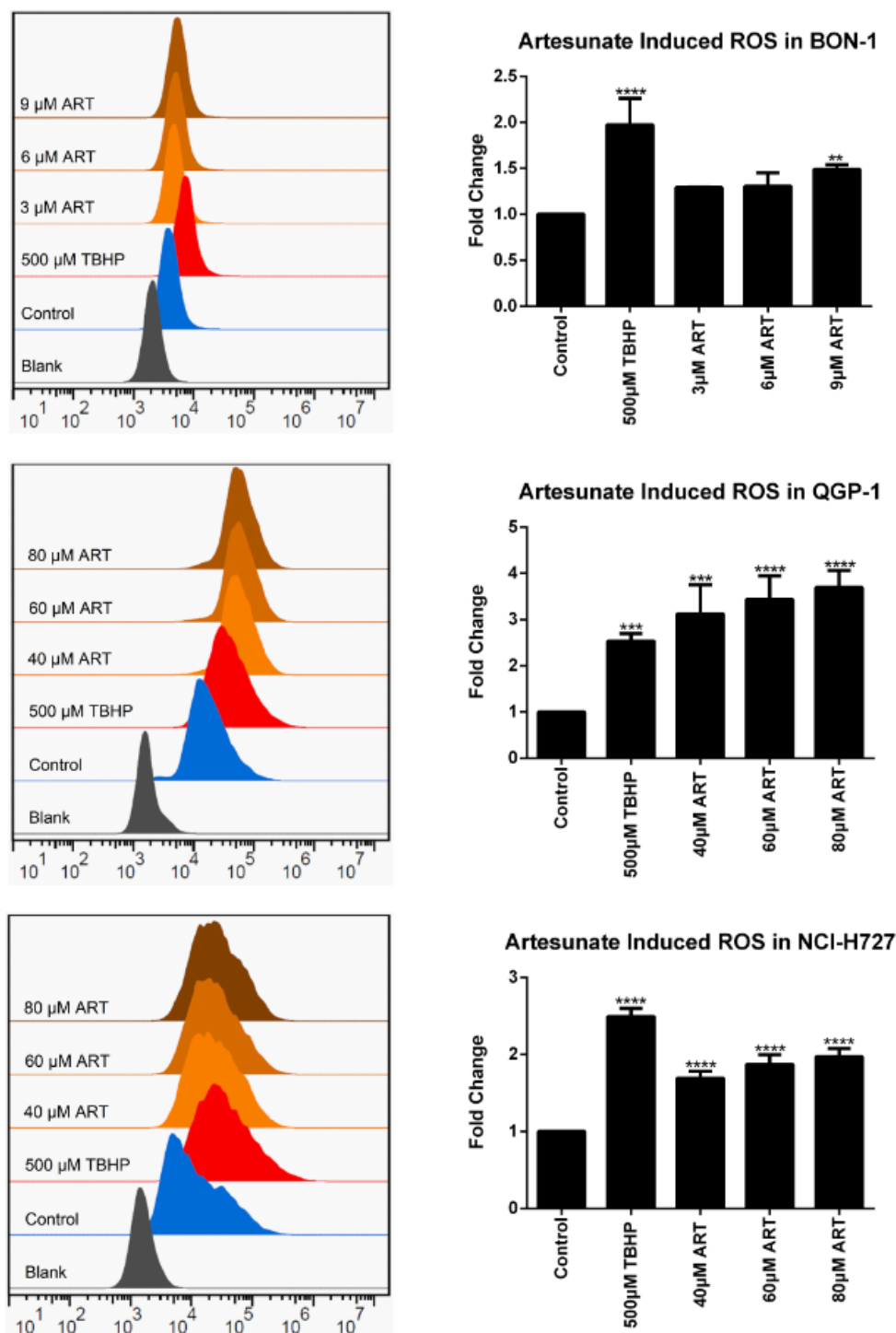


**Figure 15. Artesunate-induced ROS generation in NET cell lines**

Artesunate-induced ROS generation in NET cell lines. 500 μM tert-butyl hydroperoxide (TBHP), was applied as positive control. Asterisks “\*” represent significant differences between control and treated samples. “\*” indicates  $p < 0.05$ , “\*\*” indicates  $p < 0.01$ , “\*\*\*\*” indicates  $p < 0.0001$  and “\*\*\*\*\*” indicates  $p < 0.00001$ . The figure was constructed by the thesis author through GraphPad Prism 8 and FlowJo.

### 3.2.4 Detection of cell cycle arrest

As shown in **Figure 16**, 0.1  $\mu\text{M}$  doxorubicin as a positive control significantly induced G2/M arrest in all three cell lines after incubation for 24 h. ART significantly induced G0/G1 arrest in BON-1 and NCI-H727 cells ( $p < 0.05$ ) compared to untreated cells.  $69.93 \pm 1.10$  ( $p = 0.015$ ),  $72.60 \pm 3.39$  ( $p = 0.009$ ) and  $67.83 \pm 5.05\%$  ( $p = 0.044$ ) of cells were arrested in the transition from G0/G1 to S phase in BON-1 cells upon treatment with 3, 6 and 9 ART, respectively, compared to  $55.50 \pm 1.40\%$  in untreated samples. Similarly,  $58.27 \pm 1.12$  ( $p = 0.0002$ ),  $57.13 \pm 2.32$  ( $p = 0.0015$ ) and  $57.33 \pm 1.29\%$  ( $p = 0.0010$ ) of cells were arrested in the G0/G1 phase by the treatment of 40, 60 and 80 ART compared to  $50.93 \pm 3.19\%$  in untreated NCI-H727 cells. Regarding the QGP-1 cell line, instead of G0/G1 arrest, cell division was blocked at the transition from the G2/M phase to the G0/G1 phase with  $18.77 \pm 3.33$  and  $24.13 \pm 6.00\%$ , if treated with 60 and 80  $\mu\text{M}$  ART compared to  $16.77 \pm 3.79\%$  in untreated control samples but without significance. However, if treated with 40  $\mu\text{M}$  ART, there was a slight rise in G0/G1 phase with a percentage of  $65.50 \pm 9.20\%$  compared to control ( $63.37 \pm 4.48\%$ ).

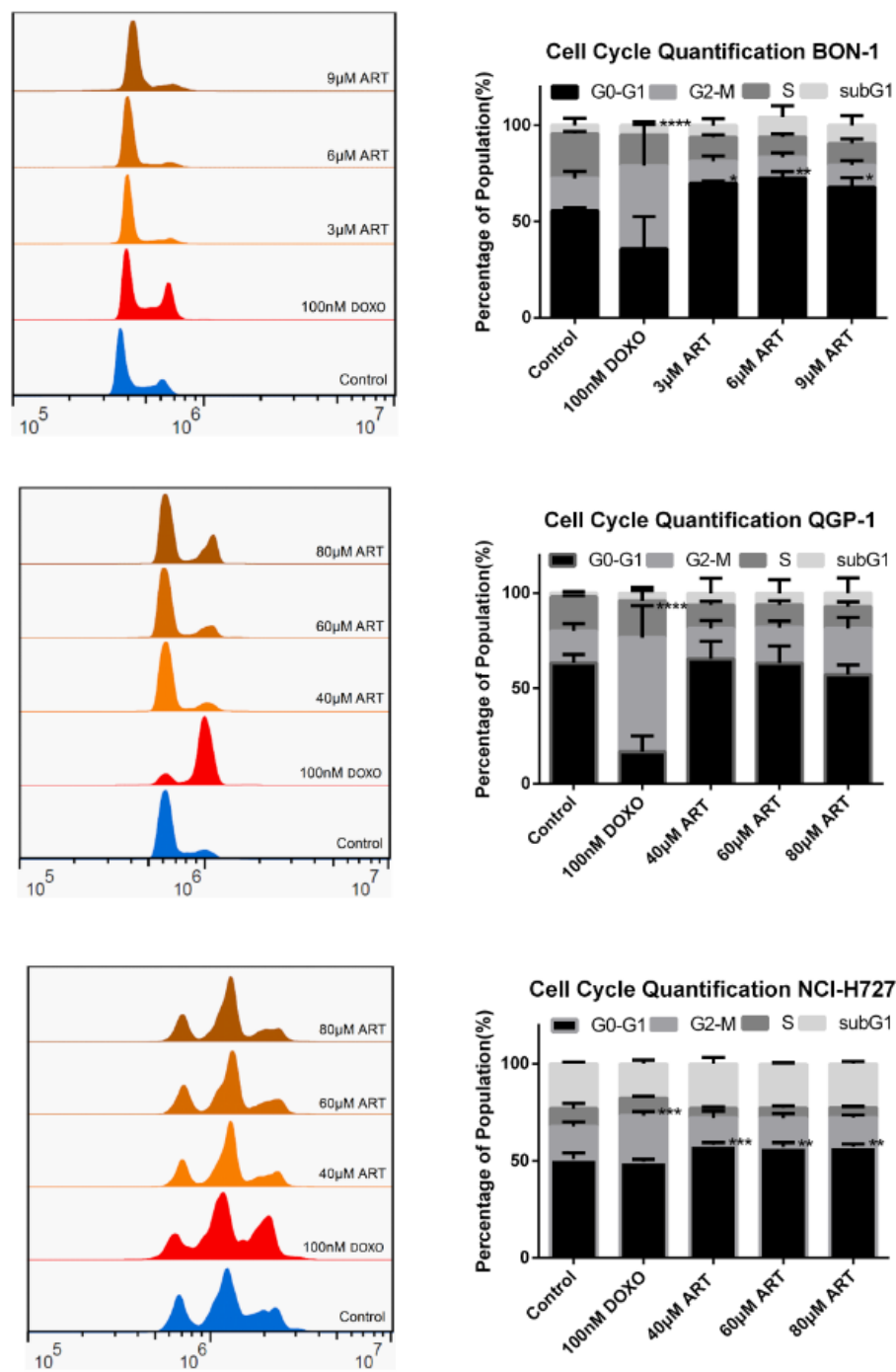


**Figure 16. Artesunate-induced cell cycle arrest in NET cell lines**

Artesunate-induced cell cycle arrest in NET cell lines. Doxorubicin (DOXO, 100 nM) was applied as a positive control. Untreated samples served as negative control (NC). Figures on the left-hand side are histograms plotted against PI absorbance detected by FL-2 of the flow cytometer. The bar diagrams on the right-hand side represent the percentages of each cell phase. Results from top to bottom show the BON-1, QGP-1 and NCI-H727 cells, respectively. Asterisks “\*” represent significant differences between control and treated samples. “\*” indicates  $p < 0.05$ , “\*\*” indicates  $p < 0.01$ , “\*\*\*” indicates  $p < 0.001$  and “\*\*\*\*” indicates  $p < 0.0001$ . The figure was constructed by the thesis author through GraphPad Prism 8 and FlowJo.

### 3.2.5 Detection of ferroptosis

Microarray results showed the transcription of genes related to ferroptosis was affected by ART. Therefore, we used a known ferroptosis inhibitor, ferrostatin-1, and an iron chelator, deferoxamine (**Figure 17**) to investigate, whether inhibition of ferroptosis could rescue cell viability. The cytotoxicity of ART was inhibited by 10  $\mu\text{M}$  ferrostatin-1 or 0.5  $\mu\text{M}$  deferoxamine (**Figure 17A**) with 5-time and 9.5-time AUC escalation in BON-1 cells, respectively. However, only deferoxamine (2.5-time AUC escalation), but not ferrostatin-1 inhibited cell death in NCI-H727 cells (**Figure 17C**), which indicated ART-induced cell death in NCI-H727 cells was iron- rather than lipid peroxidation-dependent. Unexpectedly, neither ferrostatin-1 nor deferoxamine alleviated cell death in QGP-1 cells (**Figure 17B**), indicating that ferroptosis may not play a role for ART's effects in this cell line.

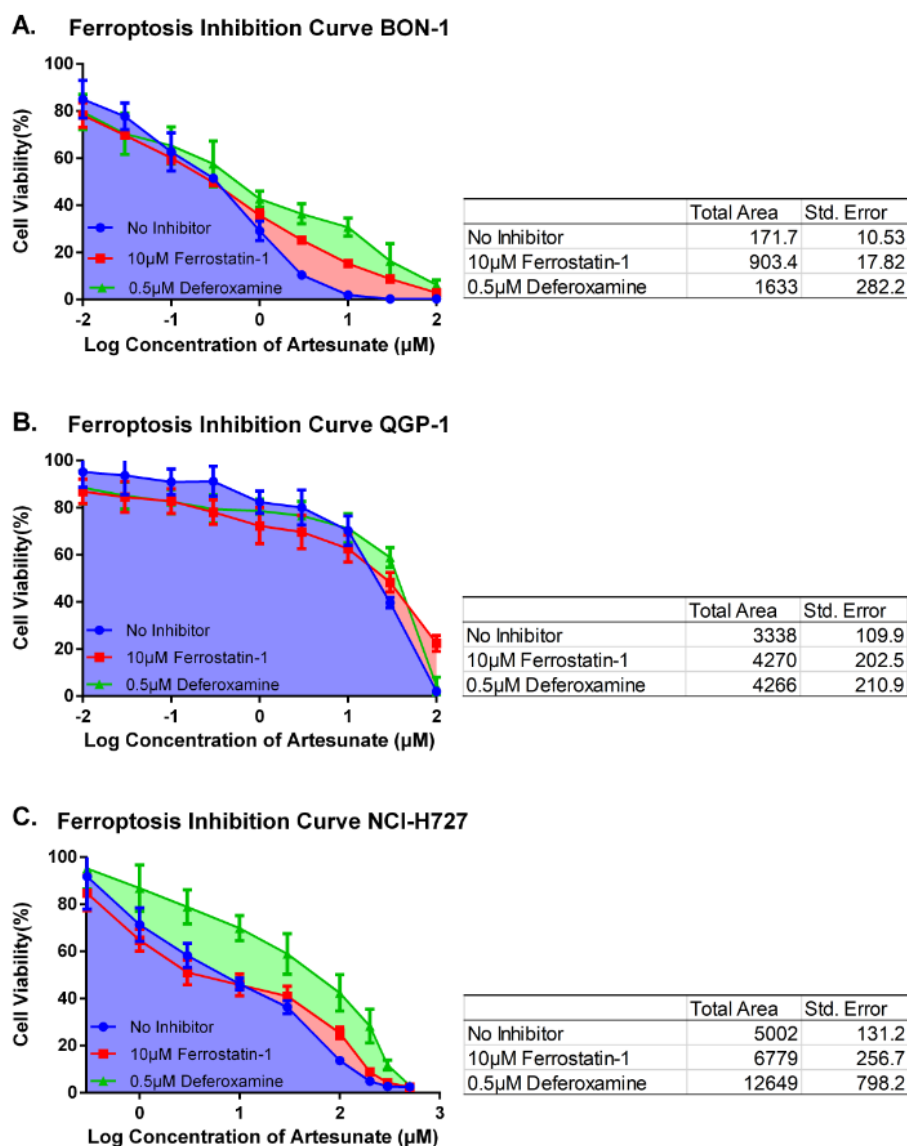


**Figure 17. Ferroptosis inhibition**

Ferroptosis inhibition. Green lines indicate cells pre-treated with 0.5  $\mu\text{M}$  deferoxamine. Red lines indicate cells pre-treated with 10  $\mu\text{M}$  ferrostatin-1, while blue lines indicate cells without pre-treatment of any inhibitors. Cell viability of (A) BON-1, (B) QGP-1 and (C) NCI-H727 cells with or without pre-treatment of inhibitors is shown. The X-axis shows log<sub>10</sub> transformed concentrations of ART, while the Y-axis shows cell viability. AUC parameters are shown in the adjacent table. The figure was drawn by the thesis author through GraphPad Prism 8.

### 3.2.6 Detection of autophagy

As shown in **Figure 18**, introduction of 3-MA alleviated cell vulnerability upon ART treatment in all three cell lines and at all time-points from 24 h to 72 h. Instead, the results did not show cellular self-protective defense, and autophagy induced by ART resulted in cell death. The rescue effect was strongest in QGP-1 cells followed by NCI-H727 and BON-1 cells, especially at lower ART concentrations. The weaker ability of escalating cell viability in the two latter cell lines indicated that there might exist other cell death modes than autophagy. However, the

protective ability of 3-MA reached its limit, if cells were treated with higher concentrations of ART or treatments for longer times to 72 h.

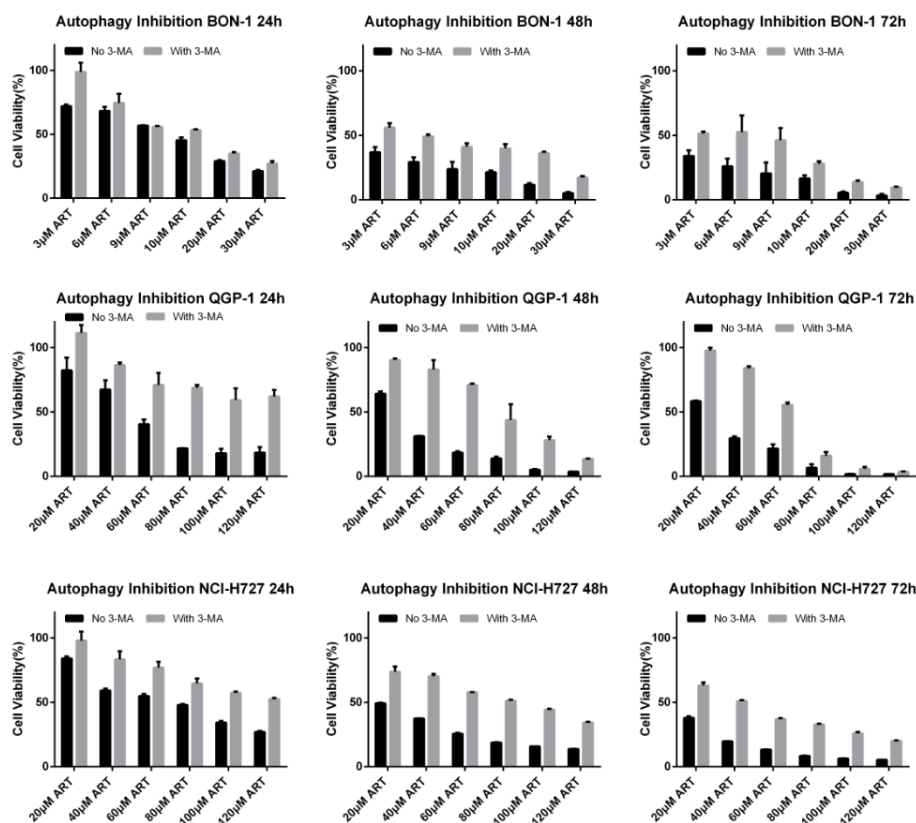


**Figure 18. Matrix of autophagy inhibition**

Matrix of autophagy inhibition. Within the matrix, the figures from the top to the bottom show results obtained from BON-1, QGP-1 and NCI-H727 cells, respectively, while from the left to the right-hand side, the results after 24 h, 48 h and 72 h, respectively, is shown. The data were obtained from one group member Madeleine Böckers and the figure was drawn by the thesis author. The figure was constructed by the thesis author through GraphPad Prism 8.

### 3.2.7 Detection of apoptosis by flow cytometer

In order to determine apoptotic cell death, we double-stained cells with annexin V conjugated to APC fluorophore and PI. The results showed a clear apoptotic effect upon treatment of BON-1 cells with ART in a time-dependent manner (**Figure 19**). After incubation for 24, 48 and 72 h, 10  $\mu\text{M}$  ART gave rise to  $11.20 \pm 4.35$ ,  $16.10 \pm 4.37$ , and  $27.21 \pm 3.75$  % apoptotic cells (both early and late apoptotic cells), respectively. Similarly,  $10.15 \pm 2.81$ ,  $28.02 \pm 7.12$  and  $53.35 \pm 0.07$  % apoptotic cells were observed upon treatment with 20  $\mu\text{M}$  ART for 24 h, 48 h and 72 h, while  $11.75 \pm 3.45$ ,  $27.28 \pm 8.81$   $\mu\text{M}$  and  $84.00 \pm 0.14$  % were measured after incubation with 30  $\mu\text{M}$  ART. Interestingly, the extension of drug incubation times magnified the dose effects. However, this method was not appropriate for the detection of apoptosis in QGP-1 and NCI-H727 cells due to the fact that even untreated samples showed high percentages of damaged

cells after the staining procedure (data not shown). Therefore, we applied the TUNEL assay for the detection of apoptosis in QGP-1 and NCI-H727 cells.

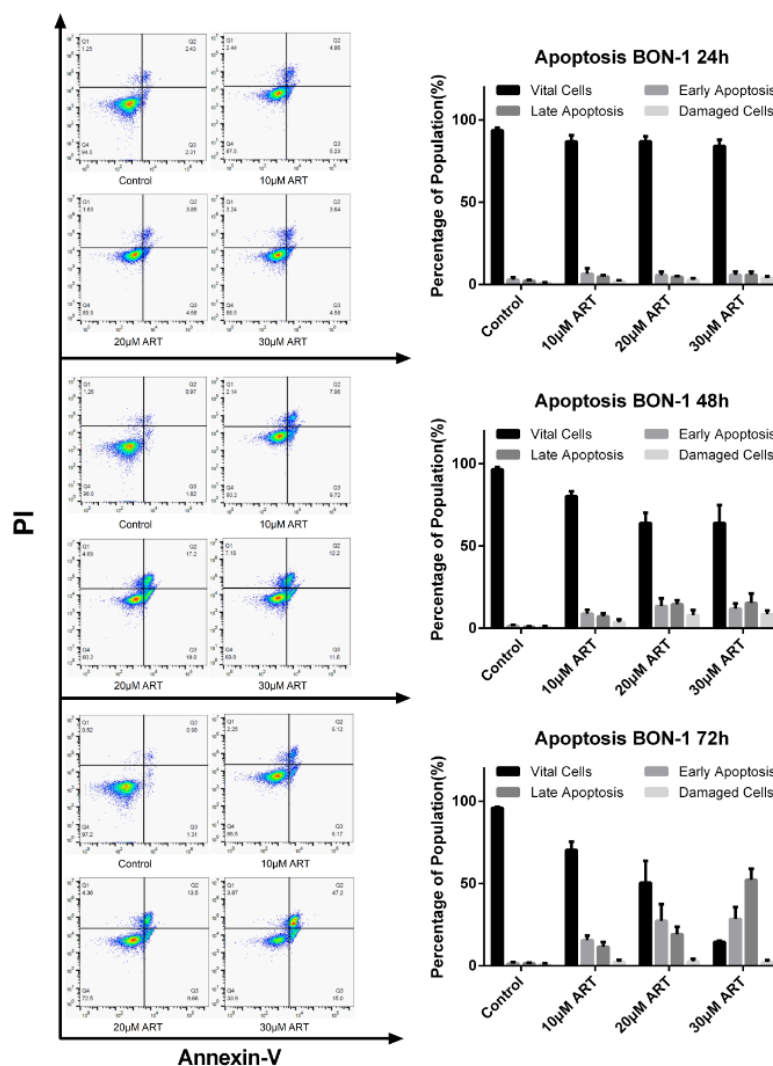


**Figure 19. Apoptosis in BON-1 cells as detected by flow cytometer**

Apoptosis in BON-1 cells as detected by flow cytometer. The left-hand side shows flow cytometer plots. The X-axis indicates annexin-V-APC signals detected by FL-1. The Y-axis indicates PI signals detected by FL-3. Cross gating was applied to distinguish cell population among annexin-V -/PI - (vital cells), annexin-V +/PI - (early apoptotic cells), annexin-V +/PI + (late apoptotic cells) and annexin-V -/PI + (damaged cells/secondary necrotic cells). The results were from three time points (24 h, 48 h and 72 h incubation) from top to bottom. The quantification results are shown on the right-hand side. The figure was constructed by the thesis author through GraphPad Prism 8 and FlowJo.

### 3.2.8 Detection of apoptosis in situ

Considering the limited capacity to detect apoptosis by flow cytometer, we applied the TUNEL assay to detect DNA fragmentation associated with early stages of apoptosis. In non-treated cells, DNA fragmentation was almost undetectable in all NET cell lines (**Figure 20**). The results were consistent with apoptosis detected with flow cytometer in BON-1 cells. Apoptotic cells were detectable after 24 h incubation. ART induced apoptosis with increasing concentrations

and elongation of the incubation time. By contrast, there were limited numbers of apoptotic cells detectable in the QGP-1 and NCI-H727 cell lines (**Figure 20**), despite that cell growth was severely inhibited and a considerable number of cells were detached from plates. This indicates that apoptosis was not the predominant cell death manner in QGP-1 and NCI-H727 cells.

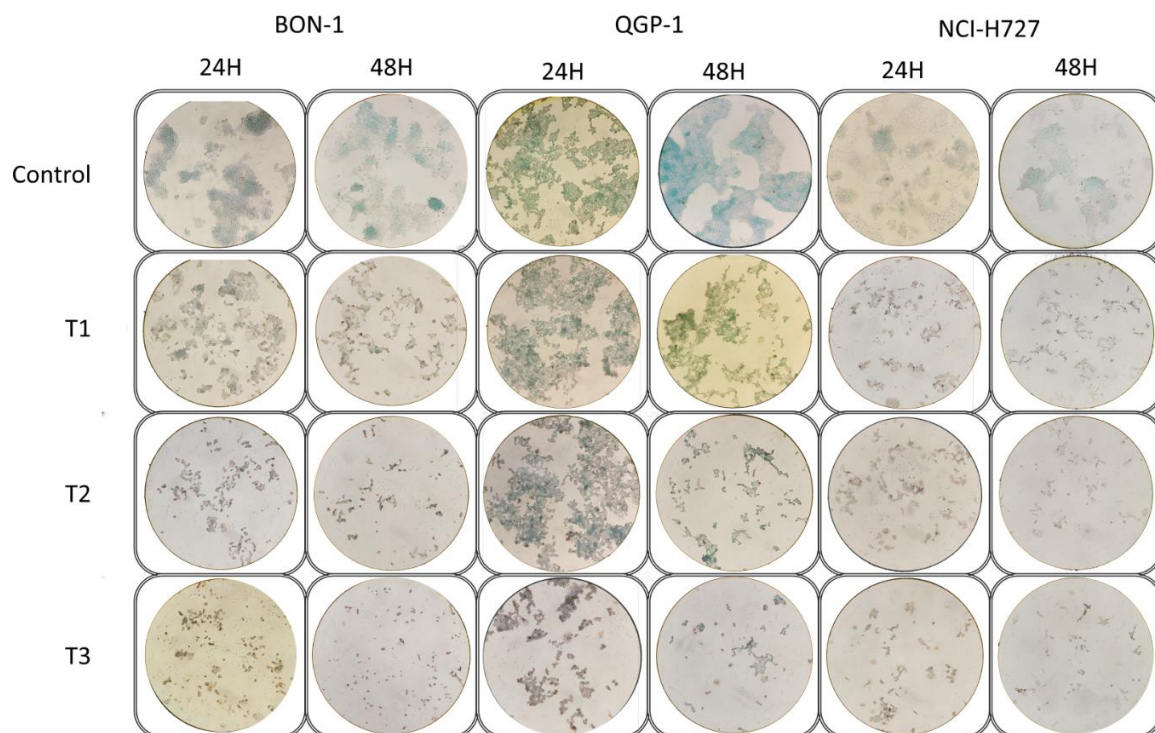


**Figure 20. Apoptosis detection in situ**

Apoptosis detection *in situ*. Brown staining represents DNA fragmentation. Cells were treated with different concentrations of ART for 24 h and 48 h in BON-1, QGP-1 and NCI-H727 cells, respectively. Methyl green was applied as counter staining dye, which shows green color. Untreated samples served as control. T1, T2 and T3 indicate three different concentrations (10  $\mu$ M, 20  $\mu$ M, 30  $\mu$ M for BON-1 cells and 40  $\mu$ M, 60  $\mu$ M, 80  $\mu$ M for QGP-1 and NCI-H727 cells). The figure was constructed by the thesis author through office PowerPoint.

### 3.2.9 Western blotting

To further study the mechanisms underlying ART against NET cell lines on the molecular level, we performed Western blotting to detect ER-stress-related and apoptosis-regulating proteins. As shown in **Figure 21**, treatment of ART for 24 h (3  $\mu$ M for BON-1 cells and 40  $\mu$ M for QGP-1 and NCI-H727 cells, respectively) clearly induced ER-stress through PERK signal transduction in all NETs, since there was an obvious phosphorylation of eIF2 $\alpha$ . Besides, we investigated ER-stress induced autophagy by detecting Atg12 abundance. However, free Atg12 was not detectable in our experiment. Instead we observed a decrease of the Atg12-Atg5

complex, which may represent a dynamic metabolic change, since complexed Atg12-Atg5 further conjugates Atg16L to form pre-autophagosomes. To confirm the fate of cells experiencing ER-stress, we further detected cell cycle, autophagy and apoptosis determinant proteins, *i.e.* p21, LC3B, PARP and caspases (**Figure 22**). An increase of cleaved PARP and cleaved caspase 8 was detected in BON-1 cells in a dose-dependent manner after 24 h. However, subsequent executioner caspases *e.g.* caspase 3 and 7 were not activated (data not shown), which indicated that ART induced apoptosis in BON-1 cells was caspase-independent cell death (CICD) [206–208]. By contrast, neither PARP cleavage nor activation of caspases (data not shown) was increased in QGP-1 and NCI-H727 cells after ART treatment for 24 h. These results explained our results from flow cytometer and TUNEL assay, where ART clearly induced apoptosis in BON-1 cells, but not in QGP-1 and NCI-H727 cells. Interestingly, a clear conversion of LC3-I to its lower migrating form LC3-II was observed in a dose-dependent manner in all NET cell lines, which further proved ER-stress induced autophagy. Similarly, p21 was up-regulated in all NET cell lines after 24 h. Noticeably, in spite of the fact that ART treatment induced cell arrest by p21, how p21 expression increased upon different concentration of ART treatment was distinct from one cell line to another. Upon treatment with low ART concentrations, p21 was most dramatically up regulated in BON-1 cells. However, the extent of upregulation contradicted the increase of drug concentration. By contrast, p21 up-regulation in QGP-1 and NCI-H727 cells concurrently increased with higher ART concentrations and dropped only at extreme high concentrations. This finding brought us to the assumption that p21 alteration in our study probably played a role as a regulator. The drop of p21 up-regulation possibly gave rise to final cell death induction. In order to prove this assumption, we detected p21 expression after drug incubation for 48 h (**Figure 23**). The results showed p21 was consistently up-regulated in apoptosis resistant NCI-H727 cells in comparison to BON-1 cells, where p21 expression was called back after 48 h when severe apoptosis occurred. In the case of QGP-1 cells, initially up-regulated p21 after 24 h turned to be down regulated after 48 h which may allow QGP-1 cells to escape cell cycle arrest. Moreover, we were interested in whether p21 alteration will affect autophagy process. Therefore, we detected LC3B after drug treatment for 48 h as well. We observed a continuous rise of LC3B expression in a dose-dependent manner, which indicated that p21 alteration did not affect the process of autophagy (**Figure 23**).

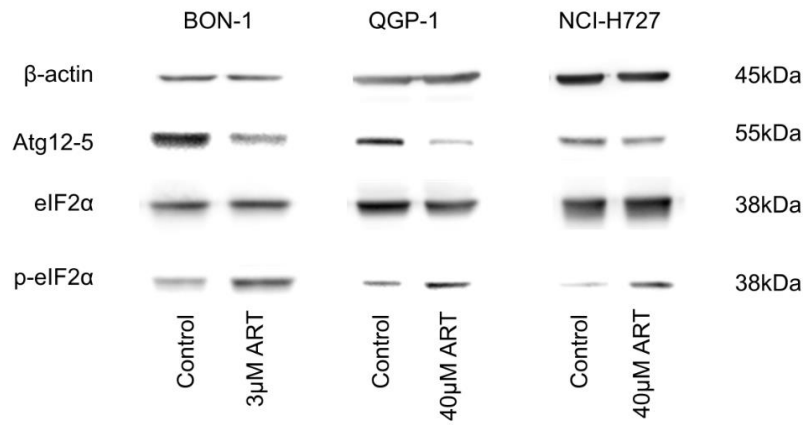


**Figure 21. ART induced ER-stress as detected by Western blotting**

ART induced ER-stress as detected by Western blotting. Results were obtained after ART treatment for 24 h. The figure was constructed by the thesis author through ImageJ and office Excel.

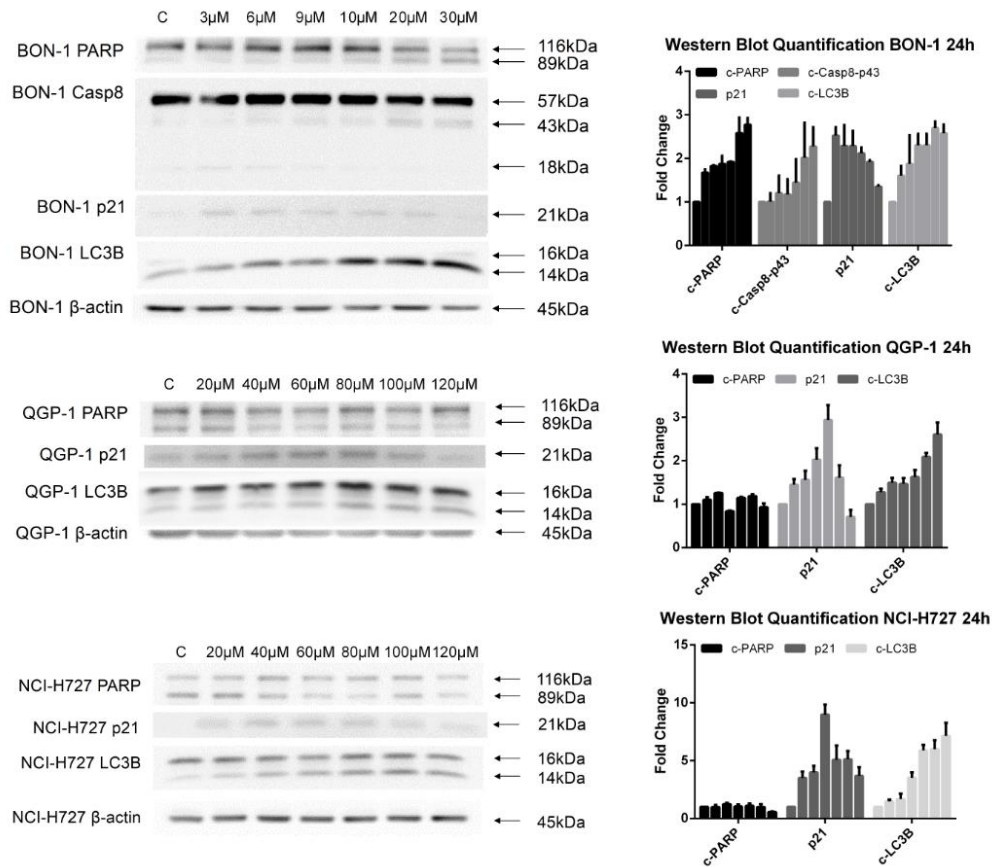


**Figure 22. Western blotting and quantification 24h**

Molecular downstream analysis from Western blotting and quantification. Results were obtained after ART treatment for 24 h. The figure was constructed by the thesis author through GraphPad Prism 8, ImageJ and office Excel.

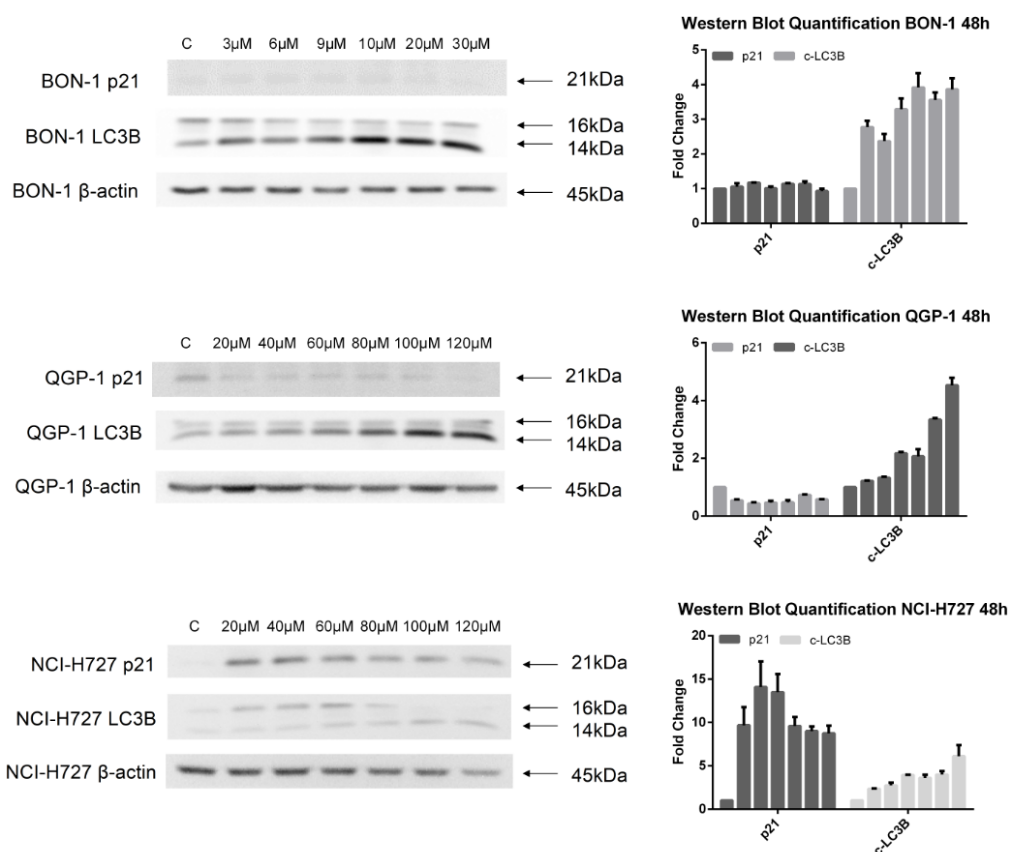


**Figure 23. Western blotting and quantification 48h**

Molecular downstream analysis from Western blotting and quantification. Results were obtained after ART treatment for 48 h. The figure was constructed by the thesis author through GraphPad Prism 8, ImageJ and office Excel.

### 3.2.10 Detection of Mitochondrial Membrane Potential

In order to prove the caspase-independent cell death in BON-1 cells, we additionally detected mitochondrial membrane potential by JC-1 staining in BON-1 cells. As shown in **Figure 24**, the percentage of cells harboring JC-1 monomers as an indication of mitochondrial disruption gradually increased from  $4.15 \pm 0.75\%$  to  $9.20 \pm 1.79\%$  if treated with  $3 \mu\text{M}$  to  $30 \mu\text{M}$  ART compared to  $1.01 \pm 0.17\%$  in control samples treated for 24 h. These percentages dramatically rose up to the extent ranging from  $42.55 \pm 8.70\%$  to  $54.83 \pm 5.03\%$  compared to  $1.63 \pm 0.35\%$  in control samples after 48 h. The results showed a both dose and time-dependent mitochondrial membrane disruption induced by ART, where dissipation of the mitochondrial electrochemical potential gradient concurrently happened with apoptosis.

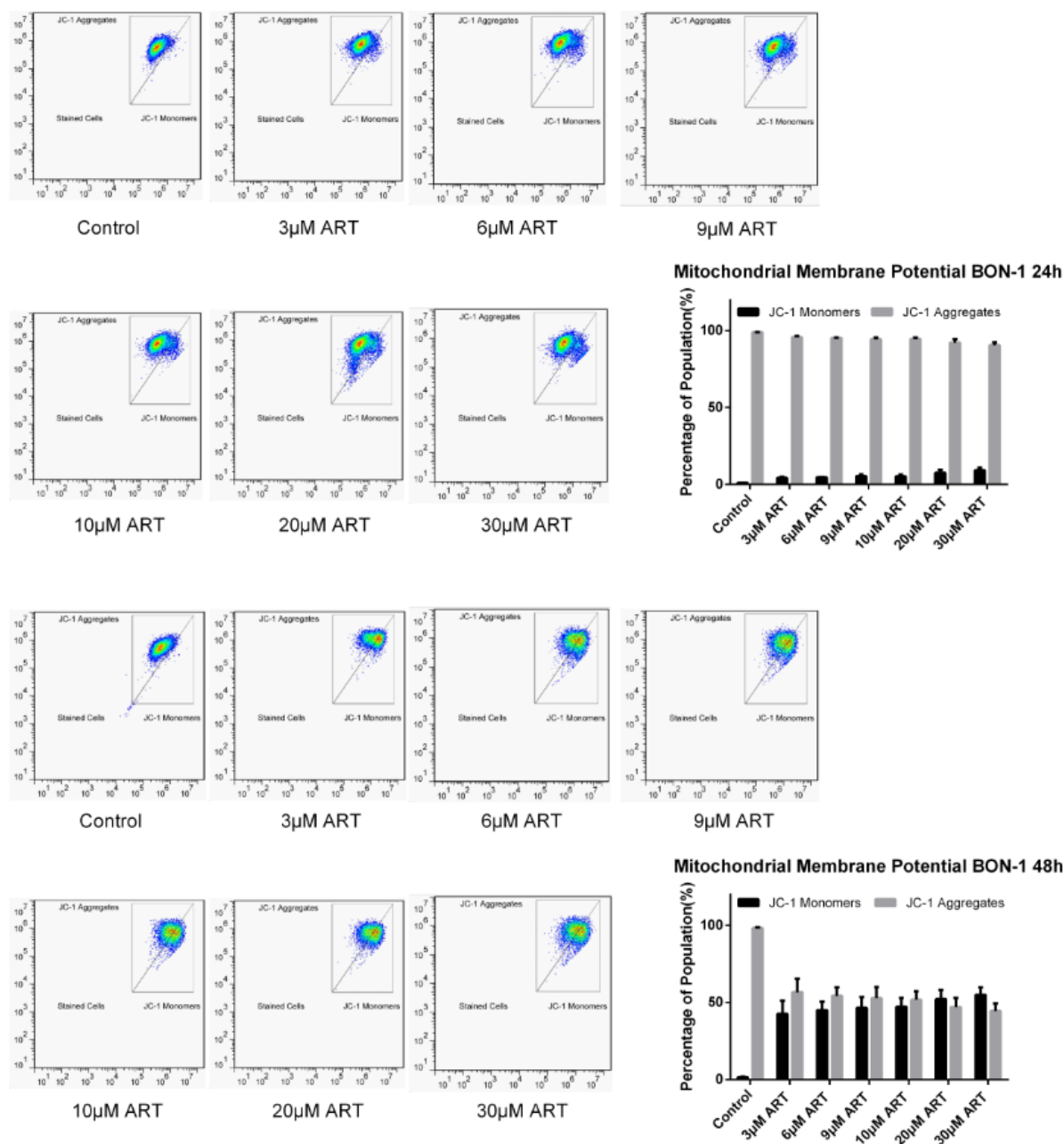


**Figure 24. Mitochondrial membrane potential as detected by flow cytometer**

Mitochondrial membrane potential as detected by flow cytometer. The figure composes flow cytometer plots and bar charts quantification. Untreated samples serve as negative control. The X-axis in flow cytometer plots shows signals detected by FL-1, which indicates JC-1 monomers. The Y-axis shows signals detected by FL-2, which indicates JC-1 aggregates. The percentages of cells harboring JC-1 monomers or aggregates obtained from 24 h and 48 h incubation are shown in bar charts, respectively. The figure was constructed by the thesis author through GraphPad Prism 8 and FlowJo.

### 3.2.11 Brief summary

In the present study, we analyzed the modes of action of ART in three NET cell lines and found interesting signaling pathways, which can possibly be triggered by EGFR inhibition [205], leading to the differential induction of apoptosis, autophagy, and ferroptosis in these cell lines.

Moreover, considering the specificity of NETs in the secretory capacity, the endoplasmic reticulum homeostasis may be an appealing target.

## 4 Discussion

### 4.1 EGFR and its role in multiple cancer types

Our results strongly indicated that protein rather than mRNA expression reflects the prognostic value of EGFR. This may have important implications, since data obtained by mRNA microarray and next generation sequencing technologies may be less reliable than data from protein arrays or immunohistochemical analyses in prognosis. Recently, the nuclear expression of EGFR comes into the focus of attention, which can be only monitored by methods based on protein visualization and localization. Furthermore, the fact that both mcEGFR and nEGFR expression was rather associated with low T stage and positive mcEGFR was related to low grade, thus well tissue differentiation, implied that the oncogenic function of EGFR may be more related to nascent stages of carcinogenesis than to advanced and progressive tumors, which may as well explain at least partially the occurrence of secondary resistance against EGFR-directed therapy. EGFR is well-known as oncogenic signal regulating proliferation apoptosis and differentiation and thereby contributes to carcinogenesis. The development of specific small molecules and antibodies targeted to EGFR represents an attractive clinical implementation [209,210].

EGFR overexpression is related with *EGFR* gene amplification, receptor-activating mutations, or deficiency of negative regulatory mechanisms [211]. Here, we investigated prognostic value of *EGFR* mRNA expression by mining the data deposited in the GEO and Oncomine databases. Although there are studies revealing that high *EGFR* mRNA [212–214] or even gene copy number [215] were correlated with poor clinical outcomes or pathological characteristics, a more systematic evaluation of published studies did not validate the proposed impact of *EGFR* mRNA expression. The inconsistency partially may be attributed to the choice of the EGFR probe. Microarray chips normally provided several probes targeting the same gene. Expression intensity according to different probes can extraordinarily differ, which may even lead to completely opposite conclusions. We used the optimal probe for our analysis based on the concept of jetset probe [216], which means only those probes providing comparatively better overall specificity, coverage and robustness were chosen. Since no correlation was found based on mRNA expression, we assessed 30 independent studies assuming that EGFR protein expression might be a more promising prognostic factor than *EGFR* mRNA expression.

As demonstrated by elegant analyses, there exist two distinct patterns of EGFR expression. Upon stimulation with ligands, mcEGFR undergoes COPI-mediated retrograde trafficking from

the Golgi apparatus to the endoplasmic reticulum. With the help of importin  $\beta 1$  and Sec61 $\beta$ , mcEGFR can be shuttled from outer nuclear membrane to inner nuclear membrane and finally released into nucleoplasm and become nEGFR [213,217]. Therefore, we took one step further and investigated, whether protein expression patterns as membranous and cytoplasmic or nuclear expression would make a difference in regard of affecting clinical outcomes or pathological characteristics. In the current study, we observed a clear positive correlation between mcEGFR and nEGFR ( $p < 0.001$ ). Furthermore, both mcEGFR and nEGFR expressions were unexpectedly associated with T stage in an adverse manner ( $p < 0.001$  and  $p = 0.004$ ; respectively). Positive mcEGFR was related to well differentiation ( $p = 0.027$ ). We also revealed the diverse distribution patterns of both mcEGFR and nEGFR within different tumor types.

## 4.2 Artesunate and its effects on NETs

Our findings suggested that investigation on cellular response confined to a single signaling pathway and cell death mode is over simplified. The landscape of cellular responses should be formed to generate an overview of drug effect. In our case, multiple cellular responses were induced by ART in three NET cell lines (BON-1, QGP-1 and NCI-H727). Microarray hybridization demonstrated a significant up-regulation of ATF3, ATF4, ATF5, DDIT3 (also known as CHOP), DDIT4 and TRIB3 transcription in all three NET cell lines upon ART treatment. Most of these up-regulated genes are considered as key effectors of ER-stress [218], which is physiologically triggered by an overload of unfolded proteins in the ER lumen and also possibly caused by EGFR inhibition in clinic [205]. Induction of ER-stress subsequently activated downstream signal transduction, which was collectively termed as unfolded protein response (UPR) [219]. Coincidentally, pancreatic neuroendocrine tumors may be one class of solid tumor that are particularly sensitive to protein folding stress due to their superior secretory activity. However, ER-stress can be either cytoprotective against stress stimuli or cytotoxic by activating cell death signaling depending on context. In our study, the NET cell lines initially responded to ART by activating UPR via eIF2 $\alpha$  phosphorylation, which further up-regulated ATF4 and DDIT3. Expectedly, ROS accumulation was detected due to cross-talk between ER-stress and oxidative stress [220]. It was also reported that persistent ER-stress induced ROS [221]. However, ROS induction was highest in QGP-1 cells with more than three-fold increase followed by NCI-H727 cells with more than 1.5- fold increase, but lowest in the in most sensitive BON-1 cell line with a fold-change below 1.5-fold upon ART treatment. Subsequent autophagy was induced in all NET cell lines with clear accumulation of LC3-II. Autophagy inhibition experiments further demonstrated ART induced autophagy broke proteostasis

balance and lead to cell death instead of restoring proteostasis in all NETs. Autophagy induction in BON-1 cells was accompanied with apoptosis on both cellular and molecular levels. PI/annexin-V dual staining and in situ DNA fragmentation assays showed apoptosis induction after ART treatment for 24 h. Accumulation of cleaved PARP, caspase 8 and LC3-II was concurrently observed after 24 h in a dose-dependent manner. However, no executioner caspases cleavage was observed, indicating caspase-independent cell death (CICD), whereby activated caspase 8 cleaves BID and provokes translocation of the latter to mitochondria catalyzing mitochondrial outer membrane permeabilization and cytochrome c release [222]. The determination of the mitochondrial membrane potential further proved our prediction with clear accumulation of JC-1 monomers fluorescence signal, indicating mitochondrial membrane disruption. However, no obvious apoptosis was detected in QGP-1 and NCI-H727 cells. Interestingly, if we looked in more detail into cell specificity, we found that the BON-1 cell line is NRAS-mutated, while both QGP-1 and NCI-H727 cell lines are KRAS-mutated [223,224]. It was previously reported that NRAS mutation increased the vulnerability to mitochondrial apoptosis, while KRAS mutation mediated apoptosis resistance [225,226]. Our study provided strong evidence for this effect pattern. Moreover, upon the disruptive cellular events within cells, p21 seemed to play a regulatory role. Encountering severe metabolic stress, cell growth was significantly arrested in G0/G1 in both BON-1 and NCI-H727 cells and G2/M in QGP-1 cells to some extent. However, the arrest was broken by p21 callback regulation in BON-1 cells after drug incubation for 48 h, if the cells were committed to apoptosis on a large scale, which was on the contrary to NCI-H727 cells harboring consistent p21 up regulation. In the case of QGP-1 cells, p21 regulation was more complicated, because it was initially up-regulated after drug incubation for 24 h as a stress response followed by down-regulation after drug incubation for 48 h. We suspected the role of callback to normal regulation differed from a real down-regulation of p21. However, how p21 was exactly involved in the networks within cells remained unclear at this state.

## 5 Material and Methods

### 5.1 Tumor cases

A total number of 502 formalin-fixed and paraffin-embedded tumor cases covering 27 tumor types have been obtained from different sources: Ovarian and endometrial carcinoma biopsies were provided by Prof. Jose Schneider and belong to the tumor banks of Hospital Universitario de Cruces, Bilbao, Spain and Hospital Universitario Valdecilla, Santander, Spain, respectively, and were to a large extent used in previous studies on oncogenic activation in gynecologic tumors. Relevant data and ethical approval by Wandsworth Ethics Committee (Wandsworth, UK, Ref: 08/H0803/3) regarding colon cancer has been published by us [17]. Further tumor biopsies have been obtained from Dr. Zahir Yassin (Tayba Cancer Centre, Khartoum, Sudan) with ethical approval from the National Medicines and Poisons Board, Sudan (dated: September 20, 2015; Ref.: TQM/Pir-F/4). In addition, two tissue microarrays (TMAs) BC000119 (Biomax Inc., Derwood, USA) and T8235713 (Biocat, Heidelberg, Germany) were commercially available. Three further TMAs were provided by the Tissue Bank of the Institute of Pathology, University Medical Center, Mainz, Germany) with ethical approval from The Ethics Committee of the State Authorization Association for Medical Issues (Landesärztekammer) Rheinland Pfalz (dated: March 22, 2018; Ref.. 2018-13179). All patients gave informed consent prior to participation. All tumor cases information refers to Supplementary Table S1.

### 5.2 Statistical evaluation of the GEO and Oncomine databases

*EGFR* mRNA expression data and corresponding overall survival time, TNM stage and grade information were obtained from the GEO (<https://www.ncbi.nlm.nih.gov/geo/>) and Oncomine (<https://www.oncomine.org/>) databases. Normalized and log-2 transformed *EGFR* mRNA expression values of jetset probes were further determined as "low" or "high" using both median and mean as the cut-off value. Thirty datasets covering 15 cancer types were analyzed for time-to-event distributions estimated with Kaplan–Meier curves with log-rank test as assessing significance method. Associations of *EGFR* mRNA expression level with pathological characteristics were determined by Pearson's  $\chi^2$ -test. The above mentioned statistical analyses were performed using IBM SPSS Statistics version 23 (IBM, USA). Statistical differences with p-values less than 0.05 were considered as significant.

### 5.3 Search strategy

Thirty independent studies based on immunohistochemical EGFR determination from Pubmed engine (<https://www.ncbi.nlm.nih.gov/pubmed>) were identified by combining the search terms “EGFR”, “expression”, “predictor”, “biomarker” and “prognosis/prognostic” for estimating EGFR protein expression and its correlation with clinical outcomes in comparison to analyses derived from the GEO and Oncomine databases based on mRNA expression.

### 5.4 Immunohistochemistry and statistical application

Immunohistochemistry was performed on 502 biopsies using EGFR rabbit monoclonal antibody (Clone EP38Y; Thermo Fisher Scientific, Dreieich, Germany) as primary antibody. The staining procedure has been previously published by us [18]. Quantification of immunostainings was performed by using Panoramic Desk (3D Histotech Panoramic digital slide scanner, Budapest, Hungary). Membranous and cytoplasmic EGFR (mcEGFR) was quantified by MembraneQuant software by using H-Score. A minimum of each three representative areas per tumor were scanned and the mean values together with standard deviations were calculated. One-hundred-four cases were excluded for nuclear EGFR (nEGFR) analysis due to the limitation in distinguishing extremely positive mcEGFR and existence of nEGFR. The other 398 cases were manually graded regarding nEGFR expression.

We used one-way ANOVA to exert mean comparison of mcEGFR H-score within different cancer types, TNM stage and grade, respectively. Independent t-test was used to determine variation in distribution of mcEGFR H-score in nEGFR negative and positive groups. mcEGFR and nEGFR were further categorized into four degrees or negative and positive groups according to expression intensity. As to mcEGFR H-scores, values below 20 were grouped as negative; H-scores ranging from 20 to 115 as weakly positive, from 115 to 210 as moderate positive and above 210 as strongly positive. The later three groups were all considered as positive. The signal-to-noise cutoff of mcEGFR H-score was determined by H-score obtained from negative controls (omission of primary antibody during staining procedure). nEGFR was similarly grouped as negative, weak, moderate and strong positive immunostaining or as negative and positive groups. As categorical data, both mcEGFR and nEGFR and their association with pathological TNM stage and grade was assessed by Pearson's  $\chi^2$ -test. Above statistical analyses were performed by using IBM SPSS Statistics version 23 (IBM, USA). Statistical differences with p-values less than 0.05 were considered as significant. Noticeably, as to grade-relevant analyses, cases graded as G0 were excluded, well differentiated to moderate

differentiated cases were grouped as low grade, while moderate-to-poorly differentiated to poorly differentiated cases were grouped as high grade.

## 5.5 Cell lines

The pancreatic neuroendocrine tumor cell line BON-1 was grown in DMEM/F12 Ham (Life Technologies, Darmstadt, Germany) and QGP-1 cells were grown in RPMI 1640 (Life Technologies). The bronchial carcinoid cell line NCI-H727 cells were grown in RPMI 1640 (Life Technologies). All the cell lines were obtained from the University Medical Center of the Johannes Gutenberg University. All media were supplemented with 10% fetal bovine serum (Life Technologies) and 1% penicillin/streptomycin (Life Technologies). Cell lines were incubated at 37°C in a humidified atmosphere of 5% CO<sub>2</sub> and 95% air.

## 5.6 Cytotoxicity determination

The *in vitro* activity of ART was evaluated by resazurin reduction assay [227]. Aliquots of 5000 cells per well were seeded and treated with step-wise increasing concentrations from 0.003 to 100 µM ART (SAOKIM, Vĩnh Phúc, Vietnam) for 72 h in a 96-well plate followed by addition of 0.01% w/v resazurin sodium salt (Sigma-Aldrich, Taufkirchen, Germany) in distilled water for 4 h. Fluorescence signals generated from the metabolized product of resazurin were measured by an Infinite M2000 Pro plate reader (Tecan, Crailsheim, Germany). The log transformed 50% inhibition concentrations (logIC<sub>50</sub>) were calculated as mean ± standard deviations from three independent experiment with six parallel measurements each.

## 5.7 Microarray hybridization

Total RNA was extracted from BON-1 cells following treatment of 3 µM ART for 24 h, while QGP-1 and NCI-H727 cells were treated with 40 µM ART using the InviTrap Spin Universal RNA Mini Kit (STRATEC Molecular, Berlin, Germany) protocol. RNA concentrations were measured by NanoDrop 1000 (Biotechnologie, Erlangen, Germany). Microarray hybridizations were performed by the Genomics and Proteomics Core Facility at the German Cancer Research Center (DKFZ, Heidelberg). Briefly, aliquots of each 1 µg total RNA for both untreated and treated sample pairs were processed with Human HT-12 v4 Expression BeadChip Kits (Illumina, San Diego, CA, USA). All samples were analyzed in duplicates. Raw data were normalized with R using function `normalize.quantile` of `bioconductor` package `preprocessCore` (R Foundation for Statistical Computing, Vienna, Austria). Gene expressions were further evaluated by `Chipster 15` with 0.97 SD filter. Empirical Bayes and BH were applied as

significance calculation and correction method, respectively. Signaling networks and relationships among significantly regulated genes ( $p < 0.01$ ) were analyzed by Ingenuity Pathway Analysis (IPA, Ingenuity Systems, Redwood, CA, USA).

### **5.8 Quantitative real-time RT-PCR**

Quantitative real-time RT-PCR was applied to validate the microarray hybridization results. In total 6 significantly regulated genes from each cell line were selected from IPA analyses. Primers were designed for the selected genes and were synthesized by Eurofins MWG Operon (Ebersberg, Germany) (See supplementary Table S3). RNA samples used for microarray hybridization were reverse transcribed to cDNA according to a protocol of the RevertAid H Minus First Strand cDNA Synthesis Kit (Thermo Scientific, Darmstadt, Germany). Quantification of cDNA was subsequently performed on CFX384 Real-Time PCR Detection System (Bio-Rad, München, Germany) using Hot Start Taq EvaGreen qPCR Mix (Axon Scientific, Göttingen, Germany). The cDNA was initially denatured at 95 °C for 15 min followed by 40 cycles of strand separation at 95 °C for 15 s, annealing at 60 °C for 20 s and elongation at 72 °C for 1 min. All samples were analyzed in duplicate. The correlation between microarray hybridization and quantitative real-time RT-PCR results was obtained by Pearson linear regression and represented as R square.

### **5.9 Reactive oxygen species (ROS) generation**

Reactive oxygen species (ROS) were quantified with the fluorescent probe 2',7'-dichlorodihydrofluorescein diacetate (H2DCFH-DA), a chemically reduced form of fluorescein. The formation of highly fluorescent 2',7'-dichlorofluorescein following cleavage of the acetate groups by intracellular esterase and oxidation status was monitored by an Accuri C6 flow cytometer (Becton-Dickinson, Heidelberg, Germany) using the FL-1 detector<sup>16</sup>. Cells were harvested using 0.25% trypsin-EDTA (Life Technologies, Germany) upon reaching 70% confluency. Aliquots of  $1 \times 10^6$  cells were counted and incubated with 1  $\mu$ M H2DCFH-DA (Sigma-Aldrich, Taufkirchen, Germany) for 30 min in the dark at 37 °C followed by 500  $\mu$ M tert-butyl hydroperoxide (TBHP, Sigma-Aldrich) and ART at increasing concentrations (3, 6 and 9  $\mu$ M for BON-1 cells or 40, 60, and 80  $\mu$ M for QGP-1 and NCI-H727 cells, respectively) for 2 h treatment, respectively. N-acetylcysteine (20 mM) was used as antioxidant to reverse ROS generation. The experiments were repeated three times.

### 5.10 Detection of cell cycle arrest by flow cytometer

Aliquots of  $5 \times 10^5$  cells per well cells were seeded into 6-well plates for 24 h allowing attachment. The cells were subsequently treated with ART (3, 6 and 9  $\mu\text{M}$  for BON-1 cells and 40, 60 and 80  $\mu\text{M}$  for QGP-1 and NCI-H727 cells, respectively) for 24 h. Following harvest with 0.25% trypsin, cells were washed with cold PBS once and fixed in 1 mL cold 70% ethanol on ice for 4 h. Then, cells were washed twice with cold PBS followed by 100  $\mu\text{g}/\text{mL}$  RNase A (Sigma-Aldrich) treatment. Cells were stained with 50  $\mu\text{g}/\text{mL}$  propidium iodide (PI, Sigma-Aldrich) and detected with an Accuri C6 flow cytometer (Becton Dickinson) with the FL-2 detector<sup>16</sup>. Doxorubicin (DOXO, 100 nM) as established standard chemotherapy was applied as positive control. Results were obtained from three independent experiments and represented as mean  $\pm$  SD of the population percentage.

### 5.11 Ferroptosis inhibition

Aliquots of 5000 cells per well were seeded in 96-well plates for 24 h allowing attachment. Then the cells were pre-treated with 0.5  $\mu\text{M}$  iron chelator deferoxamine and 10  $\mu\text{M}$  ferroptosis inhibitor ferrostatin-1 (Sigma–Aldrich), respectively, for 2 h at 37 °C. Subsequent ART treatment was conducted as described above for cytotoxicity determination without removing deferoxamine and ferrostatin-1. Noticeably, we altered the treatment concentration range for NCI-H727 cells from 0.3 to 500  $\mu\text{M}$  in order to optimize the overall observation. Results were obtained from three independent experiments with each six parallel measurements and represented as area under the curve (AUC)  $\pm$  SD instead of IC<sub>50</sub> values due to the overlapping of curves at specific cell viability of 50%.

### 5.12 Autophagy inhibition

Aliquots of 5000 cells per well were seeded in a 96-well plate for 24 h allowing attachment and then pre-treated with 5 mM 3-methyladenine (3-MA, Sigma–Aldrich) or medium containing corresponding DMSO as control for 2 h at 37 °C prior to the application of subsequent ART at different concentrations (3, 6, 9, 10, 20, and 30  $\mu\text{M}$  for BON-1 cells and 20, 40, 60, 80, 100 and 120  $\mu\text{M}$  for QGP-1 and NCI-H727 cells, respectively) for 24 h, 48 h and 72 h respectively. Cell viability was determined as described above for cytotoxicity determination without removing 3-methyladenine.

### 5.13 Apoptosis detection with flow cytometer

Aliquots of  $5 \times 10^5$  cells per well were seeded into 6-well plates and incubated for 24 h allowing attachment. Cells were subsequently treated with ART (10, 20 and 30  $\mu\text{M}$  for BON-1 cells and 40, 60, 80  $\mu\text{M}$  for QGP-1 and NCI-H727 cells, respectively) for 24, 48 and 72 h followed by double-staining with propidium iodide (PI) and annexin V-APC using the Apoptosis Detection Kit APC (Thermo Fisher Scientific) according to the manufacturer's protocol. Data were obtained using an Accuri C6 flow cytometer (Becton Dickinson). Fluorescence signals from PI and annexin V-APC staining were collected by using the FL-3 and FL-4 detectors, respectively. The experiments were repeated three times.

### 5.14 In situ apoptosis detection

Aliquots of  $5 \times 10^5$  cells per well were seeded into 6-well plates and incubated for 24 h allowing attachment. Cells were subsequently treated with ART (10, 20 and 30  $\mu\text{M}$  for BON-1 cells and 40, 60 and 80  $\mu\text{M}$  for QGP-1 and NCI-H727 cells, respectively) for 24 h and 48 h. DNA fragmentation was detected with a specific digoxigenin-nucleotide label on 3'OH strand termini, which allowed binding of a peroxidase-conjugated anti-digoxigenin antibody (TUNEL assay). Bound peroxidase further converted the chromogenic substrate 3,3'-diaminobenzidine tetrahydrochloride (DAB, Thermo Scientific) into a permanent brown-colored product. The experiments were conducted by using ApopTag peroxidase in situ apoptosis detection kit (Merck, Darmstadt, Germany). Each experiment was repeated three times.

### 5.15 Western blotting

Cells were treated with different concentration of ART (3, 6, 9, 10, 20, and 30  $\mu\text{M}$  for BON-1 cells and 20, 40, 60, 80, 100 and 120  $\mu\text{M}$  for QGP-1 and NCI-H727 cells, respectively) and incubated for 24 h and 48 h. Total protein extraction was performed using M-PER mammalian protein extraction reagent (Thermo Scientific) with addition of a protease inhibitor cocktail (Thermo Scientific) and a phosphatase inhibitor cocktail (Thermo Scientific). Several antibodies regarding ER-stress induced autophagy (eIF2 $\alpha$ , Phospho-eIF2 $\alpha$ , Atg12 and LC3B from Cell Signaling, Frankfurt, Germany), apoptosis (PARP, Caspase 3, Caspase 7, Caspase 8 and Caspase 9 from Cell signaling) and cell cycle arrest (p21 from Cell Signaling) were applied to investigate the cellular modes of action of ART in NET cells.  $\beta$ -Actin was included as internal control (Cell Signaling). All antibodies were applied at a 1:1000 dilution in 5% albumin

fraction V (Carl Roth GmbH, Karlsruhe, Germany). Quantification of bands intensity was performed with ImageJ and described as mean  $\pm$  SEM from three repetitions.

### **5.16 Mitochondrial membrane potential detection**

Aliquots of  $5 \times 10^5$  cells per well were seeded into 6-well plates for 24 h allowing attachment. The BON-1 cells were subsequently treated with 3, 6, 9, 10, 20 and 30  $\mu$ M ART for 24 h and 48 h, respectively. Mitochondrial membrane potential was detected with tetraethylbenzimidazolylcarbocyanine iodide (JC-1) probe provided with the mitochondria staining kit (Sigma-Aldrich). JC-1 accumulates in mitochondria under normal conditions due to the electrochemical potential gradient which gives a red fluorescence but disperses throughout the entire cells if the mitochondria are disrupted which gives green fluorescence. The experiment was conducted according to the manufacturer with minor adjustment. Cells were harvested with 0.25% trypsin and washed once with PBS prior to application of JC-1 and detected with flow cytometer. JC-1 aggregates were detected with the FL-2 detector while JC-1 monomers were detected with FL-1. The results were obtained from three repetitions.

## 6 Summary and conclusion

The study emphasized on two parts. The first part aimed at assessing the role of a canonic oncogene encoding protein EGFR in diverse tumor types. In this part, we successfully distinguished its expression pattern in different solid neoplastic types and suggested its superior function in the nascent stage than the advanced stage during the carcinogenesis. These findings may be especially valuable in guiding EGFR targeted therapies in clinic.

Inspired by its broad expression in different solid tumors, we were exceptionally interested in investigating its potential as a therapeutic target in a less frequent tumor type, namely NETs, which currently lack effective treatment. As demonstrated by multiple elegant studies, EGFR is highly expressed and activated in NETs. Some TKIs has been already implicated in NETs treatment in clinic trials. However, resistance to gefitinib and erlotinib has emerged in NETs due to a lack of activating mutations and occurrence of the resistance mutation T790M. Even worse, the third generation TKI osimertinib which specifically targets at T790M EGFR fails to overcome resistance, because of the phenotypic neuroendocrine transformation in NETs [10,12]. As to EGFR directed antibodies, no clear evidence was available regarding their effect on NETs. However, diverse mechanisms attributing to cetuximab (a typical EGFR targeting antibody) resistance have been revealed [13]. Therefore, we were encouraged to investigate an artemisinin-like compound, ART, which showed inhibitory potential against EGFR and reluctance in drug resistance development. Moreover, ART can impede the heterodimerization of EGFR with HER2 [19] and inhibits angiogenesis [228], which are resistance mediating mechanisms proposed for cetuximab. Three EGFR-expressing NET cell lines BON-1, QGP-1 and NCI-H727 were utilized for investigation. We discovered a convergent network involving ER-stress induction, which can possibly caused by the EGFR inhibition [205], followed by p21-regulated multiple modes of cell death. Therefore, we highlighted the possibility of ART application in NETs treatment.

Taken all together, the taken home messages we would like to strengthen are as the following:

- EGFR expresses in a broad range of solid tumors. Hence, the anti-EGFR therapies should have wider span of application.
- EGFR plays a more important role in the nascent stage than the advanced stage during carcinogenesis, which on one hand may guide its application in clinic, on the other hand partially explain the drug resistance development.

- 
- Downstream of EGFR, ART induces multiple cell death modes in NET cell lines, which are regulated by p21.
  - ER-stress inducer may be especially potent in the NETs suppression.

## 7 Future perspective

The present study has shed light on the role of EGFR in early carcinogenesis and provided novel ideas on its clinic implementation. Besides, the effect of ART in the less frequent cancer type, NETs, was investigated.

However, these findings reveal several limitations. Firstly, the inadequate and heterogeneous information on the available datasets from GEO and Oncomine makes it extremely difficult to draw an overall conclusion about the prognostic value of *EGFR* mRNA. Secondly, an issue that was not addressed in this study was the *in vivo* effect of ART on NETs, if the drug dynamics and immune environment were put into consideration. Further investigations regarding *in vivo* study are strongly recommended. Thirdly, this research has thrown up many open questions like the exact target of ART and mechanism of p21 regulation. Another possible area of future research would be investigation on multiple ER-stress inducers in the treatment of NETs.

## 8 References

- [1] J. A. Gilbert, L. J. Adhikari, R. V. Lloyd, J. Rubin, P. Haluska, J. M. Carboni, M. M. Gottardis, M. M. Ames, *Molecular markers for novel therapies in neuroendocrine (carcinoid) tumors*, *Endocrine-related cancer* **2010**, *17*, pp. 623–636.
- [2] P. L. Peghini, M. Iwamoto, M. Raffeld, Y.-J. Chen, S. U. Goebel, J. Serrano, R. T. Jensen, *Overexpression of epidermal growth factor and hepatocyte growth factor receptors in a proportion of gastrinomas correlates with aggressive growth and lower curability*, *Clinical cancer research : an official journal of the American Association for Cancer Research* **2002**, *8*, pp. 2273–2285.
- [3] T. Shah, D. Hochhauser, R. Frow, A. Quaglia, A. P. Dhillon, M. E. Caplin, *Epidermal growth factor receptor expression and activation in neuroendocrine tumours*, *Journal of neuroendocrinology* **2006**, *18*, pp. 355–360.
- [4] A. Di Florio, V. Sancho, P. Moreno, G. Delle Fave, R. T. Jensen, *Gastrointestinal hormones stimulate growth of Foregut Neuroendocrine Tumors by transactivating the EGF receptor*, *Biochimica et biophysica acta* **2013**, *1833*, pp. 573–582.
- [5] J. A. Gilbert, L. J. Adhikari, R. V. Lloyd, T. R. Halfdanarson, M. H. Muders, M. M. Ames, *Molecular markers for novel therapeutic strategies in pancreatic endocrine tumors*, *Pancreas* **2013**, *42*, pp. 411–421.
- [6] M. Höpfner, A. P. Sutter, B. Gerst, M. Zeitz, H. Scherübl, *A novel approach in the treatment of neuroendocrine gastrointestinal tumours. Targeting the epidermal growth factor receptor by gefitinib (ZD1839)*, *British journal of cancer* **2003**, *89*, pp. 1766–1775.
- [7] F. Aroldi, P. Bertocchi, F. Meriggi, C. Abeni, C. Ogliosi, L. Rota, C. Zambelli, C. Bnà, A. Zaniboni, *Tyrosine Kinase Inhibitors in EGFR-Mutated Large-Cell Neuroendocrine Carcinoma of the Lung? A Case Report*, *Case reports in oncology* **2014**, *7*, pp. 478–483.
- [8] A. D. Herrera-Martínez, J. Hofland, L. J. Hofland, T. Brabander, F. A. L. M. Eskens, M. A. Gálvez Moreno, R. M. Luque, J. P. Castaño, W. W. de Herder, R. A. Fielders, *Targeted Systemic Treatment of Neuroendocrine Tumors*, *Drugs* **2019**, *79*, pp. 21–42.
- [9] M. Kidd, S. Schimmack, B. Lawrence, D. Alaimo, I. M. Modlin, *EGFR/TGF $\alpha$  and TGF $\beta$ /CTGF Signaling in Neuroendocrine Neoplasia*, *Neuroendocrinology* **2013**, *97*, pp. 35–44.
- [10] J. A. Gilbert, R. V. Lloyd, M. M. Ames, *Lack of mutations in EGFR in gastroenteropancreatic neuroendocrine tumors*, *The New England journal of medicine* **2005**, *353*, pp. 209–210.

- [11] T. Makino, T. Mikami, Y. Hata, H. Otsuka, S. Koezuka, K. Isobe, N. Tochigi, K. Shibuya, S. Homma, A. Iyoda, *Comprehensive Biomarkers for Personalized Treatment in Pulmonary Large Cell Neuroendocrine Carcinoma, The Annals of thoracic surgery* **2016**, *102*, pp. 1694–1701.
- [12] S. Baglivo, V. Ludovini, A. Sidoni, G. Metro, B. Ricciuti, A. Siggillino, A. Rebonato, S. Messina, L. Crinò, R. Chiari, *Large Cell Neuroendocrine Carcinoma Transformation and EGFR-T790M Mutation as Coexisting Mechanisms of Acquired Resistance to EGFR-TKIs in Lung Cancer, Mayo Clinic proceedings* **2017**, *92*, pp. 1304–1311.
- [13] T. M. Brand, M. Iida, D. L. Wheeler, *Molecular mechanisms of resistance to the EGFR monoclonal antibody cetuximab, Cancer biology & therapy* **2011**, *11*, pp. 777–792.
- [14] H. Ma, Q. Yao, A.-M. Zhang, S. Lin, X.-X. Wang, L. Wu, J.-G. Sun, Z.-T. Chen, *The effects of artesunate on the expression of EGFR and ABCG2 in A549 human lung cancer cells and a xenograft model, Molecules (Basel, Switzerland)* **2011**, *16*, pp. 10556–10569.
- [15] T. Efferth, A. Sauerbrey, A. Olbrich, E. Gebhart, P. Rauch, H. O. Weber, J. G. Hengstler, M.-E. Halatsch, M. Volm, K. D. Tew et al., *Molecular modes of action of artesunate in tumor cell lines, Molecular pharmacology* **2003**, *64*, pp. 382–394.
- [16] V. B. Konkimalla, J. A. McCubrey, T. Efferth, *The role of downstream signaling pathways of the epidermal growth factor receptor for Artesunate's activity in cancer cells, CCDT* **2009**, *9*, pp. 72–80.
- [17] S. Krishna, S. Ganapathi, I. C. Ster, M. E. M. Saeed, M. Cowan, C. Finlayson, H. Kovacevics, H. Jansen, P. G. Kremsner, T. Efferth et al., *A Randomised, Double Blind, Placebo-Controlled Pilot Study of Oral Artesunate Therapy for Colorectal Cancer, EBioMedicine* **2015**, *2*, pp. 82–90.
- [18] F.-W. Michaelsen, M. E. M. Saeed, J. Schwarzkopf, T. Efferth, *Activity of Artemisia annua and artemisinin derivatives, in prostate carcinoma, Phytomedicine : international journal of phytotherapy and phytopharmacology* **2015**, *22*, pp. 1223–1231.
- [19] A. L. Greenshields, W. Fernando, D. W. Hoskin, *The anti-malarial drug artesunate causes cell cycle arrest and apoptosis of triple-negative MDA-MB-468 and HER2-enriched SK-BR-3 breast cancer cells, Experimental and molecular pathology* **2019**, *107*, pp. 10–22.
- [20] T. Efferth, *Cancer combination therapy of the sesquiterpenoid artesunate and the selective EGFR-tyrosine kinase inhibitor erlotinib, Phytomedicine : international journal of phytotherapy and phytopharmacology* **2017**, *37*, pp. 58–61.

- [21] T. Efferth, T. Ramirez, E. Gebhart, M.-E. Halatsch, *Combination treatment of glioblastoma multiforme cell lines with the anti-malarial artesunate and the epidermal growth factor receptor tyrosine kinase inhibitor OSI-774*, *Biochemical pharmacology* **2004**, *67*, pp. 1689–1700.
- [22] R. S. Miller, Q. Li, L. R. Cantilena, K. J. Leary, G. A. Saviolakis, V. Melendez, B. Smith, P. J. Weina, *Pharmacokinetic profiles of artesunate following multiple intravenous doses of 2, 4, and 8 mg/kg in healthy volunteers*, *Malaria journal* **2012**, *11*, p. 255.
- [23] A. M. Dondorp, F. Nosten, P. Yi, D. Das, A. P. Phyto, J. Tarning, K. M. Lwin, F. Arie, W. Hanpithakpong, S. J. Lee et al., *Artemisinin resistance in Plasmodium falciparum malaria*, *The New England journal of medicine* **2009**, *361*, pp. 455–467.
- [24] T. Efferth, *From ancient herb to modern drug*, *Seminars in cancer biology* **2017**, *46*, pp. 65–83.
- [25] N. J. White, T. T. Hien, F. H. Nosten, *A Brief History of Qinghaosu*, *Trends in parasitology* **2015**, *31*, pp. 607–610.
- [26] Y. Lubell, S. Yeung, A. M. Dondorp, N. P. Day, F. Nosten, E. Tjitra, M. Abul Faiz, E. B. Yunus, N. M. Anstey, S. K. Mishra et al., *Cost-effectiveness of artesunate for the treatment of severe malaria*, *Tropical medicine & international health : TM & IH* **2009**, *14*, pp. 332–337.
- [27] L. L. Capasso, *Antiquity of cancer*, *International journal of cancer* **2005**, *113*, pp. 2–13.
- [28] S. I. Hajdu, *Pathfinders in oncology from ancient times to the end of the Middle Ages*, *Cancer* **2016**, *122*, pp. 1638–1646.
- [29] N. Papavramidou, T. Papavramidis, T. Demetriou, *Ancient Greek and Greco-Roman methods in modern surgical treatment of cancer*, *Annals of surgical oncology* **2010**, *17*, pp. 665–667.
- [30] F. Bray, J. Ferlay, I. Soerjomataram, R. L. Siegel, L. A. Torre, A. Jemal, *Global cancer statistics 2018*, *CA: a cancer journal for clinicians* **2018**, *68*, pp. 394–424.
- [31] F. Macdonald, A. G. Casson, C. H. J. Ford, *Molecular biology of cancer*, BIOS Scientific Publishers, London, **2005**.
- [32] Y. A. Fouad, C. Aanei, *Revisiting the hallmarks of cancer*, *American journal of cancer research* **2017**, *7*, pp. 1016–1036.
- [33] D. Hanahan, R. A. Weinberg, *The hallmarks of cancer*, *Cell* **2000**, *100*, pp. 57–70.
- [34] D. Hanahan, R. A. Weinberg, *Hallmarks of cancer*, *Cell* **2011**, *144*, pp. 646–674.

- [35] A. P. Feinberg, M. A. Koldobskiy, A. Göndör, *Epigenetic modulators, modifiers and mediators in cancer aetiology and progression*, *Nature reviews. Genetics* **2016**, *17*, pp. 284–299.
- [36] C. Vicente-Dueñas, I. Romero-Camarero, C. Cobaleda, I. Sánchez-García, *Function of oncogenes in cancer development*, *The EMBO journal* **2013**, *32*, pp. 1502–1513.
- [37] R. J. Bevan, P. T. C. Harrison, *Threshold and non-threshold chemical carcinogens*, *Regulatory toxicology and pharmacology : RTP* **2017**, *88*, pp. 291–302.
- [38] P. Boffetta, F. Islami, *The contribution of molecular epidemiology to the identification of human carcinogens*, *Annals of oncology : official journal of the European Society for Medical Oncology* **2013**, *24*, pp. 901–908.
- [39] P. Greenwald, *NCI cancer prevention and control research*, *Preventive medicine* **1993**, *22*, pp. 642–660.
- [40] V. Vedham, R. L. Divi, V. L. Starks, M. Verma, *Multiple infections and cancer*, *Technology in cancer research & treatment* **2014**, *13*, pp. 177–194.
- [41] M. C. White, L. A. Peipins, M. Watson, K. F. Trivers, D. M. Holman, J. L. Rodriguez, *Cancer prevention for the next generation*, *The Journal of adolescent health : official publication of the Society for Adolescent Medicine* **2013**, *52*, S1-7.
- [42] A. Diaz de Leon, I. Pedrosa, *Imaging and Screening of Kidney Cancer*, *Radiologic clinics of North America* **2017**, *55*, pp. 1235–1250.
- [43] M. S. Grandhi, A. K. Kim, S. M. Ronnekleiv-Kelly, I. R. Kamel, M. A. Ghasebeh, T. M. Pawlik, *Hepatocellular carcinoma*, *Surgical oncology* **2016**, *25*, pp. 74–85.
- [44] M. Shamsi, J. Pirayesh Islamian, *Breast cancer*, *Nuclear medicine review. Central & Eastern Europe* **2017**, *20*, pp. 45–48.
- [45] R. Aarthy, S. Mani, S. Velusami, S. Sundarsingh, T. Rajkumar, *Role of Circulating Cell-Free DNA in Cancers*, *Molecular diagnosis & therapy* **2015**, *19*, pp. 339–350.
- [46] Y. Pan, G. Liu, F. Zhou, B. Su, Y. Li, *DNA methylation profiles in cancer diagnosis and therapeutics*, *Clinical and experimental medicine* **2018**, *18*, pp. 1–14.
- [47] A.-L. Volckmar, H. Sülthmann, A. Riediger, T. Fioretos, P. Schirmacher, V. Endris, A. Stenzinger, S. Dietz, *A field guide for cancer diagnostics using cell-free DNA*, *Genes, chromosomes & cancer* **2018**, *57*, pp. 123–139.
- [48] M.-S. Zeng, *Noncoding RNAs in Cancer Diagnosis*, *Advances in experimental medicine and biology* **2016**, *927*, pp. 391–427.

- [49] L. R. Duska, E. C. Kohn, *The new classifications of ovarian, fallopian tube, and primary peritoneal cancer and their clinical implications*, *Annals of oncology : official journal of the European Society for Medical Oncology* **2017**, 28, viii8-viii12.
- [50] L. Bertero, F. Massa, J. Metovic, R. Zanetti, I. Castellano, U. Ricardi, M. Papotti, P. Cassoni, *Eighth Edition of the UICC Classification of Malignant Tumours*, *Virchows Archiv : an international journal of pathology* **2018**, 472, pp. 519–531.
- [51] J. Galon, F. Pagès, F. M. Marincola, H. K. Angell, M. Thurin, A. Lugli, I. Zlobec, A. Berger, C. Bifulco, G. Botti et al., *Cancer classification using the Immunoscore*, *Journal of translational medicine* **2012**, 10, p. 205.
- [52] D. H. Johnson, J. H. Schiller, P. A. Bunn, *Recent clinical advances in lung cancer management*, *Journal of clinical oncology : official journal of the American Society of Clinical Oncology* **2014**, 32, pp. 973–982.
- [53] O. Peart, *Breast intervention and breast cancer treatment options*, *Radiologic technology* **2015**, 86, 535M-558M; quiz 559-62.
- [54] J. Qiao, Z. Liu, Y.-X. Fu, *Adapting conventional cancer treatment for immunotherapy*, *Journal of molecular medicine (Berlin, Germany)* **2016**, 94, pp. 489–495.
- [55] J. Zugazagoitia, C. Guedes, S. Ponce, I. Ferrer, S. Molina-Pinelo, L. Paz-Ares, *Current Challenges in Cancer Treatment*, *Clinical therapeutics* **2016**, 38, pp. 1551–1566.
- [56] B. Oronsky, P. C. Ma, D. Morgensztern, C. A. Carter, *Nothing But NET*, *Neoplasia (New York, N.Y.)* **2017**, 19, pp. 991–1002.
- [57] A. Dasari, C. Shen, D. Halperin, B. Zhao, S. Zhou, Y. Xu, T. Shih, J. C. Yao, *Trends in the Incidence, Prevalence, and Survival Outcomes in Patients With Neuroendocrine Tumors in the United States*, *JAMA oncology* **2017**, 3, pp. 1335–1342.
- [58] S. Pedraza-Arévalo, M. D. Gahete, E. Alors-Pérez, R. M. Luque, J. P. Castaño, *Multilayered heterogeneity as an intrinsic hallmark of neuroendocrine tumors*, *Reviews in endocrine & metabolic disorders* **2018**, 19, pp. 179–192.
- [59] D. Man, J. Wu, Z. Shen, X. Zhu, *Prognosis of patients with neuroendocrine tumor*, *Cancer management and research* **2018**, 10, pp. 5629–5638.
- [60] A. E. Hendifar, A. M. Marchevsky, R. Tuli, *Neuroendocrine Tumors of the Lung*, *Journal of thoracic oncology : official publication of the International Association for the Study of Lung Cancer* **2017**, 12, pp. 425–436.
- [61] R. A. Ramirez, A. Chauhan, J. Gimenez, K. E. H. Thomas, I. Kokodis, B. A. Voros, *Management of pulmonary neuroendocrine tumors*, *Reviews in endocrine & metabolic disorders* **2017**, 18, pp. 433–442.

- [62] A. O. Oladejo, *GASTROENTEROPANCREATIC NEUROENDOCRINE TUMORS (GEP-NETS) - APPROACH TO DIAGNOSIS AND MANAGEMENT*, *Annals of Ibadan postgraduate medicine* **2009**, 7, pp. 29–33.
- [63] C. Shen, A. Dasari, Y. Xu, S. Zhou, D. Gu, Y. Chu, D. M. Halperin, Y. T. Shih, J. C. Yao, *Pre-existing Symptoms and Healthcare Utilization Prior to Diagnosis of Neuroendocrine Tumors*, *Scientific reports* **2018**, 8, p. 16863.
- [64] A. I. Vinik, C. Chaya, *Clinical Presentation and Diagnosis of Neuroendocrine Tumors*, *Hematology/oncology clinics of North America* **2016**, 30, pp. 21–48.
- [65] J. Crona, B. Skogseid, *GEP- NETS UPDATE*, *European journal of endocrinology* **2016**, 174, R275-90.
- [66] I. Uri, S. Avniel-Polak, D. J. Gross, S. Grozinsky-Glasberg, *Update in the Therapy of Advanced Neuroendocrine Tumors*, *Current treatment options in oncology* **2017**, 18, p. 72.
- [67] J. Hofland, W. T. Zandee, W. W. de Herder, *Role of biomarker tests for diagnosis of neuroendocrine tumours*, *Nature reviews. Endocrinology* **2018**, 14, pp. 656–669.
- [68] D. L. Chan, S. J. Clarke, C. I. Diakos, P. J. Roach, D. L. Bailey, S. Singh, N. Pavlakis, *Prognostic and predictive biomarkers in neuroendocrine tumours*, *Critical reviews in oncology/hematology* **2017**, 113, pp. 268–282.
- [69] J. Y. Kim, S.-M. Hong, J. Y. Ro, *Recent updates on grading and classification of neuroendocrine tumors*, *Annals of diagnostic pathology* **2017**, 29, pp. 11–16.
- [70] G. Rindi, D. S. Klimstra, B. Abedi-Ardekani, S. L. Asa, F. T. Bosman, E. Brambilla, K. J. Busam, R. R. de Krijger, M. Dietel, A. K. El-Naggar et al., *A common classification framework for neuroendocrine neoplasms*, *Modern pathology : an official journal of the United States and Canadian Academy of Pathology, Inc* **2018**, 31, pp. 1770–1786.
- [71] I. M. Modlin, L. Bodei, M. Kidd, *Neuroendocrine tumor biomarkers*, *Best practice & research. Clinical endocrinology & metabolism* **2016**, 30, pp. 59–77.
- [72] I. M. Modlin, K. Oberg, A. Taylor, I. Drozdov, L. Bodei, M. Kidd, *Neuroendocrine tumor biomarkers*, *Neuroendocrinology* **2014**, 100, pp. 265–277.
- [73] M. Dior, J. Dreanic, C. Prioux-Klotz, B. Brieuau, C. Brezault, R. Coriat, *Tumeurs neuroendocrines de l'intestin grêle*, *Presse medicale (Paris, France : 1983)* **2017**, 46, pp. 4–10.
- [74] T. Ito, L. Lee, R. T. Jensen, *Treatment of symptomatic neuroendocrine tumor syndromes*, *Expert opinion on pharmacotherapy* **2016**, 17, pp. 2191–2205.

- [75] P. L. Kunz, *Carcinoid and neuroendocrine tumors*, *Journal of clinical oncology : official journal of the American Society of Clinical Oncology* **2015**, *33*, pp. 1855–1863.
- [76] J. R. Strosberg, T. R. Halfdanarson, A. M. Bellizzi, J. A. Chan, J. S. Dillon, A. P. Heaney, P. L. Kunz, T. M. O'Dorisio, R. Salem, E. Segelov et al., *The North American Neuroendocrine Tumor Society Consensus Guidelines for Surveillance and Medical Management of Midgut Neuroendocrine Tumors*, *Pancreas* **2017**, *46*, pp. 707–714.
- [77] S. Cohen, *The stimulation of epidermal proliferation by a specific protein (EGF)*, *Developmental biology* **1965**, *12*, pp. 394–407.
- [78] S. Cohen, G. Carpenter, L. King, *Epidermal growth factor-receptor-protein kinase interactions. Co-purification of receptor and epidermal growth factor-enhanced phosphorylation activity*, *The Journal of biological chemistry* **1980**, *255*, pp. 4834–4842.
- [79] S. Cohen, H. Ushiro, C. Stoscheck, M. Chinkers, *A native 170,000 epidermal growth factor receptor-kinase complex from shed plasma membrane vesicles*, *The Journal of biological chemistry* **1982**, *257*, pp. 1523–1531.
- [80] H. Ushiro, S. Cohen, *Identification of phosphotyrosine as a product of epidermal growth factor-activated protein kinase in A-431 cell membranes*, *The Journal of biological chemistry* **1980**, *255*, pp. 8363–8365.
- [81] M. J. Wieduwilt, M. M. Moasser, *The epidermal growth factor receptor family*, *Cellular and molecular life sciences : CMLS* **2008**, *65*, pp. 1566–1584.
- [82] N. E. Hynes, H. A. Lane, *ERBB receptors and cancer*, *Nature reviews. Cancer* **2005**, *5*, pp. 341–354.
- [83] P. Wee, Z. Wang, *Epidermal Growth Factor Receptor Cell Proliferation Signaling Pathways*, *Cancers* **2017**, *9*.
- [84] J. L. Reiter, D. W. Threadgill, G. D. Eley, K. E. Strunk, A. J. Danielsen, C. S. Sinclair, R. S. Pearsall, P. J. Green, D. Yee, A. L. Lampland et al., *Comparative genomic sequence analysis and isolation of human and mouse alternative EGFR transcripts encoding truncated receptor isoforms*, *Genomics* **2001**, *71*, pp. 1–20.
- [85] A. Guillaudeau, K. Durand, B. Bessette, A. Chaunavel, I. Pommepeuy, F. Progetti, S. Robert, F. Caire, H. Rabinovitch-Chable, F. Labrousse, *EGFR soluble isoforms and their transcripts are expressed in meningiomas*, *PloS one* **2012**, *7*, e37204.
- [86] A. Ullrich, L. Coussens, J. S. Hayflick, T. J. Dull, A. Gray, A. W. Tam, J. Lee, Y. Yarden, T. A. Libermann, J. Schlessinger, *Human epidermal growth factor receptor cDNA sequence and aberrant expression of the amplified gene in A431 epidermoid carcinoma cells*, *Nature* **1984**, *309*, pp. 418–425.

- [87] R. Roskoski, *The ErbB/HER family of protein-tyrosine kinases and cancer*, *Pharmacological research* **2014**, 79, pp. 34–74.
- [88] M. Bajaj, M. D. Waterfield, J. Schlessinger, W. R. Taylor, T. Blundell, *On the tertiary structure of the extracellular domains of the epidermal growth factor and insulin receptors*, *Biochimica et Biophysica Acta (BBA) - Protein Structure and Molecular Enzymology* **1987**, 916, pp. 220–226.
- [89] H. Ogiso, R. Ishitani, O. Nureki, S. Fukai, M. Yamanaka, J.-H. Kim, K. Saito, A. Sakamoto, M. Inoue, M. Shirouzu et al., *Crystal Structure of the Complex of Human Epidermal Growth Factor and Receptor Extracellular Domains*, *Cell* **2002**, 110, pp. 775–787.
- [90] E. R. Purba, E.-I. Saita, I. N. Maruyama, *Activation of the EGF Receptor by Ligand Binding and Oncogenic Mutations*, *Cells* **2017**, 6.
- [91] K. M. Ferguson, M. B. Berger, J. M. Mendrola, H.-S. Cho, D. J. Leahy, M. A. Lemmon, *EGF Activates Its Receptor by Removing Interactions that Autoinhibit Ectodomain Dimerization*, *Molecular Cell* **2003**, 11, pp. 507–517.
- [92] K. R. Schmitz, A. Bagchi, R. C. Roovers, P. M. P. van Bergen en Henegouwen, K. M. Ferguson, *Structural evaluation of EGFR inhibition mechanisms for nanobodies/VHH domains*, *Structure (London, England : 1993)* **2013**, 21, pp. 1214–1224.
- [93] H. Sihto, M. Puputti, L. Pulli, O. Tynninen, W. Koskinen, L.-M. Aaltonen, M. Tanner, T. Böhling, T. Visakorpi, R. Bützow et al., *Epidermal growth factor receptor domain II, IV, and kinase domain mutations in human solid tumors*, *Journal of molecular medicine (Berlin, Germany)* **2005**, 83, pp. 976–983.
- [94] A. Ullrich, L. Coussens, J. S. Hayflick, T. J. Dull, A. Gray, A. W. Tam, J. Lee, Y. Yarden, T. A. Libermann, J. Schlessinger et al., *Human epidermal growth factor receptor cDNA sequence and aberrant expression of the amplified gene in A431 epidermoid carcinoma cells*, *Nature* **1984**, 309, pp. 418–425.
- [95] K. M. Ferguson, *Structure-based view of epidermal growth factor receptor regulation*, *Annual review of biophysics* **2008**, 37, pp. 353–373.
- [96] M. Abe, Y. Kuroda, M. Hirose, Y. Watanabe, M. Nakano, T. Handa, *Inhibition of autophosphorylation of epidermal growth factor receptor by small peptides in vitro*, *British journal of pharmacology* **2006**, 147, pp. 402–411.
- [97] I. N. Maruyama, *Mechanisms of activation of receptor tyrosine kinases*, *Cells* **2014**, 3, pp. 304–330.

- [98] J. Stamos, M. X. Sliwkowski, C. Eigenbrot, *Structure of the epidermal growth factor receptor kinase domain alone and in complex with a 4-anilinoquinazoline inhibitor*, *The Journal of biological chemistry* **2002**, 277, pp. 46265–46272.
- [99] M. A. Hasenahuer, G. P. Barletta, S. Fernandez-Alberti, G. Parisi, M. S. Fornasari, *Pockets as structural descriptors of EGFR kinase conformations*, *PloS one* **2017**, 12, e0189147.
- [100] A. Kumar, E. T. Petri, B. Halmos, T. J. Boggon, *Structure and clinical relevance of the epidermal growth factor receptor in human cancer*, *Journal of clinical oncology : official journal of the American Society of Clinical Oncology* **2008**, 26, pp. 1742–1751.
- [101] D. A. Tice, J. S. Biscardi, A. L. Nickles, S. J. Parsons, *Mechanism of biological synergy between cellular Src and epidermal growth factor receptor*, *Proceedings of the National Academy of Sciences of the United States of America* **1999**, 96, pp. 1415–1420.
- [102] K. S. Gajiwala, *EGFR*, *Protein science : a publication of the Protein Society* **2013**, 22, pp. 995–999.
- [103] K. Gill, J. L. Macdonald-Obermann, L. J. Pike, *Epidermal growth factor receptors containing a single tyrosine in their C-terminal tail bind different effector molecules and are signaling-competent*, *The Journal of biological chemistry* **2017**, 292, pp. 20744–20755.
- [104] M. R. Schneider, E. Wolf, *The epidermal growth factor receptor ligands at a glance*, *Journal of cellular physiology* **2009**, 218, pp. 460–466.
- [105] S. Rayego-Mateos, R. Rodrigues-Diez, J. L. Morgado-Pascual, F. Valentijn, J. M. Valdivielso, R. Goldschmeding, M. Ruiz-Ortega, *Role of Epidermal Growth Factor Receptor (EGFR) and Its Ligands in Kidney Inflammation and Damage*, *Mediators of inflammation* **2018**, 2018, p. 8739473.
- [106] J. Chen, F. Zeng, S. J. Forrester, S. Eguchi, M.-Z. Zhang, R. C. Harris, *Expression and Function of the Epidermal Growth Factor Receptor in Physiology and Disease*, *Physiological Reviews* **2016**, 96, pp. 1025–1069.
- [107] W. Han, H.-W. Lo, *Landscape of EGFR signaling network in human cancers*, *Cancer letters* **2012**, 318, pp. 124–134.
- [108] Z. Xie, Y. Chen, E.-Y. Liao, Y. Jiang, F.-Y. Liu, S. D. Pennypacker, *Phospholipase C-gamma1 is required for the epidermal growth factor receptor-induced squamous cell carcinoma cell mitogenesis*, *Biochemical and biophysical research communications* **2010**, 397, pp. 296–300.

- [109] B. Margolis, N. Li, A. Koch, M. Mohammadi, D. R. Hurwitz, A. Zilberstein, A. Ullrich, T. Pawson, J. Schlessinger, *The tyrosine phosphorylated carboxyterminus of the EGF receptor is a binding site for GAP and PLC-gamma*, *The EMBO journal* **1990**, *9*, pp. 4375–4380.
- [110] P. Chen, H. Xie, M. C. Sekar, K. Gupta, A. Wells, *Epidermal growth factor receptor-mediated cell motility*, *The Journal of cell biology* **1994**, *127*, pp. 847–857.
- [111] J. Schlessinger, *Phospholipase Cgamma activation and phosphoinositide hydrolysis are essential for embryonal development*, *Proceedings of the National Academy of Sciences of the United States of America* **1997**, *94*, pp. 2798–2799.
- [112] H. Xie, M. A. Pallero, K. Gupta, P. Chang, M. F. Ware, W. Witke, D. J. Kwiatkowski, D. A. Lauffenburger, J. E. Murphy-Ullrich, A. Wells, *EGF receptor regulation of cell motility*, *Journal of cell science* **1998**, *111 ( Pt 5)*, pp. 615–624.
- [113] T. Basu, P. H. Warne, J. Downward, *Role of Shc in the activation of Ras in response to epidermal growth factor and nerve growth factor*, *Oncogene* **1994**, *9*, pp. 3483–3491.
- [114] B. Margolis, E. Y. Skolnik, *Activation of Ras by receptor tyrosine kinases*, *Journal of the American Society of Nephrology : JASN* **1994**, *5*, pp. 1288–1299.
- [115] M. Rojas, S. Yao, Y. Z. Lin, *Controlling epidermal growth factor (EGF)-stimulated Ras activation in intact cells by a cell-permeable peptide mimicking phosphorylated EGF receptor*, *The Journal of biological chemistry* **1996**, *271*, pp. 27456–27461.
- [116] F. Marampon, C. Ciccarelli, B. M. Zani, *Down-regulation of c-Myc following MEK/ERK inhibition halts the expression of malignant phenotype in rhabdomyosarcoma and in non muscle-derived human tumors*, *Molecular cancer* **2006**, *5*, p. 31.
- [117] Y. Wang, R. Prywes, *Activation of the c-fos enhancer by the erk MAP kinase pathway through two sequence elements*, *Oncogene* **2000**, *19*, pp. 1379–1385.
- [118] S. Leppä, R. Saffrich, W. Ansorge, D. Bohmann, *Differential regulation of c-Jun by ERK and JNK during PC12 cell differentiation*, *The EMBO journal* **1998**, *17*, pp. 4404–4413.
- [119] L. Li, G.-D. Zhao, Z. Shi, L.-L. Qi, L.-Y. Zhou, Z.-X. Fu, *The Ras/Raf/MEK/ERK signaling pathway and its role in the occurrence and development of HCC*, *Oncology letters* **2016**, *12*, pp. 3045–3050.
- [120] M. P. Czech, *PIP2 and PIP3*, *Cell* **2000**, *100*, pp. 603–606.
- [121] B. Vanhaesebroeck, D. R. Alessi, *The PI3K-PDK1 connection*, *The Biochemical journal* **2000**, *346 Pt 3*, pp. 561–576.

- [122] E. Vander Haar, S.-I. Lee, S. Bandhakavi, T. J. Griffin, D.-H. Kim, *Insulin signalling to mTOR mediated by the Akt/PKB substrate PRAS40*, *Nature cell biology* **2007**, 9, pp. 316–323.
- [123] D. D. Sarbassov, D. A. Guertin, S. M. Ali, D. M. Sabatini, *Phosphorylation and regulation of Akt/PKB by the rictor-mTOR complex*, *Science (New York, N.Y.)* **2005**, 307, pp. 1098–1101.
- [124] J. Feng, J. Park, P. Cron, D. Hess, B. A. Hemmings, *Identification of a PKB/Akt hydrophobic motif Ser-473 kinase as DNA-dependent protein kinase*, *The Journal of biological chemistry* **2004**, 279, pp. 41189–41196.
- [125] M. Andjelković, T. Jakubowicz, P. Cron, X. F. Ming, J. W. Han, B. A. Hemmings, *Activation and phosphorylation of a pleckstrin homology domain containing protein kinase (RAC-PK/PKB) promoted by serum and protein phosphatase inhibitors*, *Proceedings of the National Academy of Sciences of the United States of America* **1996**, 93, pp. 5699–5704.
- [126] J. Brognard, E. Sierceki, T. Gao, A. C. Newton, *PHLPP and a second isoform, PHLPP2, differentially attenuate the amplitude of Akt signaling by regulating distinct Akt isoforms*, *Molecular Cell* **2007**, 25, pp. 917–931.
- [127] V. Stambolic, A. Suzuki, J. L. de La Pompa, G. M. Brothers, C. Mirtsos, T. Sasaki, J. Ruland, J. M. Penninger, D. P. Siderovski, T. W. Mak, *Negative regulation of PKB/Akt-dependent cell survival by the tumor suppressor PTEN*, *Cell* **1998**, 95, pp. 29–39.
- [128] J. J. O'Shea, M. Gadina, R. D. Schreiber, *Cytokine signaling in 2002*, *Cell* **2002**, 109 Suppl, S121-31.
- [129] M. David, L. Wong, R. Flavell, S. A. Thompson, A. Wells, A. C. Lerner, G. R. Johnson, *STAT activation by epidermal growth factor (EGF) and amphiregulin. Requirement for the EGF receptor kinase but not for tyrosine phosphorylation sites or JAK1*, *The Journal of biological chemistry* **1996**, 271, pp. 9185–9188.
- [130] C. D. Andl, T. Mizushima, K. Oyama, M. Bowser, H. Nakagawa, A. K. Rustgi, *EGFR-induced cell migration is mediated predominantly by the JAK-STAT pathway in primary esophageal keratinocytes*, *American journal of physiology. Gastrointestinal and liver physiology* **2004**, 287, G1227-37.
- [131] N. Koyama, M. Kashimata, H. Sakashita, H. Sakagami, E. W. Gresik, *EGF-stimulated signaling by means of PI3K, PLCgamma1, and PKC isozymes regulates branching morphogenesis of the fetal mouse submandibular gland*, *Developmental dynamics : an official publication of the American Association of Anatomists* **2003**, 227, pp. 216–226.

- [132] A. Mora, D. Komander, D. M. F. van Aalten, D. R. Alessi, *PDK1, the master regulator of AGC kinase signal transduction*, *Seminars in cell & developmental biology* **2004**, *15*, pp. 161–170.
- [133] Y. Yamamoto, D. Lee, Y. Kim, B. Lee, C. Seo, H. Kawasaki, S. Kuroda, K. Tanaka-Yamamoto, *Raf kinase inhibitory protein is required for cerebellar long-term synaptic depression by mediating PKC-dependent MAPK activation*, *The Journal of neuroscience : the official journal of the Society for Neuroscience* **2012**, *32*, pp. 14254–14264.
- [134] E. Castellano, J. Downward, *RAS Interaction with PI3K*, *Genes & cancer* **2011**, *2*, pp. 261–274.
- [135] D. E. Butler, C. Marlein, H. F. Walker, F. M. Frame, V. M. Mann, M. S. Simms, B. R. Davies, A. T. Collins, N. J. Maitland, *Inhibition of the PI3K/AKT/mTOR pathway activates autophagy and compensatory Ras/Raf/MEK/ERK signalling in prostate cancer*, *Oncotarget* **2017**, *8*, pp. 56698–56713.
- [136] T. M. Brand, M. Iida, C. Li, D. L. Wheeler, *The nuclear epidermal growth factor receptor signaling network and its role in cancer*, *Discovery medicine* **2011**, *12*, pp. 419–432.
- [137] S.-C. Wang, Y. Nakajima, Y.-L. Yu, W. Xia, C.-T. Chen, C.-C. Yang, E. W. McIntush, L.-Y. Li, D. H. Hawke, R. Kobayashi et al., *Tyrosine phosphorylation controls PCNA function through protein stability*, *Nature cell biology* **2006**, *8*, pp. 1359–1368.
- [138] K. Dittmann, C. Mayer, B. Fehrenbacher, M. Schaller, U. Raju, L. Milas, D. J. Chen, R. Kehlbach, H. P. Rodemann, *Radiation-induced epidermal growth factor receptor nuclear import is linked to activation of DNA-dependent protein kinase*, *The Journal of biological chemistry* **2005**, *280*, pp. 31182–31189.
- [139] C. Li, M. Iida, E. F. Dunn, A. J. Ghia, D. L. Wheeler, *Nuclear EGFR contributes to acquired resistance to cetuximab*, *Oncogene* **2009**, *28*, pp. 3801–3813.
- [140] W.-C. Huang, Y.-J. Chen, L.-Y. Li, Y.-L. Wei, S.-C. Hsu, S.-L. Tsai, P.-C. Chiu, W.-P. Huang, Y.-N. Wang, C.-H. Chen et al., *Nuclear translocation of epidermal growth factor receptor by Akt-dependent phosphorylation enhances breast cancer-resistant protein expression in gefitinib-resistant cells*, *The Journal of biological chemistry* **2011**, *286*, pp. 20558–20568.
- [141] K. Dittmann, C. Mayer, B. Fehrenbacher, M. Schaller, R. Kehlbach, H. P. Rodemann, *Nuclear EGFR shuttling induced by ionizing radiation is regulated by phosphorylation at residue Thr654*, *FEBS letters* **2010**, *584*, pp. 3878–3884.

- [142] M. Juchum, M. Günther, S. A. Laufer, *Fighting cancer drug resistance, Drug resistance updates : reviews and commentaries in antimicrobial and anticancer chemotherapy* **2015**, 20, pp. 12–28.
- [143] A. Kol, A. van Terwisscha Scheltinga, M. Pool, C. Gerdes, E. de Vries, S. de Jong, *ADCC responses and blocking of EGFR-mediated signaling and cell growth by combining the anti-EGFR antibodies imgatuzumab and cetuximab in NSCLC cells, Oncotarget* **2017**, 8, pp. 45432–45446.
- [144] E. Martinelli, R. de Palma, M. Orditura, F. de Vita, F. Ciardiello, *Anti-epidermal growth factor receptor monoclonal antibodies in cancer therapy, Clinical and experimental immunology* **2009**, 158, pp. 1–9.
- [145] Z. Mazorra, A. Lavastida, F. Concha-Benavente, A. Valdés, R. M. Srivastava, T. M. García-Bates, E. Hechavarría, Z. González, A. González, M. Lugiollo et al., *Nimotuzumab Induces NK Cell Activation, Cytotoxicity, Dendritic Cell Maturation and Expansion of EGFR-Specific T Cells in Head and Neck Cancer Patients, Frontiers in pharmacology* **2017**, 8, p. 382.
- [146] M. B. Topper, J. R. Tonra, B. Pytowski, S. W. Eastman, *Differentiation between the EGFR antibodies necitumumab, cetuximab, and panitumumab, JCO* **2011**, 29, e13022–e13022.
- [147] G. da Cunha Santos, F. A. Shepherd, M. S. Tsao, *EGFR mutations and lung cancer, Annual review of pathology* **2011**, 6, pp. 49–69.
- [148] H. K. Gan, A. N. Cvrljevic, T. G. Johns, *The epidermal growth factor receptor variant III (EGFRvIII), The FEBS journal* **2013**, 280, pp. 5350–5370.
- [149] R. P. Graham, A. L. Treece, N. I. Lindeman, P. Vasalos, M. Shan, L. J. Jennings, D. L. Rimm, *Worldwide Frequency of Commonly Detected EGFR Mutations, Archives of pathology & laboratory medicine* **2018**, 142, pp. 163–167.
- [150] T. M. Brand, M. Iida, N. Luthar, M. M. Starr, E. J. Huppert, D. L. Wheeler, *Nuclear EGFR as a molecular target in cancer, Radiotherapy and oncology : journal of the European Society for Therapeutic Radiology and Oncology* **2013**, 108, pp. 370–377.
- [151] K. Dittmann, C. Mayer, A. Paasch, S. Huber, B. Fehrenbacher, M. Schaller, H. P. Rodemann, *Nuclear EGFR renders cells radio-resistant by binding mRNA species and triggering a metabolic switch to increase lactate production, Radiotherapy and oncology : journal of the European Society for Therapeutic Radiology and Oncology* **2015**, 116, pp. 431–437.

- [152] C. L. Arteaga, *Overview of epidermal growth factor receptor biology and its role as a therapeutic target in human neoplasia*, *Seminars in oncology* **2002**, 29, pp. 3–9.
- [153] B. Papouchado, L. A. Erickson, A. L. Rohlinger, T. J. Hobday, C. Erlichman, M. M. Ames, R. V. Lloyd, *Epidermal growth factor receptor and activated epidermal growth factor receptor expression in gastrointestinal carcinoids and pancreatic endocrine carcinomas*, *Modern pathology : an official journal of the United States and Canadian Academy of Pathology, Inc* **2005**, 18, pp. 1329–1335.
- [154] C. Celikel, F. Eren, B. Gulluoglu, N. Bekiroglu, S. Turhal, *Relation of neuroendocrine cells to transforming growth factor-alpha and epidermal growth factor receptor expression in gastric adenocarcinomas*, *Pathology oncology research : POR* **2007**, 13, pp. 215–226.
- [155] C. Kuhnen, B. U. Winter, *EGFR-Expression in pulmonalen neuroendokrinen Zellhyperplasien*, *Der Pathologe* **2006**, 27, pp. 147–151.
- [156] F. Grillo, T. Florio, F. Ferrau, E. Kara, G. Fanciulli, A. Faggiano, A. Colao, *Emerging multitarget tyrosine kinase inhibitors in the treatment of neuroendocrine neoplasms*, *Endocrine-related cancer* **2018**, 25, R453-R466.
- [157] E. Raymond, L. Dahan, J.-L. Raoul, Y.-J. Bang, I. Borbath, C. Lombard-Bohas, J. Valle, P. Metrakos, D. Smith, A. Vinik et al., *Sunitinib malate for the treatment of pancreatic neuroendocrine tumors*, *The New England journal of medicine* **2011**, 364, pp. 501–513.
- [158] R. Moriya, S. Hokari, S. Shibata, T. Koizumi, T. Tetsuka, K. Ito, H. Hashidate, H. Tsukada, *Histological Transformation to Large Cell Neuroendocrine Carcinoma from Lung Adenocarcinoma Harboring an EGFR Mutation*, *Internal medicine (Tokyo, Japan)* **2017**, 56, pp. 2013–2017.
- [159] D. L. Klayman, *Qinghaosu (artemisinin)*, *Science (New York, N.Y.)* **1985**, 228, pp. 1049–1055.
- [160] N. J. White, S. Pukrittayakamee, T. T. Hien, M. A. Faiz, O. A. Mokuolu, A. M. Dondorp, *Malaria*, *Lancet (London, England)* **2014**, 383, pp. 723–735.
- [161] T. Efferth, M. R. Romero, D. G. Wolf, T. Stamminger, J. J. G. Marin, M. Marschall, *The antiviral activities of artemisinin and artesunate*, *Clinical infectious diseases : an official publication of the Infectious Diseases Society of America* **2008**, 47, pp. 804–811.
- [162] P. S. Twomey, B. L. Smith, C. McDermott, A. Novitt-Moreno, W. McCarthy, S. P. Kachur, P. M. Arguin, *Intravenous Artesunate for the Treatment of Severe and Complicated Malaria in the United States*, *Annals of internal medicine* **2015**, 163, pp. 498–506.

- [163] T. Efferth, *Beyond malaria, Biotechnology advances* **2018**, *36*, pp. 1730–1737.
- [164] J. Naß, T. Efferth, *The activity of Artemisia spp. and their constituents against Trypanosomiasis, Phytomedicine : international journal of phytotherapy and phytopharmacology* **2018**, *47*, pp. 184–191.
- [165] M. E. M. Saeed, S. Krishna, H. J. Greten, P. G. Kremsner, T. Efferth, *Antischistosomal activity of artemisinin derivatives in vivo and in patients, Pharmacological research* **2016**, *110*, pp. 216–226.
- [166] J. N. Lisgarten, B. Potter, R. A. Palmer, B. Chimanuka, J. Aymami, *Structure, absolute configuration, and conformation of the antimalarial drug artesunate, Journal of Chemical Crystallography* **2002**, *32*, pp. 43–48.
- [167] N. J. White, *Malaria parasite clearance, Malaria journal* **2017**, *16*, p. 88.
- [168] P. Phompradit, W. Chaijaroenkul, K. Na-Bangchang, *Cellular mechanisms of action and resistance of Plasmodium falciparum to artemisinin, Parasitology research* **2017**, *116*, pp. 3331–3339.
- [169] K. Chotivanich, J. Sattabongkot, R. Udomsangpetch, S. Looareesuwan, N. P. J. Day, R. E. Coleman, N. J. White, *Transmission-blocking activities of quinine, primaquine, and artesunate, Antimicrobial agents and chemotherapy* **2006**, *50*, pp. 1927–1930.
- [170] R. Udomsangpetch, B. Pipitaporn, S. Krishna, B. Angus, S. Pukrittayakamee, I. Bates, Y. Suputtamongkol, D. E. Kyle, N. J. White, *Antimalarial drugs reduce cytoadherence and rosetting Plasmodium falciparum, The Journal of infectious diseases* **1996**, *173*, pp. 691–698.
- [171] A. M. Dondorp, R. J. Maude, I. C. E. Hendriksen, N. P. Day, N. J. White, *Artesunate dosing in severe falciparum malaria, The Journal of infectious diseases* **2012**, *206*, 618-9; author reply 622.
- [172] Q. Li, S. Remich, S. R. Miller, B. Ogutu, W. Otieno, V. Melendez, P. Teja-Isavadharm, P. J. Weina, M. R. Hickman, B. Smith et al., *Pharmacokinetic evaluation of intravenous artesunate in adults with uncomplicated falciparum malaria in Kenya, Malaria journal* **2014**, *13*, p. 281.
- [173] K. F. Ilett, B. T. Ethell, J. L. Maggs, T. M. E. Davis, K. T. Batty, B. Burchell, T. Q. Binh, T. A. Le Thu, N. C. Hung, M. Pirmohamed et al., *Glucuronidation of dihydroartemisinin in vivo and by human liver microsomes and expressed UDP-glucuronosyltransferases, Drug metabolism and disposition: the biological fate of chemicals* **2002**, *30*, pp. 1005–1012.

- [174] J. Keiser, N. A. N'Guessan, K. D. Adoubryn, K. D. Silué, P. Vounatsou, C. Hatz, J. Utzinger, E. K. N'Goran, *Efficacy and safety of mefloquine, artesunate, mefloquine-artesunate, and praziquantel against Schistosoma haematobium*, *Clinical infectious diseases : an official publication of the Infectious Diseases Society of America* **2010**, *50*, pp. 1205–1213.
- [175] J. Keiser, J. Utzinger, *Artemisinins and synthetic trioxolanes in the treatment of helminth infections*, *Current opinion in infectious diseases* **2007**, *20*, pp. 605–612.
- [176] W. E. Ho, H. Y. Peh, T. K. Chan, W. S. F. Wong, *Artemisinins*, *Pharmacology & therapeutics* **2014**, *142*, pp. 126–139.
- [177] T. Efferth, H. Dunstan, A. Sauerbrey, H. Miyachi, C. R. Chitambar, *The anti-malarial artesunate is also active against cancer*, *International journal of oncology* **2001**, *18*, pp. 767–773.
- [178] S. R. Meshnick, Y. Z. Yang, V. Lima, F. Kuypers, S. Kamchonwongpaisan, Y. Yuthavong, *Iron-dependent free radical generation from the antimalarial agent artemisinin (qinghaosu)*, *Antimicrobial agents and chemotherapy* **1993**, *37*, pp. 1108–1114.
- [179] P. M. O'Neill, V. E. Barton, S. A. Ward, *The molecular mechanism of action of artemisinin--the debate continues*, *Molecules (Basel, Switzerland)* **2010**, *15*, pp. 1705–1721.
- [180] S. Zhang, G. S. Gerhard, *Heme activates artemisinin more efficiently than hemin, inorganic iron, or hemoglobin*, *Bioorganic & medicinal chemistry* **2008**, *16*, pp. 7853–7861.
- [181] S. A.-L. Laurent, C. Loup, S. Mourgues, A. Robert, B. Meunier, *Heme alkylation by artesunic acid and trioxaquine DU1301, two antimalarial trioxanes*, *Chembiochem : a European journal of chemical biology* **2005**, *6*, pp. 653–658.
- [182] A. M. Lisewski, J. P. Quiros, C. L. Ng, A. K. Adikesavan, K. Miura, N. Putluri, R. T. Eastman, D. Scandfeld, S. J. Regenbogen, L. Altenhofen et al., *Supragenomic network compression and the discovery of EXP1 as a glutathione transferase inhibited by artesunate*, *Cell* **2014**, *158*, pp. 916–928.
- [183] D. S. Ellis, Z. L. Li, H. M. Gu, W. Peters, B. L. Robinson, G. Tovey, D. C. Warhurst, *The chemotherapy of rodent malaria, XXXIX. Ultrastructural changes following treatment with artemisinin of Plasmodium berghei infection in mice, with observations of the localization of 3H-dihydroartemisinin in P. falciparum in vitro*, *Annals of tropical medicine and parasitology* **1985**, *79*, pp. 367–374.

- [184] F. ter Kuile, N. J. White, P. Holloway, G. Pasvol, S. Krishna, *Plasmodium falciparum*, *Experimental parasitology* **1993**, 76, pp. 85–95.
- [185] J. Li, B. Zhou, *Biological actions of artemisinin*, *Molecules (Basel, Switzerland)* **2010**, 15, pp. 1378–1397.
- [186] U. Eckstein-Ludwig, R. J. Webb, I. D. A. van Goethem, J. M. East, A. G. Lee, M. Kimura, P. M. O'Neill, P. G. Bray, S. A. Ward, S. Krishna, *Artemisinins target the SERCA of Plasmodium falciparum*, *Nature* **2003**, 424, pp. 957–961.
- [187] B. Arnou, C. Montigny, J. P. Morth, P. Nissen, C. Jaxel, J. V. Møller, M. Le Maire, *The Plasmodium falciparum Ca(2+)-ATPase PfATP6*, *Biochemical Society transactions* **2011**, 39, pp. 823–831.
- [188] D. Cardi, A. Pozza, B. Arnou, E. Marchal, J. D. Clausen, J. P. Andersen, S. Krishna, J. V. Møller, M. Le Maire, C. Jaxel, *Purified E255L mutant SERCA1a and purified PfATP6 are sensitive to SERCA-type inhibitors but insensitive to artemisinins*, *The Journal of biological chemistry* **2010**, 285, pp. 26406–26416.
- [189] J. Wang, C.-J. Zhang, W. N. Chia, C. C. Y. Loh, Z. Li, Y. M. Lee, Y. He, L.-X. Yuan, T. K. Lim, M. Liu et al., *Haem-activated promiscuous targeting of artemisinin in Plasmodium falciparum*, *Nature communications* **2015**, 6, p. 10111.
- [190] V. B. Kasaragod, T. J. Hausrat, N. Schaefer, M. Kuhn, N. R. Christensen, I. Tessmer, H. M. Maric, K. L. Madsen, C. Sottriffer, C. Villmann et al., *Elucidating the Molecular Basis for Inhibitory Neurotransmission Regulation by Artemisinins*, *Neuron* **2019**, 101, 673-689.e11.
- [191] D. M. Sabatini, R. K. Barrow, S. Blackshaw, P. E. Burnett, M. M. Lai, M. E. Field, B. A. Bahr, J. Kirsch, H. Betz, S. H. Snyder, *Interaction of RAFT1 with gephyrin required for rapamycin-sensitive signaling*, *Science (New York, N.Y.)* **1999**, 284, pp. 1161–1164.
- [192] C. Shi, H. Li, Y. Yang, L. Hou, *Anti-inflammatory and immunoregulatory functions of artemisinin and its derivatives*, *Mediators of inflammation* **2015**, 2015, p. 435713.
- [193] E. Gugliandolo, R. D'Amico, M. Cordaro, R. Fusco, R. Siracusa, R. Crupi, D. Impellizzeri, S. Cuzzocrea, R. Di Paola, *Neuroprotective Effect of Artesunate in Experimental Model of Traumatic Brain Injury*, *Frontiers in neurology* **2018**, 9, p. 590.
- [194] M. Kuang, Y. Cen, R. Qin, S. Shang, Z. Zhai, C. Liu, X. Pan, H. Zhou, *Artesunate Attenuates Pro-Inflammatory Cytokine Release from Macrophages by Inhibiting TLR4-Mediated Autophagic Activation via the TRAF6-Beclin1-PI3KC3 Pathway*, *Cellular physiology and biochemistry : international journal of experimental cellular physiology, biochemistry, and pharmacology* **2018**, 47, pp. 475–488.

- [195] H. Lu, B. Wang, N. Cui, Y. Zhang, *Artesunate suppresses oxidative and inflammatory processes by activating Nrf2 and ROS-dependent p38 MAPK and protects against cerebral ischemia-reperfusion injury*, *Molecular medicine reports* **2018**, *17*, pp. 6639–6646.
- [196] Z. Yang, J. Ding, C. Yang, Y. Gao, X. Li, X. Chen, Y. Peng, J. Fang, S. Xiao, *Immunomodulatory and anti-inflammatory properties of artesunate in experimental colitis*, *Current medicinal chemistry* **2012**, *19*, pp. 4541–4551.
- [197] D. E. Jeong, H. J. J. Song, S. Lim, S. J. J. Lee, J. E. Lim, D.-H. Nam, K. M. Joo, B. C. Jeong, S. S. Jeon, H. Y. Choi et al., *Repurposing the anti-malarial drug artesunate as a novel therapeutic agent for metastatic renal cell carcinoma due to its attenuation of tumor growth, metastasis, and angiogenesis*, *Oncotarget* **2015**, *6*, pp. 33046–33064.
- [198] V. Konkimalla, J. McCubrey, T. Efferth, *The Role of Downstream Signaling Pathways of the Epidermal Growth Factor Receptor for Artesunates Activity in Cancer Cells*, *CCDT* **2009**, *9*, pp. 72–80.
- [199] S.-Z. Zang, Y.-R. Yang, S.-S. Zhao, Y.-X. Li, X.-Y. Gao, C.-L. Zhong, *In silico insight into EGFR treatment in patients with lung carcinoma and T790M mutations*, *Experimental and therapeutic medicine* **2017**, *13*, pp. 1735–1740.
- [200] C. L. Arteaga, *Epidermal growth factor receptor dependence in human tumors*, *The oncologist* **2002**, *7 Suppl 4*, pp. 31–39.
- [201] R. Ranjbar, F. Nejatollahi, A. S. Nedaei Ahmadi, H. Hafezi, A. Safaie, *Expression of Vascular Endothelial Growth Factor (VEGF) and Epidermal Growth Factor Receptor (EGFR) in Patients With Serous Ovarian Carcinoma and Their Clinical Significance*, *Iranian journal of cancer prevention* **2015**, *8*, e3428.
- [202] J. H. Torres-Jasso, A. R. Bustos-Carpinteyro, J. R. Garcia-Gonzalez, J. Peregrina-Sandoval, J. A. Cruz-Ramos, E. Santiago-Luna, J. Y. Sanchez-Lopez, *Epidermal growth factor receptor expression in gastric tumors and its relationship with the germline polymorphisms - 216 GT, -191 CA, (CA) n IVS1, and R521K*, *Indian journal of cancer* **2016**, *53*, pp. 345–348.
- [203] T. Mukohara, *Expression of epidermal growth factor receptor (EGFR) and downstream-activated peptides in surgically excised non-small-cell lung cancer (NSCLC)*, *Lung Cancer* **2003**, *41*, pp. 123–130.
- [204] J. P. Kallio, P. Hirvikoski, H. Helin, P. Kellokumpu-Lehtinen, T. Luukkaala, T. L. J. Tammela, P. M. Martikainen, *Membranous location of EGFR immunostaining is*

- associated with good prognosis in renal cell carcinoma, *British journal of cancer* **2003**, 89, pp. 1266–1269.
- [205] S. Hong, Y. Gu, Z. Gao, L. Guo, W. Guo, X. Wu, Y. Shen, Y. Sun, X. Wu, Q. Xu, *EGFR inhibitor-driven endoplasmic reticulum stress-mediated injury on intestinal epithelial cells*, *Life sciences* **2014**, 119, pp. 28–33.
- [206] A. Bürkle, *PARP and the Release of Apoptosis-Inducing Factor from Mitochondria*. In: *Poly(ADP-Ribosyl)ation.*, Springer-Verlag, s.l., **2006**.
- [207] R. Feltham, J. E. Vince, K. E. Lawlor, *Caspase-8*, *Clinical & translational immunology* **2017**, 6, e124.
- [208] Hong S.J., Dawson T.M., Dawson V.L., *PARP and the Release of Apoptosis-Inducing Factor from Mitochondria*. In: *Poly(ADP-Ribosyl)ation.*, Landes Bioscience/Eurekah.com; Springer Science+Business Media, Georgetown, Tex., New York, N.Y., **2006**.
- [209] T. Efferth, *Signal transduction pathways of the epidermal growth factor receptor in colorectal cancer and their inhibition by small molecules*, *Current medicinal chemistry* **2012**, 19, pp. 5735–5744.
- [210] O. Kadioglu, J. Cao, M. E. M. Saeed, H. J. Greten, T. Efferth, *Targeting epidermal growth factor receptors and downstream signaling pathways in cancer by phytochemicals*, *Targeted oncology* **2015**, 10, pp. 337–353.
- [211] A. Franovic, L. Gunaratnam, K. Smith, I. Robert, D. Patten, S. Lee, *Translational up-regulation of the EGFR by tumor hypoxia provides a nonmutational explanation for its overexpression in human cancer*, *Proceedings of the National Academy of Sciences of the United States of America* **2007**, 104, pp. 13092–13097.
- [212] A. Ema, M. Waraya, K. Yamashita, K. Kokubo, H. Kobayashi, K. Hoshi, Y. Shinkai, H. Kawamata, K. Nakamura, H. Nishimiya et al., *Identification of EGFR expression status association with metastatic lymph node density (ND) by expression microarray analysis of advanced gastric cancer*, *Cancer medicine* **2015**, 4, pp. 90–100.
- [213] J. A. Q. A. Faria, C. de Andrade, A. M. Goes, M. A. Rodrigues, D. A. Gomes, *Effects of different ligands on epidermal growth factor receptor (EGFR) nuclear translocation*, *Biochemical and biophysical research communications* **2016**, 478, pp. 39–45.
- [214] H. Fujita, K. Ohuchida, K. Mizumoto, S. Itaba, T. Ito, K. Nakata, J. Yu, T. Kayashima, A. Hayashi, R. Souzaki et al., *High EGFR mRNA expression is a prognostic factor for reduced survival in pancreatic cancer after gemcitabine-based adjuvant chemotherapy*, *International journal of oncology* **2011**, 38, pp. 629–641.

- [215] H. S. Park, M. H. Jang, E. J. Kim, H. J. Kim, H. J. Lee, Y. J. Kim, J. H. Kim, E. Kang, S.-W. Kim, I. A. Kim et al., *High EGFR gene copy number predicts poor outcome in triple-negative breast cancer*, *Modern pathology : an official journal of the United States and Canadian Academy of Pathology, Inc* **2014**, 27, pp. 1212–1222.
- [216] Q. Li, N. J. Birkbak, B. Györffy, Z. Szallasi, A. C. Eklund, *Jetset*, *BMC bioinformatics* **2011**, 12, p. 474.
- [217] H.-W. Lo, M. Ali-Seyed, Y. Wu, G. Bartholomeusz, S.-C. Hsu, M.-C. Hung, *Nuclear-cytoplasmic transport of EGFR involves receptor endocytosis, importin beta1 and CRM1*, *Journal of cellular biochemistry* **2006**, 98, pp. 1570–1583.
- [218] S. Song, J. Tan, Y. Miao, Q. Zhang, *Crosstalk of ER stress-mediated autophagy and ER-phagy*, *Journal of cellular physiology* **2018**, 233, pp. 3867–3874.
- [219] P. Walter, D. Ron, *The unfolded protein response*, *Science (New York, N.Y.)* **2011**, 334, pp. 1081–1086.
- [220] A. Dandekar, R. Mendez, K. Zhang, *Cross talk between ER stress, oxidative stress, and inflammation in health and disease*, *Methods in molecular biology (Clifton, N.J.)* **2015**, 1292, pp. 205–214.
- [221] H. M. A. Zeeshan, G. H. Lee, H.-R. Kim, H.-J. Chae, *Endoplasmic Reticulum Stress and Associated ROS*, *International journal of molecular sciences* **2016**, 17, p. 327.
- [222] G. Kroemer, S. J. Martin, *Caspase-independent cell death*, *Nature Medicine* **2005**, 11, 725 EP -.
- [223] A. Pender, I. Garcia-Murillas, S. Rana, R. J. Cutts, G. Kelly, K. Fenwick, I. Kozarewa, D. Gonzalez de Castro, J. Bhosle, M. O'Brien et al., *Efficient Genotyping of KRAS Mutant Non-Small Cell Lung Cancer Using a Multiplexed Droplet Digital PCR Approach*, *PloS one* **2015**, 10, e0139074.
- [224] T. Vandamme, M. Peeters, F. Dogan, P. Pauwels, E. van Assche, M. Beyens, G. Mortier, G. Vandeweyer, W. de Herder, G. van Camp et al., *Whole-exome characterization of pancreatic neuroendocrine tumor cell lines BON-1 and QGP-1*, *Journal of molecular endocrinology* **2015**, 54, pp. 137–147.
- [225] N. Dolgikh, M. Hugle, M. Vogler, S. Fulda, *NRAS-Mutated Rhabdomyosarcoma Cells Are Vulnerable to Mitochondrial Apoptosis Induced by Coinhibition of MEK and PI3K $\alpha$* , *Cancer research* **2018**, 78, pp. 2000–2013.
- [226] L. Yang, Y. Zhou, Y. Li, J. Zhou, Y. Wu, Y. Cui, G. Yang, Y. Hong, *Mutations of p53 and KRAS activate NF- $\kappa$ B to promote chemoresistance and tumorigenesis via*

- dysregulation of cell cycle and suppression of apoptosis in lung cancer cells, Cancer letters* **2015**, 357, pp. 520–526.
- [227] J. O'Brien, I. Wilson, T. Orton, F. Pognan, *Investigation of the Alamar Blue (resazurin) fluorescent dye for the assessment of mammalian cell cytotoxicity, European journal of biochemistry* **2000**, 267, pp. 5421–5426.
- [228] B. Krusche, J. Arend, T. Efferth, *Synergistic inhibition of angiogenesis by artesunate and captopril in vitro and in vivo, Evidence-based complementary and alternative medicine : eCAM* **2013**, 2013, p. 454783.

## 9 Supplementary materials

Supplementary Table S1. Clinical features of patients

Variables	Characteristics of Patients (n=502) for mcEGFR Analysis		Characteristics of Patients (n=398) for nEGFR Analysis	
	No. of Patients	% of total patients	No. of Patients	% of total patients
<b>Age Range</b>	24-95			
<b>Gender</b>				
Female	157		132	
Male	264		205	
NA	81		61	
Sum	502		398	
<b>Tissue type</b>				
Uterus & Cervix	25	4.98%	21	5.28%
Colorectal(Colon & Rectum)	138	27.49%	108	27.14%
Breast	51	10.16%	47	11.81%
Ovary	11	2.19%	9	2.26%
Brain	6	1.20%	0	0.00%
Lung & Bronchi	47	9.36%	44	11.06%
Pancreas	42	8.37%	33	8.29%
Prostate	44	8.76%	32	8.04%
Kidney	108	21.51%	84	21.11%
Other	30	5.98%	20	5.03%
Cases in Analysis	<b>502</b>	<b>100.00%</b>	<b>398</b>	<b>100.00%</b>
Sum	502	100.00%	398	100.00%
<b>Pathologic T Stage</b>				
T1	89	17.73%	66	16.58%
T2	132	26.29%	107	26.88%
T3	115	22.91%	99	24.87%
T4	60	11.95%	47	11.81%
NA	106	21.12%	79	19.85%
Cases in Analysis	<b>396</b>	<b>78.88%</b>	<b>319</b>	<b>80.15%</b>
Sum	502	100.00%	398	100.00%
<b>Pathologic N Stage</b>				
N0	212	42.23%	168	42.21%
N1	77	15.34%	70	17.59%
N2	17	3.39%	11	2.76%
N3	1	0.20%	1	0.25%
NA	195	38.84%	148	37.19%
Cases in Analysis	<b>306</b>	<b>60.96%</b>	<b>249</b>	<b>62.56%</b>
Sum	502	100.00%	398	100.00%
<b>Pathologic M Stage</b>				
M0	333	66.33%	267	67.09%
M1	25	4.98%	20	5.03%
NA	144	28.69%	111	27.89%
Cases in Analysis	<b>358</b>	<b>71.31%</b>	<b>287</b>	<b>72.11%</b>
Sum	502	100.00%	398	100.00%
<b>Pathologic Grade</b>				
G0	16	3.19%	15	3.77%
G1	69	13.75%	55	13.82%
G1-G2(G1.5)	9	1.79%	8	2.01%
G2	157	31.27%	124	31.16%
G2-G3(G2.5)	5	1.00%	3	0.75%
G3	141	28.09%	115	28.89%
G4	1	0.20%	0	0.00%
NA	104	20.72%	78	19.60%
Cases in Analysis	<b>382</b>	<b>76.10%</b>	<b>305</b>	<b>76.63%</b>
Sum	502	100.00%	398	100.00%

Case n=1 were excluded for later analysis; G0 cases were excluded for later analysis; NA=Not available

Supplementary Table S2. Other tumor types

Tumor Type	Patiens (n=30) for mcEGFR Analysis	Patiens (n=20) for nEGFR Analysis
Head and Neck	2	2
Bladder	1	0
Esophagus	3	1
Duodenum	1	0
Fallopian Tube	1	1
Gall Bladder	2	2
Liver	3	3
Lymphoma	3	1
Parotid	1	1
Skin	1	1
Soft Tissue	1	1
Tonsil	2	1
Stomach	3	3
Testis	1	1
Thymus	1	0
Thyroid	2	1
Adrenal	1	0
Adipose	1	1
Sum	30	20

Supplementary Table S3. Primers list

Name	Sequence
ANXA13F	GCTAAAGCGAGCAGTCCTCAG
ANXA13R	GTCTGCCCCGATAAGATTTCAA
HOPXF	GAGACCCAGGGTAGTGATTTGA
HOPXR	AAAAGTAATCGAAAAGCCAAGCAC
GINS2F	CCCTGGTTTACCCGTGGAAG
GINS2R	GGGAGCAGGCGACATTTCT
HSPB1F	ACGGTCAAGACCAAGGATGG
HSPB1R	AGCGTGTATTTCCGCGTGA
KIAA0101F	ATGGTGCGGACTAAAGCAGAC
KIAA0101R	CCTCGATGAACTGATGTCGAAT
FAM46CF	TCCATTGCGCGTCAGTTTGAG
FAM46CR	GGTTGCTGTACTTGAGAAGTCC
CCNE1F	AAGGAGCGGGACACCATGA
CCNE1R	ACGGTCACGTTTGCCTTCC
MCM6F	GAGGAACTGATTCGTCCTGAGA
MCM6R	CAAGGCCCGACACAGGTAAG
E2F2F	CGTCCCTGAGTCCCAACC
E2F2R	GCGAAGTGCATACCGAGTCTT
TRIB3F	TGCCCTACAGGCACTGAGTA
TRIB3R	GTCCGAGTGAAAAAGGCGTA
STC2F	CTTACATGGGATTTGCATGACTT
STC2R	AATGGATCATCTCCTACTATCACC
DDIT4F	CTCTTCGCCCTCGTCCTT
DDIT4R	AGCCAGTGCTCAGCGTCA
ACTBF	CATGTACGTTGCTATCCAGGC
ACTBR	CTCCTTAATGTCACGCACGAT
GAPDHF	TTGGTATCGTGAAGGACTCA
GAPDHR	TGTCATCATATTGGCAGGTT

## Supplementary Table S4 (a-c). Top 10 regulated networks in NET cell lines

## a. Top 10 regulated networks in BON-1

ID	Molecules in Network
1	CSNK1A1, DDX46, DUT, ECT2, EXOSC9, FAM72C/FAM72D, FAM81A, GGH, HIST1H2BH, HNRNPH1, ISG20, KPNA2, LAMP3, LSM3, LSM5, MCM2, MCM5, NARS, Nfat (family), PABPC1, PYGB, Ras homolog, RPA3, SH3KBP1, SLC16A10, snRNP, SNRNP25, SNU13, STRN3, SUMO2, TCR, TOP2A, UNG, ZFP36, ZFP69B
2	60S ribosomal subunit, BAIAP2L1, BUB3, Cadherin, CENPA, DDX17, DEK, DIAPH3, EBP, Ephb dimer, ERBB, Hat, histone deacetylase, HJURP, HOXB5, IFRD1, LAMB3, MICB, MIS18BP1, NEUROD1, NGRN, OIP5, PRAME, PSTPIP1, RASIP1, RBBP7, RPL6, RPL22, RPL29, RPL26L1, SAP30, SCG5, SLC25A25, SRC, ZWINT
3	<b>48s, Akt, ALDH2, ASNS, Atf, ATF3, ATF4, ATF5, C1GALT1C1, CAP2, CARHSP1, CARS, CDK4/6, CEBPG, CHAC1, CTH, DDIT4, ELOVL5, Foxo, GARS, IARS, MHC Class I (complex), MTHFD2, PARM1, PCK2, PPP1R15A, PSAT1, PSPH, RDH10, SLC1A4, SLC7A5, SLC7A11, STC2, TRIB3, Vegf Receptor</b>
4	alcohol group acceptor phosphotransferase, AURKB, BUB1, BUB1B, CDC16, CENPE, Dynein, ERCC6L, ETV5, FOXM1, GCNT1, GCNT3, Gi-coupled receptor, GRB10, HPGD, KIF20A, KIFC1, KRT7, MAD2L1, Mapk, NDC80, NEK2, NUF2, PRC1, Rab5, Rho gdi, RMI1, RMI2, RPS6KA2, SAC3D1, SPC25, sphingomyelinase, STK40, TACC3, TTK
5	ASCL1, ATM/ATR, Basc, BLM, BRCA1 complex B, CDC7, CDC45, CDCA7, CHAF1A, CHAF1B, CHTF18, DLX5, DSCC1, FANCD2, FEN1, Mcm, MCM4, MCM6, MCM7, MCM10, MRN, MSH2, MSH6, MutS alpha, ORC6, Pka, PKIA, PLRG1, RFC2, RFC3, RFC4, RFC5, RPA, RPA1, TEAD2
6	ASB1, chymotrypsin, CKAP2, DTYMK, EVA1A, HELLS, HOPX, HOXB8, KIAA1524, MELK, NPTX1, P glycoprotein, plasminogen activator, PRSS1, PRSS2, PRSS3, PSAP, RNF103, SAT1, secreted MMP, SERPINE2, SLC22A18, SLC31A1, Sphk, SPINK1, TFP12, TIMP4, TMEM150A, TRMT10C, trypsin, Trypsinogen, UBE2, UBE2C, UBE2H, Vegf
7	20s proteasome, Alpha catenin, ANLN, ANXA2, Ap2 alpha, ARPC5, ASPM, CEP78, DBN1, EI24, ERRF1, F Actin, FAM65A, Fcer1, GCLC, HEPACAM2, HMGB2, ITPKA, LDHA, LDL-cholesterol, MAP1LC3, MAP1LC3B, MAPK6, Myosin2, PI3K (family), PYCR1, SHC1, SORD, SQSTM1, TAX1BP1, TES, TNFRSF10B, ULK1, VEZT, ZSCAN32
8	7S NGF, Aconitase, Alpha tubulin, Beta Tubulin, C16orf59, CCT8, CDCA4, CDK1/2, Cebp, CLIC4, CXorf57, DHX15, Gamma tubulin, HIGD1A, HPRT1, ISCU, KCTD12, KIF22, MAP1B, MRPL35, P38 MAPK, Pak, PRTFDC1, RACGAP1, STMN1, SYT1, TCP1, TPT1, TUBA1A, TUBA4A, TUBB, TUBB2B, TUBB4B, TUBE1, tubulin (family)
9	Alpha Actinin, ATAD2, ATPase, BRD2, CA8, calpain, CCNA2, CHEK2, CSRP2, Cyclin A, Cyclin E, DDX39A, E2f, E2F2, EC11, Focal adhesion kinase, GINS2, GPT2, Hedgehog, IL-2R, KIF14, KNTC1, LONP1, MARS, MYCN, PGAM1, PHGDH, Rnr, RPS4X, SARS, SMARCA5, SPDL1, TM6SF1, TMED9, TYMS
10	26s Proteasome, C15orf48, Calmodulin, caspase, CCND3, Cytochrome bc1, cytochrome C, DLGAP5, EDF1, Fanc, FANCG, FANCI, FOXA1, FOXO3, GFPT1, HMGB1, ICA1, IGFBP3, LMO4, MIDN, Mitochondrial complex 1, NDUFA2, NFE2L1, Nos, NPTX2, PARP, POLE2, PRDX5, PRKAB2, Proinsulin, TIMM21, TK1, TLE1, UBE2T, ZNF277

## b. Top 10 regulated networks in QGP-1

ID	Molecules in Network
1	ACOT7, BUB3, calpain, CARHSP1, CDK2, COPB1, DCTPP1, DDX21, DUT, ETS2, EXOSC8, EXOSC9, FAM64A, Fibrinogen, FN3KRP, FOXA1, GOLT1B, IAH1, KIF11, MCM2, MRPL23, MRPS30, NKX2-1, NREP, PABPC1, PGM3, PRNP, PRR15L, RNA polymerase II, RPA2, RPL6, RRP12, TMEM237, VEGFA, ZFP69B
2	ACAT2, AGAP6 (includes others), alcohol group acceptor phosphotransferase, ATAD2, ATPase, CENPK, CENPM, EEF1E1, EIF1B, EIF4A2, ELMSAN1, EPRS, FABP5, FAM83D, GPT2, HAUS8, HSPB1, IARS, LONP1, MAPK3, MARS, P glycoprotein, P4HA2, RNF114, SEC16A, SELENBP1, STAMBPL1, TAGLN2, TRIP13, TXNL1, UBE2, UBE2C, UBE2H, YARS, YPEL5
3	adenosine-tetraphosphatase, ATP synthase, ATP5G1, ATP5I, ATP5J, BEX2, BEX3, BLVRA, C16orf59, DYNLT3, F0 ATP synthase, FAM46A, FNDC3A, FNDC3B, IBTK, Importin beta, LRRC26, MRPL11, NFkB (complex), OSBPL6, PXMP2, RIOK3, SARS, SIVA1, SLBP, SLC2A6, SLC38A2, SRP19, STRAP, TNPO1, TUBE1, UHRF1BP1, WDR34, XPOT, ZFAND5
4	ACSL3, APCDD1, ARHGAP23, CDCA4, COMTD1, EBP, ERLEC1, FA, Fanc, FANCE, FANCG, FANCL, GJB2, GLDN, GMNN, HERP, HOXB7, HOXB8, I kappa b kinase, IFRD1, MELK, Neuropilin, NRCAM, NRP1, PKDCC, PLOD1, PLOD2, SHISA2, SLC27A3, SLC7A1, SYVN1, UBE2T, Vegf, WLS, ZBED1
5	BRI3BP, CDCA7, CNBP, DNA Polymerase, DNPH1, DSCC1, EXO1, FEN1, GAMT, GCHFR, KIAA0101, LIG1, LOXL4, METTL3, MTHFD1L, MYC, NDPK, NME2, NME3, POLA2, POLbeta-POLepsilon-POLgamma-XRCC1-LIG1-PARP1-PCNA-FEN1, POLD1, PRIM2, Primase, Rfc, RFC2, RFC3, RFC5, RPA, SEPHS2, SHMT1, SLC38A1, TIMELESS, TMEM97, TYMS
6	AURKB, BCL11A, CDCA3, CDCA8, CHAF1B, DPM3, ESCO1, Focal adhesion kinase, HAUS1, HDAC1, Hedgehog, HISTONE, HMG20B, KIF20A, KLF4, KLHL13, KRT19, LAMTOR4, MutS alpha, NASP, PCGF1, PHF19, PHGDH, POLE2, RASSF2, SIPA1L2, TACC2, TFG, thyroid hormone receptor, TMEM54, TOP2A, TXNRD1, UHRF1, VitaminD3-VDR-RXR, WIPI1
7	Actin, Alpha actin, Arp2/3, CDC42EP4, CEP95, CLK1, COCH, DCTN4, Dynamin, E2F2, ELL2, HIST1H2BH, INPPL1, IRF2BP2, KIF23, MARK1, MCM3, MCM5, MCM10, NAMPT, P-TEFb, PALLD, PALMD, PSRC1, PYGB, Rac, RRM2, RTN4, SH3KBP1, SLC35D3, SLFN5, SRSF2, TIP60, TMSB15A, WASL
8	<b>ANKRA2, ARNTL, ATF3, ATF6, CYB5A, DDIT3, ERCC6L, Fc receptor, FST, GADD45A, GOT, hemoglobin, IgG, IgG1, Igg3, IL17C, JMJD1C, LMO4, MCTP1, MPP1, N-cor, NFIL3, NR1D2, PPP1R15A, PRDX2, Ras homolog, RMI2, RPRM, SOCS2, TMED7, TOB1, TSEN15, UNG, WARS, ZSCAN31</b>
9	<b>48s, AChR, ASNS, ATF4, ATF5, ATP2A3, AURK, BTG2, CD55, CDCA5, CDK2-CyclinE, CEBPG, CHAC1, CHRNAS, CNN2, CNN3, CTH, DPYSL4, EIF4F, Eif4g, ERK, GARS, GOT1, NRG (family), NUSAP1, PCDH18, PITX1, PSAT1, PSPH, RPS6KA, S100P, SERCA, STC2, TRIB3, ZSCAN32</b>
10	20s proteasome, AGAP1, ANKRD11, AP1S1, Atf, BET, CBX4, Ctbp, DBI, FAM46C, Fcer1, FSCN1, GFPT1, Jnk, LSS, MAP1LC3, MAP1LC3B, MARVELD3, MECOM, MYO10, NQO1, NT5C3A, PIGA, PLK4, PMAIP1, PNPLA8, PRKAA, PRKAB2, SESN2, SQSTM1, SUMO, SUMO-Ubc9 E2, TARS, TNFRSF21, Vla-4

## c. Top 10 regulated networks in NCI-H727

ID	Molecules in Network
1	48s, ASCL1, ASNS, ASPM, Atf, ATF3, ATF4, ATF5, BUB1, CARS, CDCA7, CEBPG, DLL3, ERK, GARS, HERPUD1, HEY1, HNRNPDL, ID1, JAG1, LAT2, MKNK2, MTHFD2, NDC80, NKX2-2, Notch, NUF2, PCK2, PPP1R15A, PSAT1, RPS6KA, SDCBP2, SPC25, STC2, TRIB3
2	7S NGF, ABCC2, ANXA13, BEST1, BEX2, c-Src, CDCP1, CYB5A, DHRS2, FAM129A, Ferritin, FHL2, Filamin, FTH1, GCLM, HBB, hemoglobin, HPCAL1, IER3, IL17RB, Integrin alpha 3 beta 1, LAMA3, LAMB3, LRRC26, Nfkb (complex), RIOK3, S100P, SHMT1, SIVA1, SLC3A2, SLC7A1, SLC7A5, SLC7A11, ST3GAL1, TRIM15
3	ADRB, BHLHE40, Cg, CXCL1, DDIT4, DTYMK, DUSP5, EPHA2, FJX1, FLNC, FNDC3B, FSH, GEM, GOT, GPAT3, HELLS, HMGCS2, KIF20A, KLF4, Lh, MCL1, Mek, MT1X, NAMPT, PDLIM3, PEG10, PHGDH, PTPase, SHISA2, SLC20A1, SRXN1, TPM1, TRIP13, UNG, Vegf
4	Basc, BMP, CCNE2, Cdk, CHAF1A, CHAF1B, Cyclin A, Cyclin E, DACH1, DSCC1, ECT2, EXO1, FEN1, FOXC1, JUN, KIAA0101, MSH2, MSH6, MutS alpha, PCNA, PELO, Rb, Rfc, RFC2, RFC3, RFC4, RFC5, SLC1A5, SLC30A1, SLC38A2, SLFN11, Smad, SUMO, TMEM109, XPOT
5	Alpha tubulin, ARG2, BLOC1S1, CLIP1, collagen, DHCR24, DYNC1H1, elastase, ERRF1, GCLC, Gcn5l, HMMR, HMOX1, Hsp27, Jnk, Lfa-1, MAFG, MAP2K1/2, mediator, NAV2, NFE2L1, NFIL3, Pak, Pdgf Ab, PHLDA1, PPP2R2A, SERTAD4, SLC12A2, Sos, STMN1, TBL1X, TIPARP, TXNRD1, UPP1, YARS
6	AKAP7, ANKRD11, APC (complex), AURK, BUB3, Cbp/p300, CCNE1, DLGAP5, Fanc, FANCG, FANCI, FANCL, GCC1, HISTONE, histone deacetylase, Histone H1, Histone h3, KCTD20, KIF15, LRP, LRRC20, MIS18BP1, MT1G, OIP5, PER2, Pkc(s), SARS, TIP60, TMPO, TOP1, Top2, TYMSOS, UBE2T, UHRF1, ZBED1
7	Actin, Adaptor protein 2, ANLN, BAIAP2L1, Calmodulin, CD3, CDK2, Clathrin, DPYSL3, DUT, FLNB, GGH, Gpcr, GPT2, HIST1H2BD, ID2, KIF14, LONP1, MARS, MCM2, MCM5, NCALD, POLA2, PRIM1, Primase, RRM1, Sfk, Shc, SPTBN1, SRC (family), TARS, TCEA3, TCR, TUBB, tubulin (complex)
8	20s proteasome, 26s Proteasome, BCR (complex), CBX4, CCNB1, DCBLD2, DDIT3, EDEM1, Eph Receptor, FOSL1, GABARAPL1, GFPT1, GRB10, Ikb, KLHL3, MAP1B, MAP1LC3B, Mapk, MHC CLASS I (family), NAAA, NREP, PARP, PRKAA, Rab5, RBCK1, Rsk, SKP2, SPRY4, SQSTM1, TK1, TNFRSF10B, tubulin (family), Ubiquitin, ULK1, WARS
9	Akt, ALDH, ALDH5A1, ASF1B, CDC7, CDC45, CDK4/6, Ctbp, CTHRC1, Cyclin A/Cdk2, Cyclin D, DGKD, DKK1, DNA Polymerase, E2f, E2F2, FKHR, GINS2, GINS3, INSM1, LEF1, Mcm, MCM3, MCM4, MCM6, MCM7, PBK, Pias, RPA, SERCA, SH2B3, Smad2/3-Smad4, TGIF1, TIPIN, Wnt
10	ASB1, ASB9, Calcineurin protein(s), caspase, Caveolin, CLIC4, Collagen Alpha1, creatine kinase, cytochrome C, cytochrome-c oxidase, DNAJB9, Hdac, HOXB8, Hsp70, Hsp90, HSPA2, MEF2, MT1A, MT1E, MT1F, MT1H, MYB, NFAT (complex), Nfat (family), NPC1, P38 MAPK, PBX3, PLAUR, RAB5A, Raf, RANBP1, SAP30, Sapk, TFDP1, TSC22D3

## 10 Appendix

### 10.1 Publications List

#### *Original publications as lead author*

- ❖ **Ge Yan**, Mohamed E.M. Saeed, Sebastian Foersch, Jose Schneider, Wilfried Roth and Thomas Efferth: *Relationship between EGFR expression and subcellular localization with cancer development and clinical outcome*. *Oncotarget*. 2019; 10:1918-1931.
- ❖ **Ge Yan** and Thomas Efferth: *Cell Harvesting Methods Affect Cellular Integrity of Adherent Cells during Apoptosis Detection*. *Anticancer Research*. 2018; 38(12):6669-6672.

#### *Original publications as co-author*

- ❖ Thomas Efferth, **Ge Yan**, *et al*: *Biopiracy versus One-World Medicine—From colonial relicts to global collaborative concepts*. *Phytomedicine*. 2019 May; 53:319-331

#### *Submitted manuscripts*

- ❖ **Ge Yan**, Madeleine Böckers, Sabine M. Klauck, Christian Fottner, Matthias M. Weber, Thomas Efferth: *p21 regulates artesunate induced multiple cell death modes in neuroendocrine tumors*. *Acta Pharmacologica Sinica b*. 2019 March
- ❖ **Ge Yan** and Thomas Efferth: *Broad spectrum cross-resistance towards anticancer drugs mediated by epidermal growth factor receptor*. *Anticancer Research*. 2018 April
- ❖ Mohamed-Elamir F. Hegazy, Masashi Fukaya, Mona Dawood, **Ge Yan**, Edmond Fleischer, Asmaa W. Zagloul, Thomas Efferth: *Vitamin K3 thio-derivative: A novel specific apoptotic inducer in sensitive and drug-resistant cancer cells*. *Investigational New Drugs*. 2019 May

#### *Posters*

- ❖ **Ge Yan**, Matthias M. Weber, Christian Fottner, Esther Mettler and Thomas Efferth. *Effect of Artesunate on Neuroendocrine Cell Line*. The 3rd Annual Meeting of the Specialty Committee of Immunology of Traditional Chinese Medicine of the World Federation of Chinese Medicine Societies. Mainz, Germany, 7-10, August, 2016.

#### *Book chapter (unpublished yet)*

- ❖ **Ge Yan** and Thomas Efferth: *Identification of chemo-sensitizer by drug repurposing to enhance the efficacy of cancer therapy*

## **10.2 Curriculum Vitae**